EXPERIMENTAL RESEARCH ON PREVENTING DEBONDING PROBLEM IN RETROFITTED RC BEAM – COLUMN JOINTS USING COMPOSITE MATERIALS

by

Hasan Altun

B.Sc., Civil Engineering, Bogazici University, 2008

Submitted to the Institute for Graduate Studies in
Science and Engineering in partial fulfillment of
the requirements for the degree of
Master of Science

Graduate Program in Civil Engineering

Boğaziçi University

2011

ACKNOWLEDGEMENTS

I would like to express my gratitude to all the people who in one way or another contributed to the development of this research. I would like to express my sincere appreciation to my advisor Assoc. Prof. Dr. Cem Yalçın; thank you for your valuable help in instructing, guiding and supporting me throughout the duration of this thesis.

Also, I would like to thank the members of my Master's thesis examination committee: Assist. Prof. Dr. Kutay Orakçal, and Assoc. Prof. Dr. Ercan Yüksel for their knowledgeable and in-depth comments and advice.

Special thanks to my friends Dr. Selçuk Altay, Dr. Osman Kaya and Tevfik Terzioğlu for encouraging me to chose this subject of the thesis for their help and suggestions during the construction and testing of the specimens, and to the technicians, Hasan Şenel, Hamdi Ayar, Ümit Melep and Mesut Kardaş for their help in the experimental phase of this research.

Carbon Fiber Reinforced Polymer Material and its adhesives were provided by BASF. Their contribution is greatly appreciated.

Further, I would like to thank my friends and colleagues: C. Aydın, S. Kaya, H. Köksal, Ç. Yiğit Şanlı, Zennure Gündoğdu Şanlı and D. Uluğtekin for their help, the support and for the fun times during MSc. I wish you all success, luck and happiness.

Finally, I would like to thank my family and my great friend R. Goch for their continuous support and encouragement.

ABSTRACT

EXPERIMENTAL RESEARCH ON PREVENTING DEBONDING PROBLEM IN RETROFITTED RC BEAM – COLUMN JOINTS USING COMPOSITE MATERIALS

Beam-column joints in existing reinforced concrete (RC) structures that were designed according to pre-1970s national design codes pose serious danger in moderate to severe earthquakes due to the fact that they were designed for gravity loads and lateral force levels that were much lower than those specified by the current codes. Common deficiencies of these joints could be summarized as; widely spaced column ties, no transverse reinforcement in the joint region, inadequate lap splicing in the column and insufficient embedment length of beam bottom reinforcement in the joints. This lack of seismic detailing may cause non-ductile behavior and excessive lateral deformation demands which cannot be accommodated, and therefore, failure mechanisms resulting in total collapse may easily develop. Thus, the shear capacity and the effective confinement of joints must be improved. This research investigates the actual behavior of such joints and debonding problem in Carbon Fiber Reinforced Polymer (CFRP) wrapping methodologies that were developed to improve the seismic behavior of such deficient joints.

In order to investigate the effect of CFRP retrofitting on the behavior of exterior beam-column joints, nearly three full-scale reinforced concrete beam-column subassemblies were produced and tested under constant axial load and reversed cyclic loading. One of the specimens was detailed according to ACI 318-09 code requirements and the remaining two specimens that are deficient in shear detailing requirements were retrofitted using CFRP sheets according to previous studies conducted by Altay’s PhD dissertation using new anchorage techniques for preventing debonding effect on CFRP from concrete surface.

Experimental and analytical results showed that the CFRP-retrofitted specimens exhibited significant behavior in terms of load carrying capacity. The desired failure mechanism, which is the hinge formation in the beam, was reached and debonding problem of the CFRP was prevented, by using increased number and improved quality of anchorages.

ÖZET

KOMPOZİT MALZEMELERLE GÜÇLENDİRİLMİŞ BETONARME KOLON-KİRİŞ BİRLEŞİM BÖLGELERİNDEKİ YÜZEY AYRIŞMA PROBLEMİNİN ORTADAN KALDIRILMASI

1970 öncesi yerel tasarım şartnamelerine dayanılarak yapılan yapıların kolon-kiriş birleşim bölgeleri sadece yerçekimi yükleri altında tasarlandığından ve de deprem yüklerini karşılayamayacak bir kapasitede olduklarından dolayı büyük tehlike arz etmektedirler. Geniş etriye aralıkları, birleşim bölgelerinde etriye olmaması, kolonlarda yetersiz bindirme boyları ve kiriş donatılarının yetersiz ankrajlanması bu elemanların genel eksiklikleridir. Sismik tasarım donatısı eksikliği bu elemanlarda gevrek davranışa ve aşırı yatay deformasyonlara neden olmaktadır. Bundan dolayı, bu elemanlarda kesme kapasitesi ve efektif sargı iyileştirmesi yapılmalıdır. Bu araştırma, belirtilen birleşim noktalarının davranışını ve karbon lifli güçlendirilmiş polimer (CFRP) malzeme ile sargılama yapılarak iyileştirme yapılan elemanlardaki yüzey ayrışmayı önleme çalışmalarını kapsakmaktadır.

CFRP sargılama ile güçlendirmenin, kolon-kiriş birleşim bölgesi davranışına etkisi, üç adet yaklaşık 1/1 oranlı, betonarme kolon-kiriş birleşim noktası numunesi üretilip, sabit eksenel yük altında, tersinir yatay kuvvetler ile test edilerek irdelenmiştir. Bu numunelerden bir tanesi, birleşim bölgesi ACI şartnamsine göre tasarlanmış olup diğer iki numune ise birleşim bölgesinde yetersiz donatıya sahip olduklarından, daha once Altay'ın doktora tez çalışmasındaki CFRP ile sargılama metodu kullanılarak, değişik ankraj teknikleriyle güçlendirilmiştir.

Deneysel ve analitik verilerin neticesinde, CFRP ile güçlendirilmiş numuneler, taşıma gücü bakımından oldukça üstün bir performans sergilemişlerdir. İstenilen göçme modu olan kirişte mesnet oluşumu gözlemlenmiş ve de arttırılan ankraj sayısı ve kalitesinden ötürü CFRP'nin beton yüzeyinden ayrışması problemi ortadan kalkmıştır.

TABLE OF CONTENTS

LIST OF FIGURES

LIST OF TABLES

LIST OF SYMBOLS / ABBREVIATIONS

C_b	Compression force of beam
C_{c1}	Compression force of top column
C_{c2}	Compression force of bottom column
CR#	Crack number
$d_{1,2}$	Readings of displacement sensors in curvature measurements
$d_{1,2}$	Diagonal distances of deformed shape of the joint shear panel
E_c	Modulus of Elasticity of concrete
E_s	Modulus of Elasticity of steel
F_{1-6}	Internal forces of truss members
f'_c	Concrete compressive strength
f_s	The stresses of longitudinal reinforcements
f_t	The tensile strength of concrete
f_u	The ultimate strength of steel, concrete and CFRP
f_y	The yield strength of reinforcement
f_{truss}	Stresses of truss members
h	Height of the joint shear panel
$h_{1,2}$	Distance of displacement sensors from the surface of the member
h_c	Distance between two displacement sensors in curvature readings.
H	Applied Lateral load
K	Secant stiffness
L	Length of beam
$L_{1,2}$	Gage length of displacement sensors in curvature readings
M	Moments of the section
n	Number of CFRP layers
N	Beam end vertical reaction
NA	Neutral Axis
P	Axial load
R_1	Vertical reaction at column support

R_2	Horizontal reaction at column support
R_3	Vertical reaction at beam support
Sg	Strain gauge
t_{FRP}	Thickness of one layer of CFRP
T_b	Tensile force of beam longitudinal reinforcement
T_{c1}	Tensile force of top column longitudinal reinforcement
t_c	Height of column and/or beam cross-section
Δ	Column top displacement
Δ/H	Drift ratio
α	The angel of diagonal cracks occurred at joint region
Δ	Relative longitudinal displacement reading taken from the displacement sensors
$\Delta_{1,2}$	Readings of displacement sensors in curvature measurements
ε_o	The strain values at the maximum strength of concrete model
ε_c	The compressive strain of extreme fiber of the section
ε_t	The tensile strain of extreme fiber of the section
ε_{sh}	The strain value where the strain hardening initiates
ε_u	The ultimate strain value of concrete and steel
ε_y	The yield strain value of steel
$\varepsilon_{1,2}$	Strains calculated from
γ	Shear deformations of the joint
κ	Curvature
ρ	Longitudinal reinforcement ratio
$\rho_{l\text{-}min}$	Minimum longitudinal reinforcement ratio
ρ_s	Transverse reinforcement ratio
σ_y	Yield stress
ACI	American Concrete Institute
ASTM	American society for testing and materials
CDE	Cumulative dissipated energy
CFRP	Carbon fiber reinforced polymer

RC	Reinforced concrete
FRP	Fiber reinforced polymer
GFRP	Glass fiber reinforced polymer
LVDT	Linear variable differential transformer
3D	Three dimensional

1. INTRODUCTION

1.1. General

In seismic areas, the strengthening of under-designed reinforced concrete (RC) structures represents a crucial issue involving technical and social aspects. Since these structures were originally designed to carry only gravity loads, they lack the ductility and the hierarchy of strength that induce a global failure mechanism appropriate for seismic conditions. Typically, columns have minimum cross-sectional dimensions with lower strength concrete and because of the widely-spaced ties, their longitudinal steel reinforcement is inadequate to satisfy the flexural and shear demands generated during an earthquake. The lack of appropriate size and spacing of column ties increases the risk of brittle and local failure mechanisms such as crushing of the unconfined concrete at the column ends, resulting instability of the longitudinal steel reinforcing bars in compression, and bond failures of those in tension when they are inadequately spliced.

RC beam-column joints require strengthening due to deficient detailing of reinforcing bars, insufficient column sections or due to increased loading on the structure. Strengthening of these joints, however, is a challenging task that poses major practical difficulties. A variety of techniques have been applied to joints with the most common ones being the construction of RC or steel jackets. Reinforced concrete jackets require intensive labor and often intricate detailing of steel in the form of diagonal collars. Moreover, concrete jackets increase the dimensions and weight of structural elements. Few attempts have been made in employing plain or corrugated steel plates. In addition to corrosion protection, these elements require special attachment through the use of either epoxy adhesives combined with bolts or special grouting.

On the other hand, strengthening of such existing structures using lightweight composite materials is becoming widespread due to their ease of installation and competitive pricing compared with traditional methods. One of these groups of lightweight

materials is fiber-reinforced polymer (FRP) materials, which are available today in the form of strips or in-situ resin impregnated sheets, are being used to strengthen a variety of RC elements, including beams, slabs, columns, and shear walls, in order to enhance the flexural, shear, and axial (through confinement) capacity of such elements.

FRP materials offer such advantages that are listed as; ease of installation, immunity to corrosion, high stiffness-to-weight and strength-to-weight ratios, availability in convenient ‘‘to apply’’ forms, and the ability to control the material’s behavior by selecting the proper orientation of the fibers. All of these features make these composite materials highly-engineered materials that are suitable for infrastructure applications.

1.2. Problem Definition

Beam-column joints of existing RC structures that were designed according to pre 1970s national design codes pose serious danger in moderate to severe earthquakes due to the fact that they carry only gravity loads and the amounts of lateral force levels are much lower than those specified by the current codes. Common deficiencies of these joints could be summarized as; widely spaced column ties, no transverse reinforcement in joint region, inadequate lap-splicing in column and insufficient embedment length of positive beam reinforcement in the joints. These lacks of seismic detailing cause non-ductile behavior. As a result, excessive lateral deformation demands could not be accommodated, and thus, failure mechanisms toward total collapse are inevitable. Thus, the shear capacity and the effective confinement of joints must be improved.

There have been many catastrophic failures reported in the past earthquakes, in particular with Turkey and Taiwan earthquakes that were occurred in 1999, which have been attributed to beam-column joints as shown in Figure 1.1. The poor design practice of beam-column joints is compounded by the high demand imposed by the adjoining flexural members (beams and columns) in the event of mobilizing their inelastic capacities to dissipate seismic energy. Unsafe design and detailing within the joint region jeopardizes the entire structure, even if other structural members conform to the design requirements.

Recent earthquakes and related studies have revealed the importance of beam-column joints and the need for retrofitting of existing beam to column connections aroused. Methods for improvement of joints such as steel jacketing, reinforced concrete jacketing, or epoxy injection have been investigated by many researchers and their positive effects were emphasized.

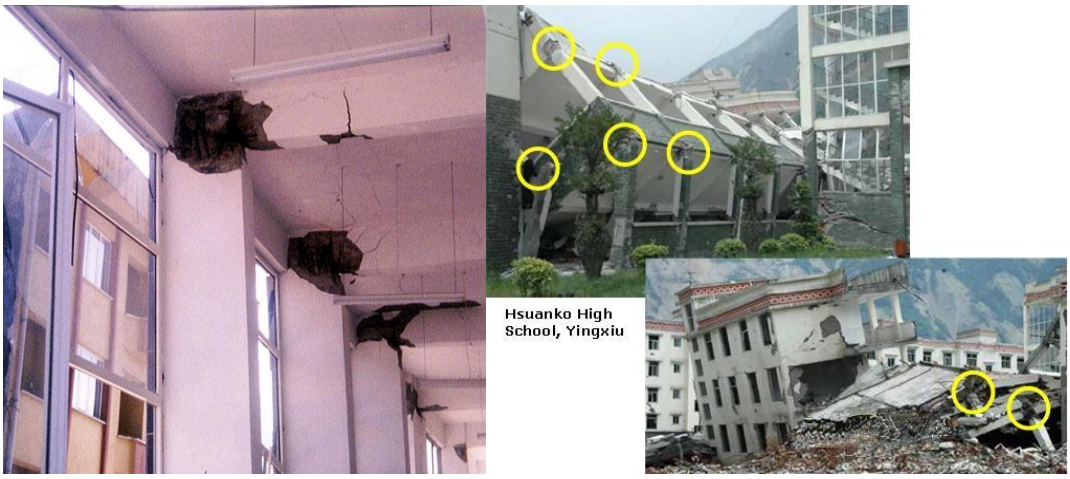

Figure 1.1. Damage of Beam-Column Joints

This research investigates the actual behavior of such joints and Carbon Fiber Reinforced Polymer (CFRP) wrapping methodologies are developed to improve the seismic behavior of such deficient joints.

1.3. Literature Review

1.3.1. Beam-Column Joint Behavior

1.3.1.1.Types of Beam-Column Joints. The geometric categories of RC beam-column connections depend on in-plane geometry, out-of-plane geometry (transverse beam(s) and/or slab(s)), and joint eccentricity. Figure 1.2 displays various types of RC beam-column connection subassemblies according to in-plane geometry. An interior connection has two longitudinal beams with a continuous column, an exterior connection has one longitudinal beam with a continuous column, and a knee connection has one longitudinal beam with a discontinuous column.

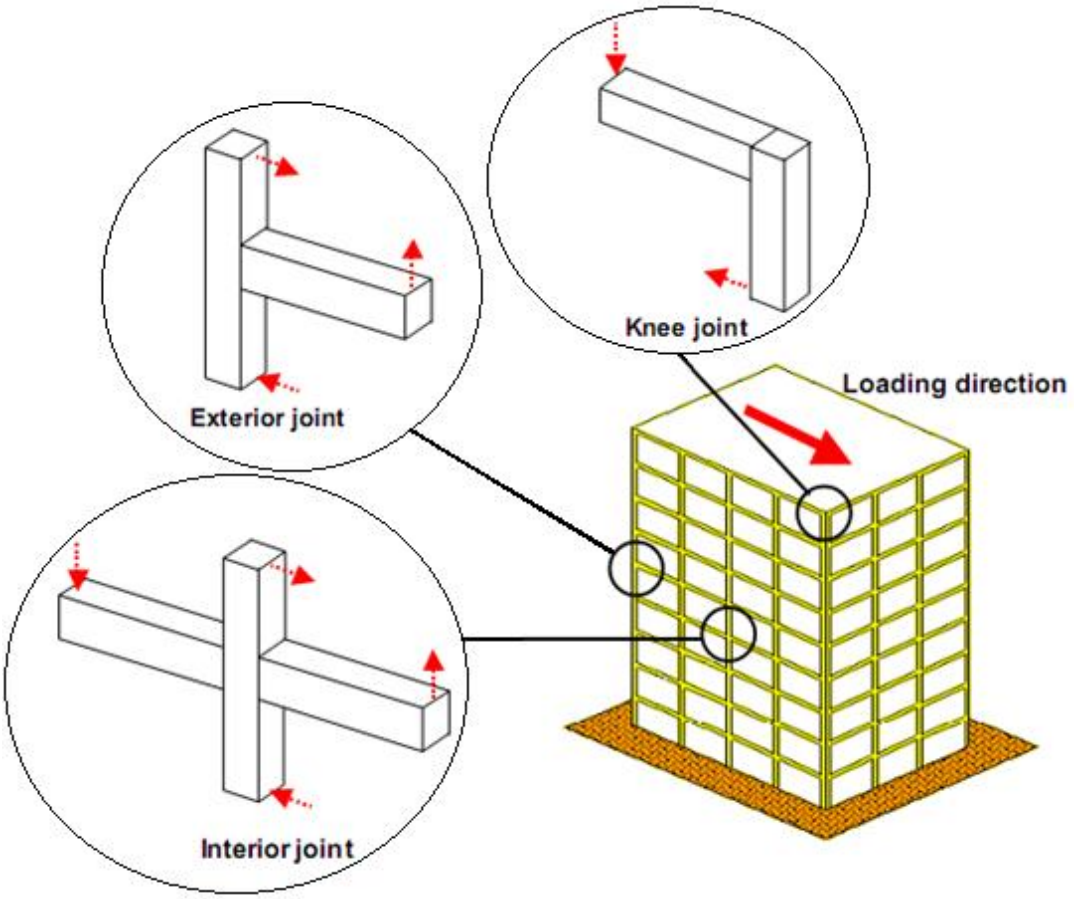

Figure 1.2. Terminology of RC Beam-Column Connections

1.3.1.2.Beam-Column Joint Behavior. The seismic design philosophy relies on providing sufficient ductility to the structure by which the structure can dissipate seismic energy. In RC beam-column connections subjected to earthquake loading, the main role of the joint panel is to transfer loads from and to the adjacent beam(s) and column(s). When only the flexural strength of well-detailed longitudinal beams limits overall response, RC beam-column connections typically display ductile behavior. This beam-hinging governing mode is usually considered as the most desirable for maintaining good global energy-dissipation without severe degradation of overall lateral load capacity. On the other hand, RC beam-column connections can exhibit less robust behavior when severe damage is concentrated within the joint panel. Therefore, understanding joint shear behavior is important toward controlling the overall performance of RC beam-column connections and frames.

Seismic action launches to joint region significant horizontal and vertical shear forces due to moment reversals in the adjacent members across the joint. As it is shown in Figure 1.3, the demand magnitudes of joint shear forces (V) and their corresponding moments (M) are much larger than those capacities in the beams and columns leading to a brittle joint shear mechanism, and thus, resulting strength and stiffness degradation according to detailing provided as shown in Figure 1.4 when subjected to cyclic loading in the inelastic range.

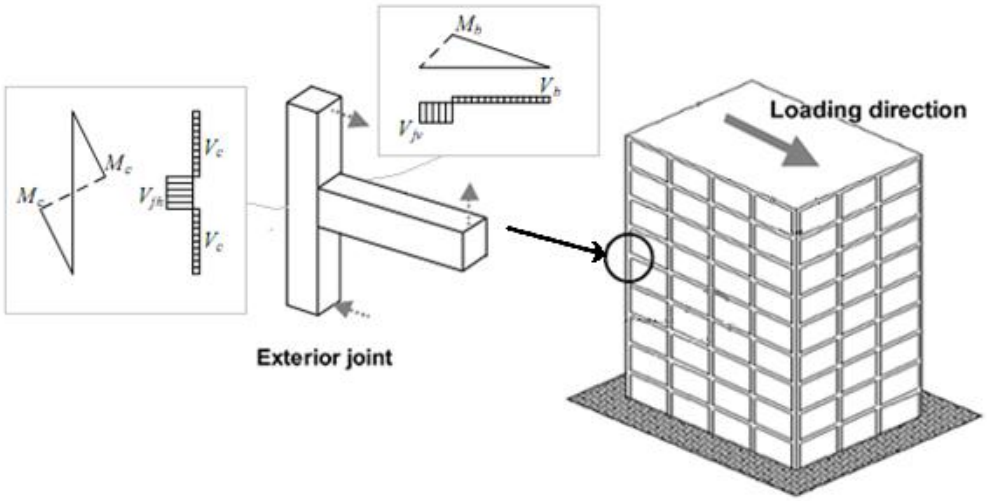

Figure 1.3. Horizontal and Vertical Shear Forces

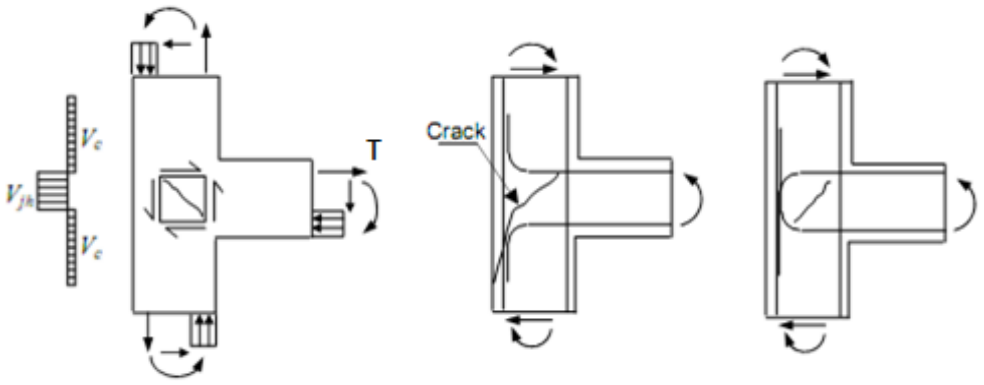

(a) Forces (b) Poor detail (c) Satisfactory detail

Figure 1.4. Forces and Detailing Requirement for Exterior Joint

All in all, the functional requirement of a joint, which is the zone of intersection of beams and columns, is to enable the adjoining members to develop and sustain their ultimate capacity. The demand on this finite size element is always severe especially under seismic loading. The joints should have adequate strength and stiffness to resist the internal forces induced by the framing members.

1.3.2. Key Parameters Controlling Beam-Column Joint Shear Behavior

As it was discussed while describing the joint behavior, beam-column connections have been identified as potentially one of the weaker components of reinforced concrete moment resisting frames subjected to seismic lateral loading, and therefore, the desired failure should be beam hinge because of the fact that RC beam-column connections can show much more brittle behavior when severe damage is concentrated within the joint panel. Thus, joint shear behavior is important with regard to controlling the overall behavior of RC beam-column connections. Well-established knowledge of RC joint shear behavior is necessary since severe damage within a joint panel may trigger deterioration of the overall performance of RC beam-column connections or frames. However, despite the importance of understanding RC joint shear behavior, a consensus on the ways in which some parameters affect joint shear strength has not been reached. There are many factors affecting RC beam-column joints and many researchers tested joints by such varying parameters. Namely, they are listed as:

- Concrete compressive strength,
- Column versus beam moment strength ratio,
- Discontinuous beam reinforcement with short embedment length,
- Anchorage of the reinforcing bars in joint region,
- Shear resisting mechanism in beam-column joint,
- Confinement of joint core,
- Axial load,
- Presence of transverse beams and floor slab.

However, there is still no consensus on some of those parameters listed above. Especially, some researchers ignore the effect of axial load on joint shear capacity but some strongly recommend that the axial load contribution may rise to its shear capacity.

Uma and Prasad (2004) generalized beam-column joint behavior such that it is controlled by bond and shear failure mechanisms, which are weak sources for energy dissipation. They summarize performance criteria for joints under seismic actions as follows:

i. The joint should have sufficient strength to enable the maximum capacities to be mobilized in the adjoining flexural members,
ii. The degradation of joints should be so limited such that the capacity of the column is not affected in carrying its design loads,
iii. The joint deformation should not result in increased storey drift.

In order to achieve these criteria, bond requirements and shear resisting mechanism should be provided. In the behavior of joint region, the desired failure should be such that plastic hinges occur in the beams, which cause critical bond conditions in the longitudinal reinforcing bars passing through the joint, and also impose high shear demand in the joint core. The joint behavior exhibits a complex interaction between bond and shear. The bond performance of the bars anchored in a joint affects the shear resisting mechanism to a significant extent. When the longitudinal bars at the joint face are stressed beyond yield splitting cracks are initiated along the bar at the joint face which is referred to as "yield penetration." Adequate development length for the longitudinal bar is to be ensured within the joint taking yield penetration into consideration. Therefore, the bond requirement has a direct implication on the sizes of the beams and columns framing into the joint.

In the case of exterior joints, the beam longitudinal reinforcement that frames into the column terminates within the joint core. The longitudinal reinforcement bar, if terminating straight, would get pulled out due to progressive loss of bond. The pull out failure of the longitudinal bars of the beam results in complete loss of flexural strength. This kind of failure is unacceptable and it could be prevented by the provision of hooks or by providing effective anchorage.

Bond strength is affected by confinement, clear distance between the bars and nature of the surface of the bar. In order to transfer the tensile forces, confinement of the embedded bars that is obtained from axial compression due to the column is very crucial for improving the bond performance. Moreover, Popov's and Bertero's (1975) common research has shown that bond performance is better if the clear distance between the longitudinal bars is less than 5 times the diameter of the bar. It should be known that the quality of concrete is also affective in the behavior of the reinforcing bar in bond.

Shear force demand is an important factor affecting the joint behavior. High shear stresses are created within the joint by the external forces acting on the face of the joint and this leads to diagonal stresses and causing diagonal cracks if tensile stresses exceed the tensile strength of concrete. Extensive cracking occur within the joint under load reversals, affecting its strength and stiffness and hence the joint becomes flexible enough which is the desired beam hinge mechanism.

As it has been shown in Figures 1.4 and 1.5, the column shear force (V_c) and corresponding joint shear (V_{jh}) in an exterior joint could be calculated as:

$$V_c = \frac{M_h}{l_c} \tag{1.1}$$

$$V_{jh} = T - V_c \tag{1.2}$$

Where T is the tension in the reinforcing bar and M_c is the moment in the column.

Effective shear area is also a crucial factor affecting joint behavior. The effective shear area A_j is defined by the width of the joint, b_j, and the depth of the joint h_j. The area effective in resisting joint shear may not be as large as the column's entire cross section area since the width of the beam, b_w and the column, b_c may differ from each other. ACI 352-02 code recommends effective joint shear area based largely on engineering approximations.

The shear resisting mechanism consists of a diagonal concrete strut action and a truss action. The diagonal concrete strut mechanism is formed by the major diagonal concrete

compression force in the joint which is produced by the vertical and horizontal compression stresses and the shear stresses on concrete at the beam and column critical sections. The truss mechanism is formed by a combination of the bond stress transfer along the beam and column longitudinal reinforcement, the tensile resistance of lateral reinforcement and compressive resistance of uniform diagonal concrete struts in the joint panel. The strength of the strut mechanism depends on the compressive strength of concrete and that of the truss mechanism on the tensile yield strength of the lateral reinforcement crossing the failure plane.

The total strength of joint contributed by each mechanism can be considered as the shear strength of the joint in the horizontal direction and is given as

$$V_{jh} = V_{ch} + V_{sh} \tag{1.3}$$

Where, V_{ch} is the contribution from the concrete strut and V_{sh} is the contribution from the truss mechanism. The internal forces developed in the strut and truss mechanisms are illustrated in Figure 1.5.

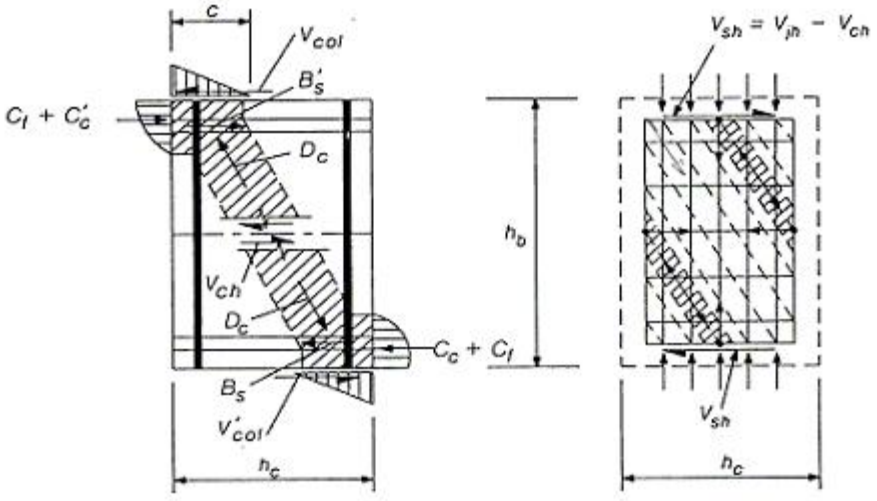

a) Strut Mechanism b) Truss Mechanism

Figure 1.5. Forces and Detailing Requirement for Exterior Joint

Under seismic loading conditions, after beam's flexural yielding, bond along the beam reinforcement deteriorates, the truss mechanism starts to diminish and the diagonal strut mechanism must resist the most dominant part of the joint shear. In such a case, the tension force in the beam reinforcement not transferred to the joint concrete by bond must be resisted by the concrete at the compression face of the joint, thus increasing the compression stress in the main strut. The concrete strut is progressively weakened by the reversed cyclic loading. At the same time, the compressive strength of the concrete is reduced by the increasing tensile strain perpendicular to the direction of main strut. The failure of the concrete strut in shear compression occurs because of those two cases. The principal role of the lateral reinforcement in this case is to confine the cracked core concrete.

In addition to these, the slab contribution to flexural resistance of the longitudinal beam results in increased joint shear which is applied directly along the compression zone of the longitudinal beams and is resisted within the joint by the inclined compression strut. However, increased force along the strut may cause compression failure in the strut.

1.3.3. Experiments Conducted on As Built Beam-Column Joints

Since 1970s, many researches dealt with reinforced concrete connections. Research on this area could be classified into experiments with quasistatic loading on bridge beam-column joints, typical building frame joints and frameworks report enhancement of both shear and bending capacity, and cyclic load tests on joints with inadequate reinforcement bond length, rehabilitated specimens, shear strengthened "T" joints, have also reported substantial improvements in ultimate capacities.

Focusing on studies conducted on typical building frame joints, several researchers have investigated RC joint shear behavior based on their constructed experimental databases for RC beam-column connection subassemblies. In their constructed databases, some experimental subassemblies experienced joint shear failure either in conjunction with or without yielding of beam reinforcement, which is referred to as "BJ" and "J" failures, respectively, while, some experimental subassemblies experienced only beam flexural

failure, which is referred to as “B” failure. For example, Kitayama et al. (1991) examined 15 interior “BJ” failures and 19 interior “J” failures from experiments conducted by them and by others. They reported two findings related to joint shear strength. First, joint shear strength seemed to be independent of column axial load, and second, joint shear strength was not enhanced by an increase in the amount of joint transverse reinforcement when the dimensionless joint transverse reinforcement ratio (total area of joint transverse reinforcement, located in the loading direction and placed between the top and bottom beam reinforcement, divided by the product of column width and the distance between the compressive and tensile resultants of the section) was already above 0.4%.

Bonacci and Pantazoupoulou (1993) collected data from experiments consisting of 34 interior “BJ” failures and 16 interior “J” failures. In collecting the experimental data, there was no restriction on the amount (how much or how little) of joint transverse reinforcement. They indicated that column axial load has no coherent influence on joint shear strength. By calculating the potential contribution of joint transverse reinforcement to joint shear strength, they suggested that the participation of joint transverse reinforcement in the shear-resistance mechanism can be significant. Goto and Joh (1996) collected data from 52 experimental interior “BJ” failures and 23 interior “J” failures, again with no limitation on the amount of joint transverse reinforcement. According to their examination, joint shear strength was dependent on concrete compressive strength, and joint transverse reinforcement also somewhat affected joint shear strength. Kamimura et al. (2000) collected data from 87 interior joint tests. In this collected data, the governing failure modes were beam flexural failure, “BJ” failures, and “J” failures. As in other previous research, there was no restriction on the amount of joint transverse reinforcement when collecting the data. They reported that the amount of joint transverse reinforcement used in a frame structure had little influence on the shear strength and joint deformation of interior connections.

Kitayama (1991) proposed a tri-linear shear stress vs. shear strain envelope curve for RC joint shear behavior by defining joint shear moduli based on 11 interior “BJ” failures and 3 interior “J” failures (that again had no restriction on the amount of joint transverse reinforcement). To determine the shear moduli after diagonal cracks occurred in the joint

panel, the following were considered: concrete compressive strength, joint transverse reinforcement, column reinforcement, column axial load, and lateral confinement by transverse beams and/or slabs. Similar to the suggestion of Kitayama (1991), Teraoka and Fujii (2000) also proposed an envelope curve of joint shear behavior, which consisted of four line segments. In their suggestion, joint shear stress (at maximum response) follows AIJ 1999 and joint shear strain at key transition points are fixed regardless of the diversity of joint panels. The proposed models of Kitayama (1991) and Teraoka and Fujii (2000) are certainly questionable for application to cases not covered by their collected experimental data, and could perhaps not even be the best for use with their respective own databases.

1.3.4. Experiments on Beam-Column Joints Retrofitted with Carbon Fiber Reinforced Polymers (CFRP)

In recent studies, many studies were focused on strengthening or existing structures and the use of fiber reinforced polymers for strengthening and repair of reinforced concrete structures seems to be an attractive solution in the field of civil engineering. Focusing on previous research, a combination of FRP in various forms bars, plates and sheets in structural enhancement have been investigated. The suitability of adhesives of different moduli has also been studied. On some occasions a combination of FRP and steel external reinforcements has been used. FRP in seismic retrofitting of strong-beam-weak-column frameworks that are prevalent in gravity load designed buildings have been investigated. Analytical models of externally reinforced beam-column joints have been presented using closed form, and finite element technique. Design methods have been suggested for shear and bending. Pushover analysis has been employed in the design of upgrading (strengthening) of bridge joint assemblies and buildings in seismic conditions.

One of the first prior using the application of carbon fiber composite jackets for the three columns joining with cap beam of an existing concrete bridge pier is Gergely et al. (1998). A displacement-based approach was used to design the carbon fiber composite wrap for the bridge bent and four full-scale specimens were tested. They confirmed that retrofit of a bridge pier for gravity load and seismic improvement of the performance of a typical bridge was feasible. Columns, cap beams, and cap beam-column joints could

benefit from the retrofit with carbon fiber composite materials and increase both the shear capacity and the ductility of the concrete pier.

In 2000, Gergely et al. have focused on a retrofit technique for RC beam column joints based on externally applied CFRP composite sheets. In their experimental study of RC T-joints, they designed, built, and tested 14 1/3-scale exterior beam-column joint specimens. The composite curing process, the CFRP layout, and the surface preparation of the concrete were the main considered parameters in this study. Also they conducted on an analytical study. For control specimens, shear damage in the beam-column joint region has caused failure at low lateral load. However, the peak lateral load has significantly increased for retrofitted specimens.

Granata and Parvin (2001) conducted an experimental study on FRP upgrade of RC beam-column joint. The objective of this research was evaluating the moment capacity of the beam-column connections wrapped with Kevlar fiber composite fabric and experimental results demonstrated significant improvement of flexural capacity of beam-column connections. They also offered that the addition of FRP overlays to the bottom of the beam-column connections provided the mechanism for shear transfer between the beam and column elements.

Mukherjee and Joshi (2005) have conducted an experimental study on the FRP composite retrofitting of adequately designed and detailed interior RC beam-column joints with anchored deficient beam bottom reinforcements. In their study, the control specimens have also been repaired and tested in order to investigate the effectiveness of retrofitting technique for damaged specimens. They have used both glass and carbon composite materials and have concluded that both of them can be efficiently used for seismic retrofitting as well as rehabilitation of reinforced concrete joints but, specimens strengthened using CFRPs have shown stiffer behavior than GFRP strengthened specimens because the stiffness of carbon is considerably higher than that of glass. Considerable increases in yield load and initial stiffness have been achieved regardless of reinforcement detailing and damage state. Test on rehabilitated specimens have suggested that FRP not

only restores original strength of specimen but also there is considerable enhancement in its yield load, initial stiffness and energy dissipation capacity.

Pantelides et al. (2008) studied on an experimental research program that regards the use of externally applied carbon fiber reinforced plastic (CFRP) jackets for seismic rehabilitation of reinforced concrete interior beam-column joints, which were designed for gravity loads. The joints had steel reinforcement details that are known to be inadequate by current seismic codes in terms of joint shear capacity due to the absence of transverse steel hoops and bond capacity of beam bottom steel reinforcing bars at the joint. Lap splicing of beam bottom steel reinforcement at the joint using externally applied longitudinal CFRP composite laminates is investigated. Improvement of joint shear capacity using diagonal CFRP composite laminates is another strengthening scheme employed. Concrete crack widths for the as-built specimens and the extent of CFRP delamination for the rehabilitated specimens at various drift ratios are reported. The test results indicated that CFRP jackets are an effective rehabilitation measure for improving the seismic performance of existing beam-column joints with inadequate seismic details in terms of increased joint shear strength and inelastic rotation capacity. In addition, CFRP laminates are effective rehabilitation measures for overcoming problems associated with beam bottom steel bars that have inadequate embedment into the beam-column joints.

Altay et al. (2010) have conducted on an experimental study involving full-scale experimental evaluation of carbon fiber-reinforced polymer CFRP rehabilitation for existing RC beam-column joints designed for gravity load with common pre-1970s deficient reinforcement details when subjected to cyclic loading. They investigated CFRP retrofit techniques to enhance the performance of joints that posses lack of shear reinforcement within the joint core and shortly embedded positive beam reinforcement. For control specimens, it has been observed that the slippage of the beam positive reinforcement is more critical than joint shear failure therefore, in the order of priority, the debonding of the shortly embedded beam bottom longitudinal reinforcements should be eliminated or delayed and the joint core should be strengthened for shear. Experimental variables studied entail the developed CFRP retrofit configurations, and magnitude of the applied column axial load. Comparative analysis of the lateral loads versus drift hysteresis

loops, stiffness degradation, and total dissipated energy curves of three as-built and three corresponding CFRP-retrofitted RC joints revealed that significant improvement in the shear capacity of the upgraded joints occurred. Moreover, the slippage of short embedded beam positive reinforcement into the joint was substantially controlled due to the developed CFRP retrofit. The results demonstrated the effectiveness of CFRP retrofit configurations in enhancing the structural performance of actual size connections.

1.3.5. Experiments on Debonding of Retrofitted Beam-Column Joints

During the last decade or so, rehabilitation of structures has been attempted through the use of fiber-reinforced polymer FRP sheets to increase the strength of structural elements. Due to its complexity and practical difficulties, limited studies have been carried out on the joint as opposed to the column or the beam FRP strengthening. Although limited in quantity, these investigations have shown the effectiveness of FRP as external reinforcement in increasing the shear and flexural capacities and ductility of the beam-column joint subassemblies is also very important because of the problem of debonding in FRP from concrete surface. It has been widely accepted that carbon fiber reinforced polymers can be used effectively to strengthen reinforced concrete members. Until now most research and applications of such strengthening methods has been focused on gluing or bolting CFRPs to the members' surface and the failure was often caused by premature de-bonding or de-lamination of the CFRP and therefore the superior tensile strength of CFRP could not be fully utilized.

Antonopoulos and Triantafillou (2003) have investigated the effect of various parameters on the behavior of shear critical exterior RC joints strengthened with FRP by testing 18 specimens. The results have demonstrated the important role of mechanical anchorages in limiting premature debonding, and they have provided important information on the investigated parameters, including: area fraction of FRP, distribution of FRP between the beam and the column, column axial load, internal joint (steel) reinforcement, initial damage, carbon versus glass fibers, sheets versus strips, and the effect of transverse beams. In this study, debonding has dominated the behavior of FRP unless very low area fractions are employed or proper mechanical anchorages are

provided. Concerning this, mechanical anchorages and wrapping of longitudinal FRP sheets with transverse layers have increased the effectiveness of both strips and sheets. However, they have pointed that for the same area fraction, flexible sheets are more effective than strips. Additionally, both the strength and the dissipated energy have increased considerably with but not proportionally (due to premature debonding) to the number of FRP layers. On the other hand, they have also concluded that increasing the FRP area fraction only in the beam is nearly as effective as it is for equal increase in both the beam and the column, implying that the effectiveness of column FRP is rather limited. Though, the effectiveness of FRP sheets in joints with a transverse beam or with joint shear reinforcement has been reduced when it is compared to planar system with no shear reinforcement. Moreover, a few parametrical study carried out in this study have indicated that even low quantities of FRP materials may provide significant enhancement of the shear capacity.

Aiello et al. (2004) investigated the bond performance between different kinds of FRP sheets and concrete. They performed the beam tests and direct shear strip tests. Concluding tests, the following remarks can be made: (1) For both beam test and direct shear strip tests increasing the FRP stiffness ultimate force and mean bond stress increase as well. The initial transfer length, evaluated by the beam tests, increases with the stiffness of the reinforcement as confirmed in the available literature. (2) For direct shear strip test the slip seems to be independent of the FRP stiffness; this anomalous result points out as the direct shear strip test is un-reliable for the slips evaluation. (3) The utilized surface treatment influenced the kind of failure. In fact, the failure varied from adhesion failure, for the specimens without treatment, to cohesion failure for the specimens with surface treatment. The utilized treatment on the concrete surface involves only a global effect on the bond between FRP sheet and concrete (i.e. failure, mean bond stress and ultimate force), while the maximum bond stress remains almost constant. (4) The mean bond stress obtained by the beam tests and the direct shear strip tests are comparable. The easier direct shear strip test represents a good alternative to more complicated bond test, especially from a design point of view. (5) The theoretical Fédération Internationale du Béton (FIB) curve fits very well experimental points mainly for the ascending branch of the curves.

Shang et Al (2005) worked on a research that is focused on the experimental results of flexural behavior of four RC beams strengthened by prestressed-CFRP sheet and one with non-prestressed-CFRP sheet in order to overcome debonding problem. Their experimental tests indicated that the prestressed-CFRP method can significantly increase the cracking load and flexural stiffness and therefore reduce deflection at working load level compared to the non-prestressed-CFRP method. They also contributed that this method can allow the better use of the CFRP's high tensile strength under the serviceability limit state and this method can effectively prevent the debonding failure which was often a failure mode of the traditional FRP strengthening method, at the ultimate limit state. In short, the use of prestressed-CFRP sheet is a feasible and effective method to strengthen concrete structures.

Experimental and theoretical researches are always necessary and interesting because of the fact that techniques are still new and suitable models are needed for a reliable design. In particular, bond between concrete and FRP is still an open problem because of the lack of a standard in tests, the great variability of parameters involved and, therefore, the difficulty for assessing a bond law of general validity.

1.3.6. Analytical Modeling of The Shear Capacity of Beam-Column Joints

Hanson and Connor (1967) reported the test results of RC interior beam-column connections and gave a quantitative definition of joint shear as a horizontal force transferred at the mid-height of a horizontal section of a beam-column connection. They suggested that joint shear failure may be precluded by limiting the joint shear stress to the level at which joint shear failure occurs. Hanson and Connor defined the joint shear V_j in an interior beam-column connection. Referring to the free body diagram in Figure 1.6,

$$V_j = T + C_s' + C_c' - V_c \tag{1.4}$$

The joint shear V_j in Figure 1.6 is an internal force acting on the free body along the horizontal plane at the mid height of the beam-column connection. This definition has been

used in the design of beam-column connections. The contribution of steel and concrete is taken into account separately.

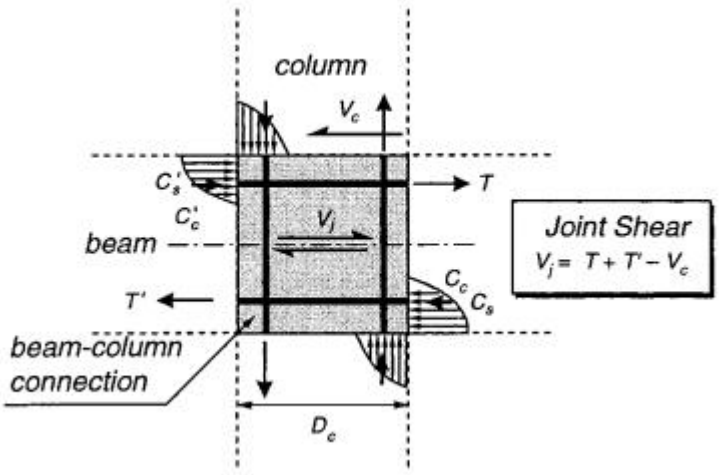

Figure 1.6. Definition of Horizontal Joint Shear in Interior RC Beam-Column Joints

The basic theory relating to the design of reinforced concrete beam-column joints is revised and extended, and the results of a series of tests conducted in the second half of 1976 are reported. It is shown that a joint which contained bond plates to prevent bond failure of the flexural reinforcement in the joint and was proportioned to limit yielding of the steel in this zone had markedly superior performance to specimens designed to comply with the American Concrete Institute ACI 318-71 code and to specimens designed according to the proposals of May 1976 for the revision of the New Zealand Ministry of Works and Development code of practice for the design of public buildings.

Scarpas (1981) made a study on the behavior of exterior beam column joints. The results are presented of tests of three reinforced concrete exterior beam-column sub-assemblies under simulated seismic loading. The main variable studied was the amount of horizontal joint shear reinforcement. A new tentative model for the mechanism of exterior joint shear resistance is proposed.

In 1996, Scot made an experimental work on 17 R/C exterior beam-column joints. Effects of depth of beam, tension steel percentage, reinforcing details of beam, and axial load were examined. He measured the strain distribution along the beam and column

reinforcing bars [43]. Gergely et al. (1998) calculated the contribution of the FRP to the shear capacity of a joint by analogy to steel stirrups, assuming that the FRP crossing a potential shear crack in the beam will exhaust its tensile capacity.

Shiohara (2001) investigated irrationality in the existing models for shear failure and examined 20 tests of RC interior beam-column connections exhibiting shear failure. Test data indicated that joint shear stress is not proportional to story shear. Joint shear increased until the end of the test in most specimens, even if the joint shear deformation apparently increased and the story shear decreased. Moment in section at the beam end decreased due to a reduction in distance between stress resultants at the column face. The cause of the deterioration of story shear was shown to originate from a finite upper limit of anchorage capacity of beam longitudinal reinforcements passing through the beam-column connection. A new mathematical model was introduced for shear failure of the beam-column connection to reflect this behavior as shown in Figure 1.7.

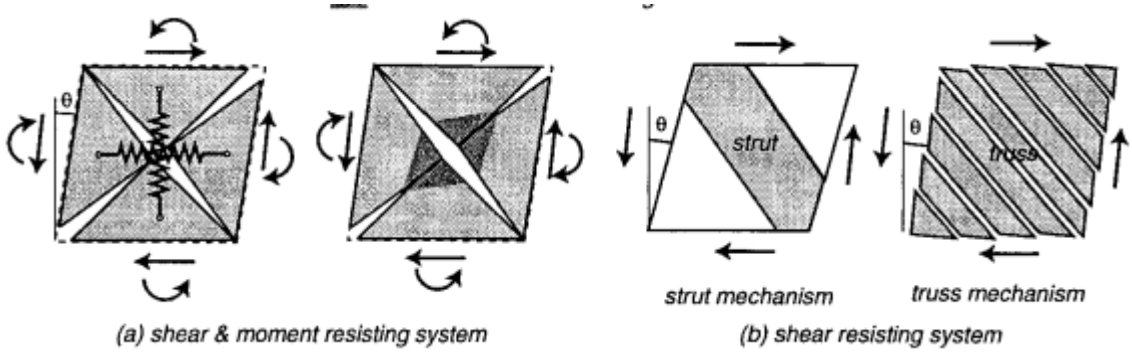

Figure 1.7. Comparison of Mechanisms for New Model and Existing Models

The model was based on divided segments, rotating due to bending moment coming from beams and columns. The equilibrium of internal forces in steel and concrete and external forces acting on beam ends and column ends are taken into account to derive the moment resisting capacity of the beam-column connection.

A simplified method, based on softened strut and tie model, for determining the shear strength of discontinuity regions failing in a diagonal compression is proposed by Hwang and Lee (1999). The method incorporates the shear resisting mechanisms as postulated by the softened strut and tie mode, and it is a function of the concrete strength, horizontal

shear reinforcement, vertical shear reinforcement and geometrical configuration of the discontinuity regions. Bakır and Boduroğlu (2002) presented a new design equation predicting the shear strength of monotonically loaded exterior beam-column joints accurately.

In 2002, Antonopoulos and Triantafillou presented analytical models in their study for the analysis of reinforced concrete joints strengthened with composite materials in the form of externally bonded reinforcement comprising unidirectional strips or flexible fabrics. The models provided equations for stresses and strains at various stages of the response (before or after yielding of the beam or column reinforcement) until the ultimate capacity is reached, defined by concrete crushing or fiber-reinforced polymer (FRP) failure due to fracture or debonding. Solutions to these equations were obtained numerically. The models provided useful information on the shear capacity of FRP-strengthened joints in terms of the quantity and configuration of the externally bonded reinforcement and may be used to design FRP patching for inadequately detailed beam-column joints. A number of case studies were examined indicating that even low quantities of FRP materials may provide significant enhancement of the shear capacity. Analytical shear strength predictions were in good agreement with test results found in the literature.

In 2009, Wang and Hsu investigated the interior shear strength of non-ductile frames strengthened with reinforced concrete jackets, but no new joint shear hoops and no dowel anchors installed into new and old concrete interface. The results show that the RC-jacketed scheme is able to efficiently rehabilitate non-ductile frames with very poor joint details. An empirical equation for calculating the joint shear strength is proposed.

1.4. Research Significance and Rationale

The present research focuses on the seismic strengthening of under-designed RC beam-column joints, which nowadays represents a strong technical and social need in many parts of the world. The innovative aspect or the proposed technique is the retrofitting of beam-column joints with fiber reinforced polymer and preventing the debonding of FRP from the surface by different anchorage techniques. Strengthening methods that may

indirectly affect the performance of existing joints (for example, adding steel bracing or shear walls) are outside the scope of this study.

An experimental investigation was conducted on near full-scaled beam-column joints. It aimed at validating different upgrading of debonding schemes and demonstrating that such a technique has the potential to become a sound and effective solution for the strengthening of RC structures located in seismic areas.

1.5. Objective and Scope

This experimental study was mainly focused on the development of an applicable FRP retrofitting technique by focusing on the prevention of debonding of CFRP from the face of the retrofitted region.

The objectives of this research could be summarized as follows:

i. to identify the effects of reinforcement detailing deficiencies on beam column joints detailed according to ACI code,
ii. to identify the effects of reinforcement detailing deficiencies and different CFRP orientations on beam column joint behavior,
iii. to develop a FRP retrofitting strategy for an existing beam column joints with certain deficiencies through full-scale experimental investigation,
iv. to create a description of an experimental program designed to assess the bond behavior of CFRP strengthening systems for RC beam-column joints.

In this research, RC beam-column joint specimens with deficiencies mentioned above were tested under constant axial load and reversed cyclic loading following a pre-defined displacement history. In the first phase of the study, a current ACI code-detailed control specimen was tested in order to investigate the effects of joint ties on seismic behavior. In addition to that, a pre1970s existing specimen strengthened with CFRP was tested. Taken into account of these test results, another CFRP-retrofitted specimen was also tested in order to overcome the mentioned deficiencies (mainly debonding) and to evaluate the effectiveness of the retrofitting scheme. After the test observations of the specimens, these results were analyzed and compared with a numeric model.

1.6. Methodology

This research investigates the actual behavior of reinforced concrete beam-column joints designed according to pre 1970s US codes and Carbon Fiber Reinforced Polymer wrapping methodologies which are developed to improve the seismic behavior of such deficient joints. In order to achieve this, previous tests conducted at the Structures Laboratory of Boğaziçi University were investigated and the main problem of FRP strengthened specimens was debonding of FRP sheets from concrete face.

In this research three specimens were produced. The first specimen was designed according to current ACI joint detailing code (ACI 318 and ACI352-02), while the other two were designed according to pre 1970s codes. In order to prevent the debonding of FRP wrap from the concrete surface, in this study, different anchorage strategies were tried and further improved in the third specimen.

1.7. Report Outline

The experimental investigation on the seismic behavior of reinforced concrete beam-column connections and retrofitting of these connections by using CFRP sheets is presented on this thesis.

In Chapter 1, brief information about the behavior of the joint under seismic action, literature review and previous research results, and the objectives of this research are given. Chapter 2 provides all the details of the experimental study with construction techniques and testing phases. Experimental results are presented with graphical data in chapter 3. Discussion and comparison of tests, and a numerical study are also presented in this chapter. In the final chapter, a summary of findings and recommendations for further research in this area are listed.

2. EXPERIMENTAL SETUP

2.1. Description of Testing Program

Seismic deficiencies of exterior beam-column joints were investigated experimentally. These joints were designed for gravity loading only according to pre-1970 USA practices. Specimens that were designed for testing in Altay's (2010) thesis work were produced for further investigation. Their original designation was US3 where beam-column joints had deficient panel shear reinforcement and also inadequate embedment depth of beam bottom reinforcement in the column.

In this series of tests, prevention of debonding of CFRP sheets from concrete surface parameter was intended to be investigated. One specimen with proper current ACI 318-2002 and 352R-20 code provisions was prepared (US3-ACI). Other two specimens were exactly as same as previously-tested US3 (US3-FRP1 and US3-FRP2). Both retrofitted specimens were strengthened with CFRP as like in Altay's study in which three layers of CFRP were used for retrofitting, however they had different anchorage application techniques.

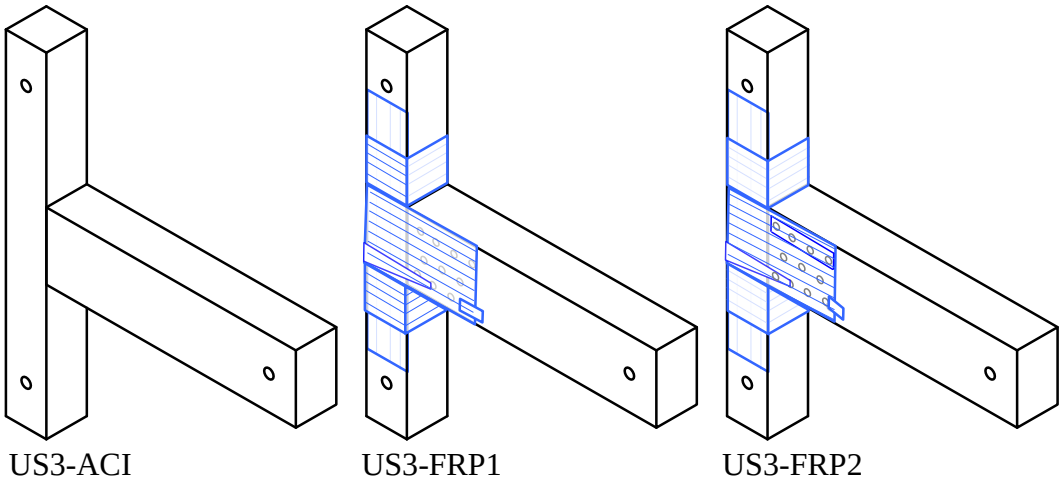

Figure 2.1. Testing Specimens

Table 2.1. Test Specimen Properties

Test #	Specimen Name	Lap Splicing Length (mm)	Short Embedment Length (mm)	Column Axial Load		FRP Wrapping Configuration
				(kN)	%	
1	US3-ACI	—	—	700	0.26	—
2	US3-FRP1	500	150	700	0.26	CFRP
3	US3-FRP2	500	150	700	0.26	CFRP

2.2. Properties of Specimens and Test Parameters

All test specimens were designed as exterior beam-column joints of a multi-story building. The reinforcement is determined such that should any failure occurs; first hinging starts at the beam. In other words, the total moment carrying capacities of the columns are higher than that of the beam. Here, moment capacity ratio of beam to column was taken as 1.24. The specimen dimensions are given in Figure 2.2 and calculated flexural capacities are revealed in Table 2.2. Accordingly, the height of the column is 2500 mm and the cross-section of the column is 300 mm x 300 mm, the length of the beam from the column face is 1850 mm and its cross-sectional dimensions are300 mm x 500 mm. The specimen was fixed to the actuator and to the ground by means of hinge supports, whereas, the beam was fixed to the strong floor via a rigid link by means of hinge supports. Therefore, the total tested column height is 1920 mm and beam length is 1650 mm.

Table 2.2. Flexural capacities of subassemblies

Subassembly	fc (MPa)	fy (MPa)	section		Reinforcement		Axial Load (kN)	Ultimate Moment (kNm)
			Width (mm)	Height (mm)	top	bottom		
Beam	30	514	300	500	3Ø20	2Ø20	0	209.7
Column	30	514	300	300	3Ø20	3Ø20	702	169.1

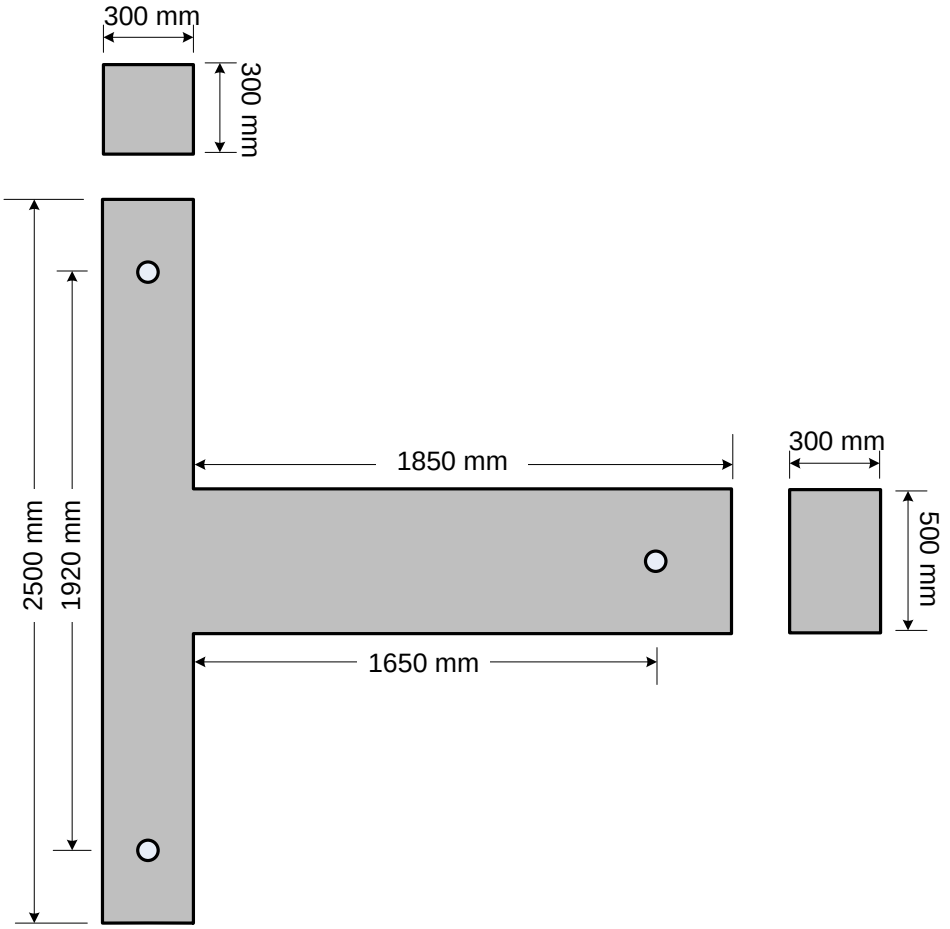

Figure 2.2. Test Specimen Dimensions

The behavior of the beam-column joints were under investigation for several years. Majority of the RC buildings under seismic loads, fail in the joint regions. In this failure mode which is commonly referred to as joint failure, cracking initiates at the beam column face and then propagates diagonally in the joint. The causes of such failures are the deficiencies in the buildings due to the lack of sufficient information at the time they were constructed. (Beres et al (1994). The deficiencies investigated in US3 Specimens can be listed as follow;

- Widely spaced column ties that provide little confinement to the concrete,
- Little or no transverse reinforcement within the joint region,
- Construction joints below and above the beam column joint,
- Insufficient embedment length of positive beam reinforcement,
- Lap splicing at the bottom portion of the top column.

The arrangement of the test specimens included all of these deficiencies while allowing us to study effect of each parameter separately. In this study US3 type specimens were examined.

2.3. Design and Construction of the Test Specimens

The main deficiencies which were studied for US3 were widely-spaced column ties that provide little or no confinement to the concrete, no transverse reinforcement in the joint panel region, construction joints below and above the beam column joint, lap splicing at the top portion of column and insufficient embedment length of positive beam reinforcement. However, in the US3-ACI design specimen these deficiencies were not present. Figures 2.3 and 2.4 show reinforcement details of ACI-detailed specimen. The deficiencies and the internal reinforcement detail of other US3 specimens were clearly shown in Figures 2.5 and 2.6.

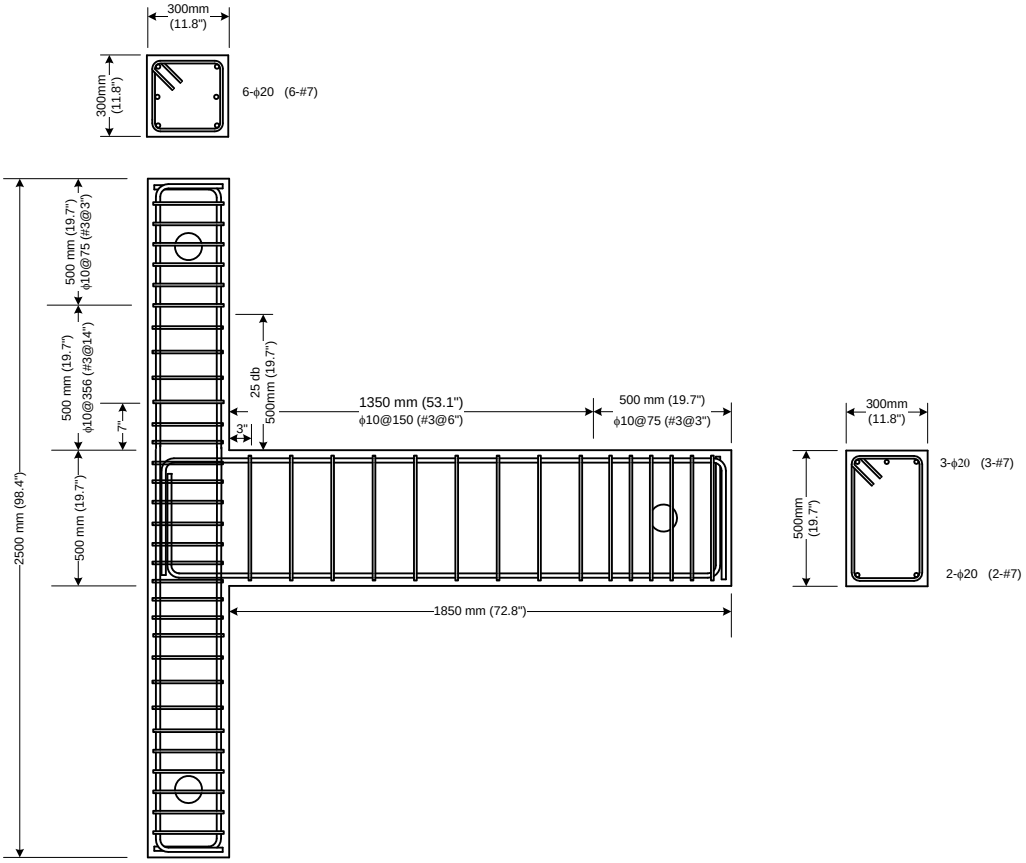

Figure 2.3. Reinforcement Details for US3-ACI

Figure 2.4. A picture of US3-ACI from the construction site

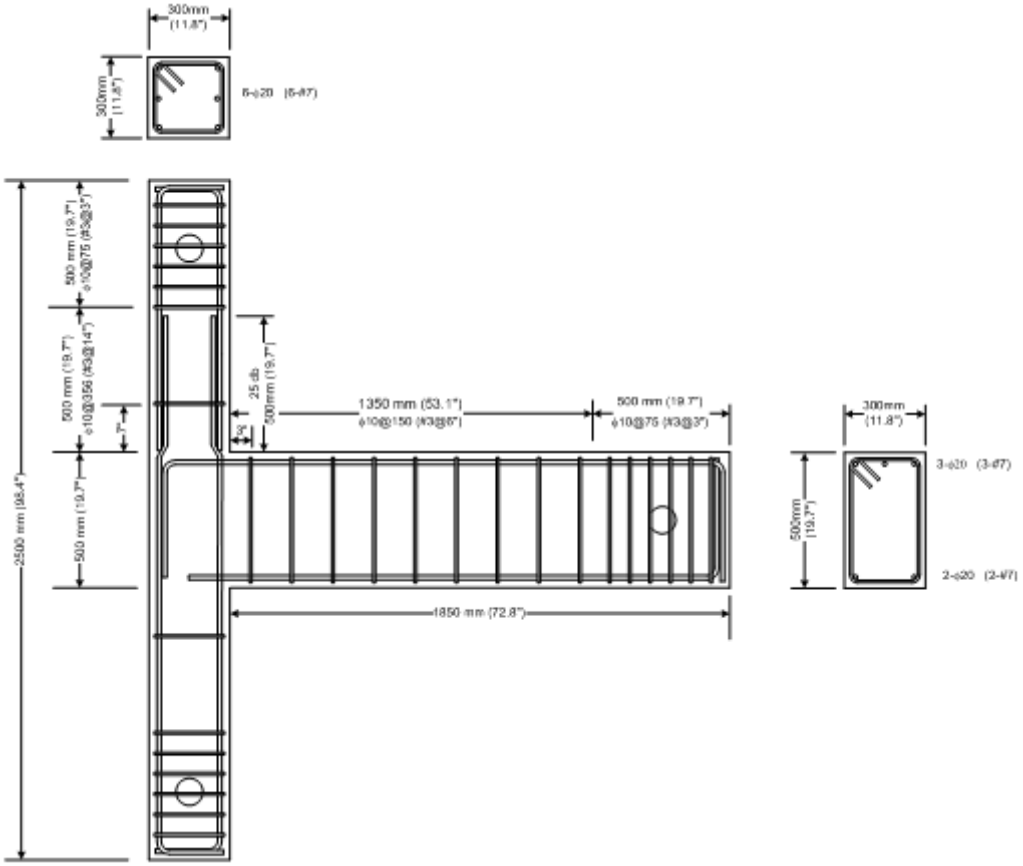

Figure 2.5. Reinforcement Details for US3-FRP1 and US3-FRP2

Figure 2.6. A picture of US3-FRP1 and US3-FRP2 from the construction site

2.4. Material Properties

2.4.1. Concrete

All of the test specimens were constructed in the structural laboratory and ready-mix concrete was used with specified concrete strength. Pouring of concrete was all done at the same time for all specimens. 12 samples of cylinders were taken for column and beams. These samples were then tested 7 days apart, 3 cylinder specimens at a time, until 28th day, which is the day the experiments started. The following Table 2.3 illustrates the test results.

Table 2.3. Test results of concrete cylinders

Specimen No.	7-Day (MPa)	14-Day (MPa)	28-Day (MPa)
1	23.27	26.52	29.19
2	22.63	28.07	31.00
3	24.17	26.78	29.68
Average Strength (MPa)	23.36	27.12	29.96

2.4.2. Steel

Deformed bars were used for both of the transversal and longitudinal reinforcement of the column and beams. According to the tests done in the Material's Laboratory the yield strengths of these steel bars were 453 MPa and 514 MPa for transversal and longitudinal steel, respectively.

2.4.3. Carbon Fiber Reinforced Polymers (CFRP)

FRP materials are widely used in different areas due to their excellent properties. In this research CFRP material, C Fiber 160, produced by BASF was used in order to determine contributions to the existing structure. In strengthened specimens, different CFRP wrapping orientation and different number of CFRP layers were applied considering the damage and crack pattern occurred in control specimens. Properties of CFRP are given in Table 2.4 and stress strain curve, as per manufacturer's data, is given in Figure 2.7.

Table 2.4. Properties of CFRP Material

Nominal Thickness	0.33 mm/ply
Ultimate Tensile Strength (0°)	3800 MPa
Tensile Modulus (0°)	227 GPa
Ultimate Rupture Strain (0°)	1.67 %
Weight	330 g/m^2
Density	1.70 -1.80 t/m^3

2.4.3.1.Theoritical thickness of CFRP Material. To calculate theoretical thickness (t_{FRP}) of the CFRP material in microns, divide weight (w_{FRP}) in g/m^2 to density (ρ_{FRP}) in t/m^3 is given by Eq (2.1).

$$t_{FRP} = \frac{w_{FRP}}{\rho_{FRP}} \tag{2.1}$$

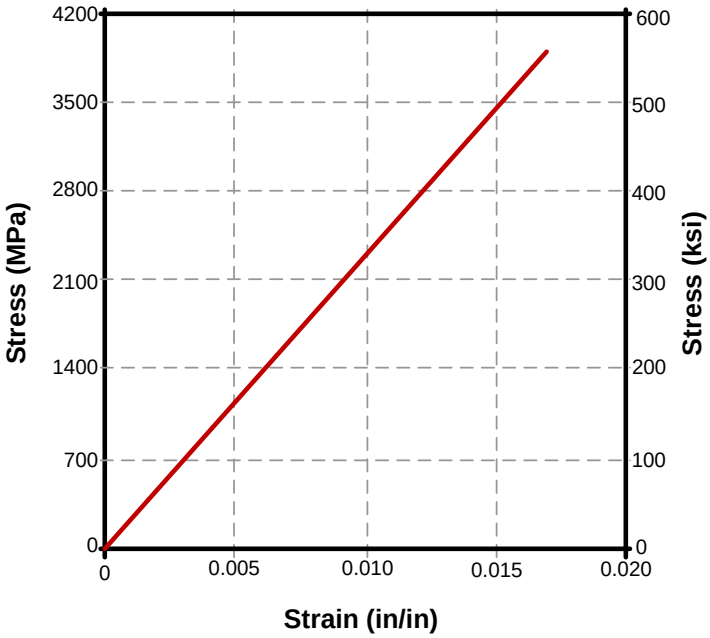

Figure 2.7. Stress-Strain Relations of CFRP sheets

2.4.4. Repairing Materials' Properties

Concresive 1406 :_This type of epoxy based repairing material produced by BASF was used for replacing with all loose concrete at the joint region. Before the application of primer, joint core and regions that will be wrapped with FRP were covered with Concresive 1406. Mechanical properties of Concresive 1406 were given in Table 2.5.

Table 2.5. Properties of Concresive 1406

Application Thickness	2 mm – 30 mm
Bending strength	25 MPa (7 days)
Compressive Strength (20°)	75 MPa (7 days)
Bond Strength	3.0 MPa (concrete) 3.5 MPa (steel)

Emaco S88C : Cement based repairing material produced by BASF was used for preparing beam support before test by improving the rigidity of the wide hinge in the beam support. Mechanical properties of Emaco S88C were given in Table 2.6.

Table 2.6. Properties of Emaco S88C

Application Thickness	Min. 10 mm
Tensile Strength (20°)	3.6 MPa (28 day)
Compressive Strength (20°)	70 MPa
Bond Strength (Steel)	14 MPa (smooth bar) 30 MPa (ribbed bar)
Bond strength (Concrete)	6.5 MPa
Modulus of Elasticity (0°)	>28 GPa

2.5. FRP Retrofitting Methodology

Installation of FRP sheets need special care and only trained technicians can install them. When combined with epoxy, FRP sheets become very strong in tension. FRP wrapping provides excellent passive type of confinement effect to the reinforced concrete member.

2.5.1. Surface Preparation

The procedure for the surface preparation for installing the CFRP sheets is as follows:

- *Preparing the surface of the specimen*: All the faces of beam column regions are first smoothened and the corners are rounded. The corner radius is about 20 mm. Increasing the radius of corner increases the confinement effects of CFRP (*Ref. Rochette*). All large gaps are filled with putty *(Concressive 1406)* and large particles are removed from the area which is going to be wrapped and cleaned up with a wire brush. And then vacuumed to obtain a clean surface. Figure 2.8-(a) shows a view after gap filling with Concressive 1406.
- *Application of the primer:* A primer (*MBrace Pimer*) which helps the connection of CFRP and concrete was applied to the surfaces with roll brush. 24 hour curing time should be passed for covering on primer. Figure 2.8-(b) shows a view after primer application to the specimen.

Filling Gaps with C1406 Primer Application Epoxy Application

Figure 2.8. Surface Preparation Steps

2.5.2. CFRP Application

After the surface is ready and the primer is dry, two component-epoxy adhesive of CFRP, MBrace Adesivo (Saturant), was prepared and CFRP fabrics were installed to the beam column joint region. No air pockets must remain under the sheets. Mixed epoxy has about 30 minute working time, after that it gets hot and dense. Therefore, the application of epoxy has to be on time and be done by professional equipment.

2.5.3. CFRP Wrapping Configuration

CFRP orientation will depend on the deficiency type. For example if transverse reinforcement is not placed within the joint, U shape or $\pm 45^{o}$ oriented CFRP can be applied by surrounding the column and extending to the beam faces until an adequate anchorage is provided for a problem with an inadequate anchorage length for the beam reinforcement.

2.5.3.1. CFRP Wrapping Orientation for US3-FRP1.

Step 1: In order to handle with the debonding effect at the surface of the beam, CFRP sheets were tried to be anchored to the beam. For that reason, four anchorage holes with 12 mm diameters were drilled at the top part of the beam with 120 mm spacing, 3

anchorage holes with 12 mm diameters were drilled at the middle part with a 180 mm and finally 2 anchorage holes were drilled with 20 mm diameters at the bottom part of the beam. After drilling process, surface repairing has done and then the premier was applied to the surface of the specimen where the CFRP being wrapped. Figure 2.9 shows the orientation of the holes.

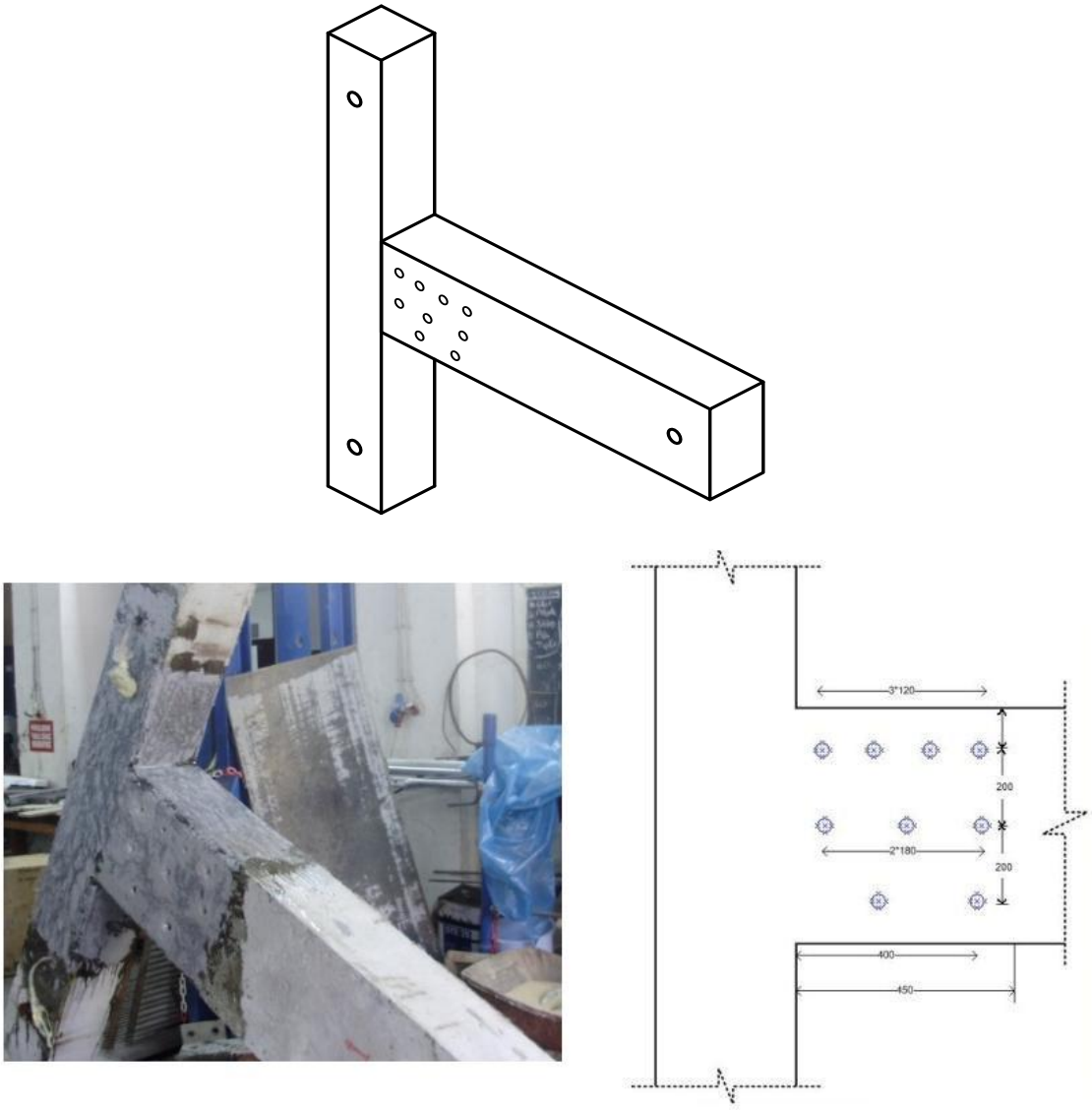

Figure 2.9. Drilling Anchorage Hole

Step 2: In the second step CFRP sheets installation has started with 3 layers of column flexural CFRP sheets on to the north and south side of the column. The length of the shapes overlays will be applied to the top and bottom face of the beam. Total length of

the CFRP sheets became 120 cm (30+30=60 *2 =120-top and bottom). The Figure 2.10 shows the application of flexural CFRP sheets.

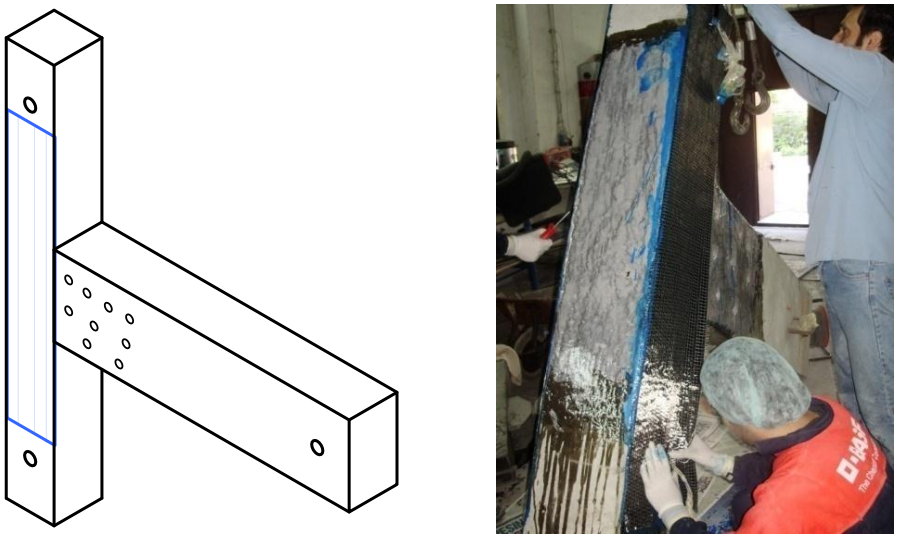

Figure 2.10. CFRP Application for Column Flexure

Step 3: The main idea for the application of the column wraps is to increase the confinement effect in the columns, which is associated with the deficiency of widely spaced column ties, in order to increase the ductility, 300 mm part of the column from the joint was wrapped with 3 layers CFRP sheets at the top column and 2 layers CFRP sheets at the bottom column as shown in Figure 2.11.

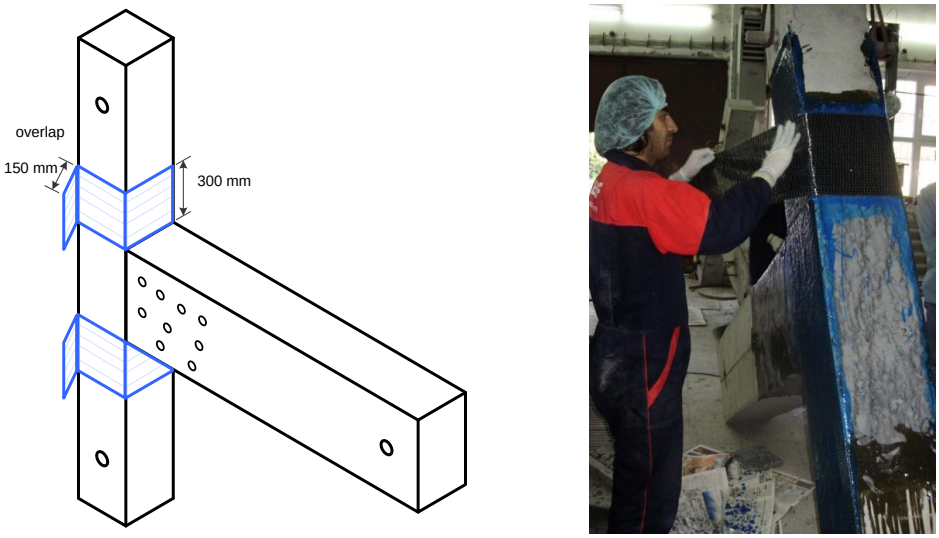

Figure 2.11.Column Wraps

Step 4: Three layer of U-shaped wrapping was applied to the joint and was extend 450 mm on the beam face. The purpose of this application was to provide additional confinement to the joint region and decrease the shear damage in the joint. Since one of the main aims was to shift the plastic hinge to the beam, the distance that was extended along the beam should be short enough to satisfy this requirement, at the same time it should be long enough to provide sufficient anchorage and strength to the member. The application drawing and a photo taken during application could be seen in Figure 2.12.

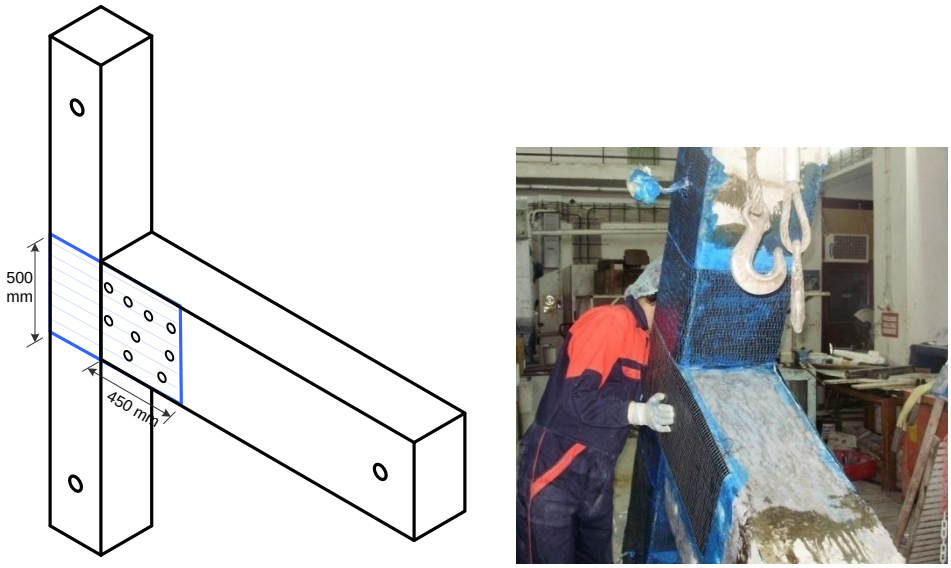

Figure 2. 12. U Shape CFRP Application

Step 5: Last step of the CFRP sheet installation was the application of the anchorage for the U-shaped wraps. The belt, which is turning around the column and passing through the first hole, near to the column, was used for preventing the slip at the short embedment length of the beam reinforcement. The other bottom hole was used for preventing the debonding of U-shaped wrapping by extending 100 mm part of the U-shape and passing through the hole to the other side of the beam. The other holes in the middle part and at the upper side were also used for preventing the occurrence of debonding by using anchorage sheets which has (500mm x 150mm) dimensions.

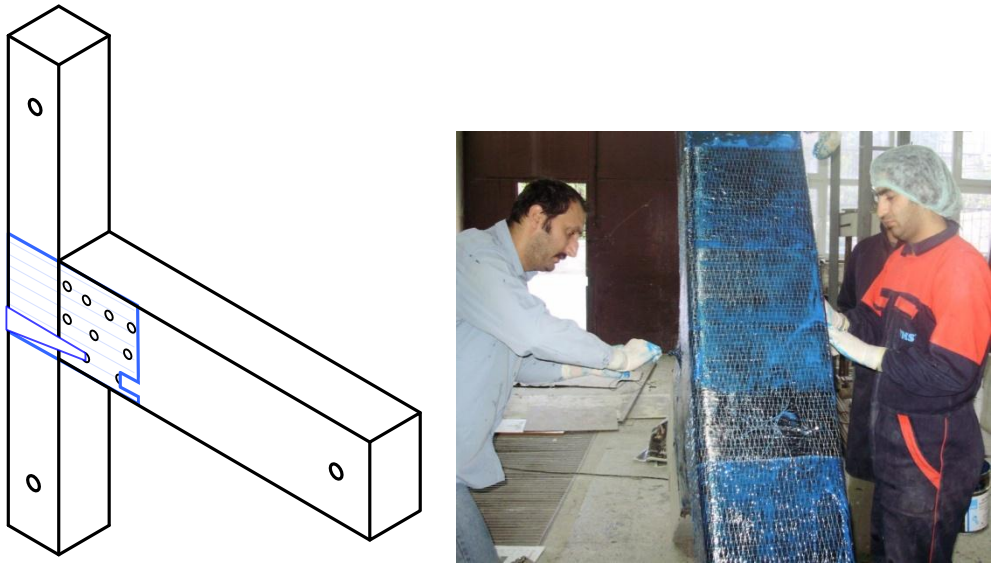

Figure 2. 13. Anchorage Application on U-Shaped Wrap

2.5.3.2.CFRP Wrapping Orientation for US3-FRP2.

Step 1: In order to increase the effectiveness of bonding, number of drilling holes in this specimen has been increased. Four anchorage holes with 20 mm diameters were drilled at the top part of the beam with 125 mm spacing, 3 anchorage holes with 12 mm diameters were drilled at the middle part with a 125 mm and lastly 4 anchorage holes were drilled with 20 mm diameters at the bottom part of the beam symmetric to the top holes. After drilling process, surface repairing has done and then the premier was applied to the surface of the specimen where the CFRP being wrapped. Figure 2.14 shows the orientation of the holes.

Step 2: In this step, CFRP sheet installation was started with 3 layers of column flexural CFRP sheets on to the north and south side of the column as done in the FRP1 specimen. The length of the shapes overlays were applied to the top and bottom face of the beam. The dimension of each ply was taken as 1200 mm x 300mm. Figure 2.15 shows the application of flexural CFRP sheets.

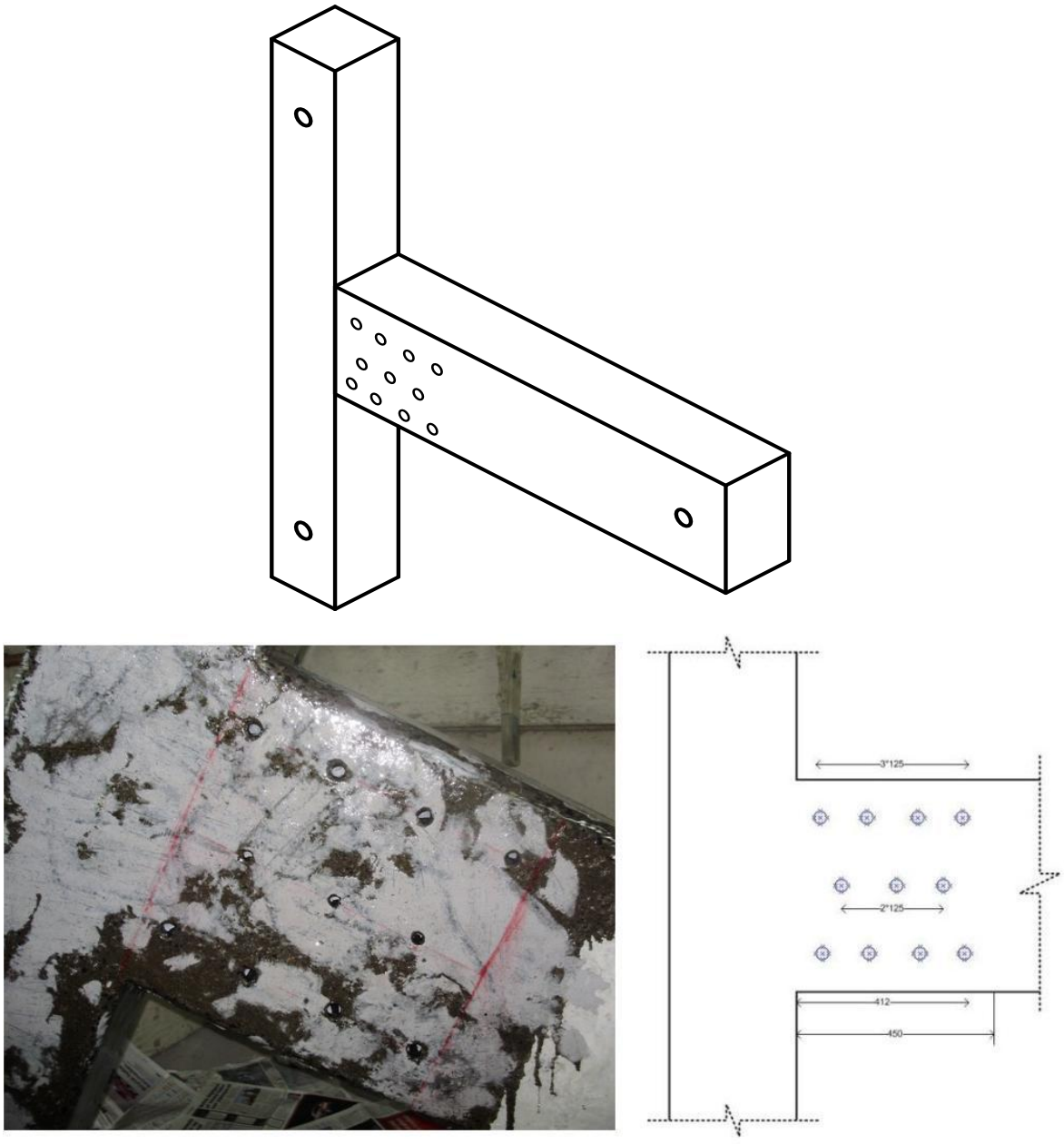

Figure 2. 14. Drilling of Anchorage Holes in US3-FRP2

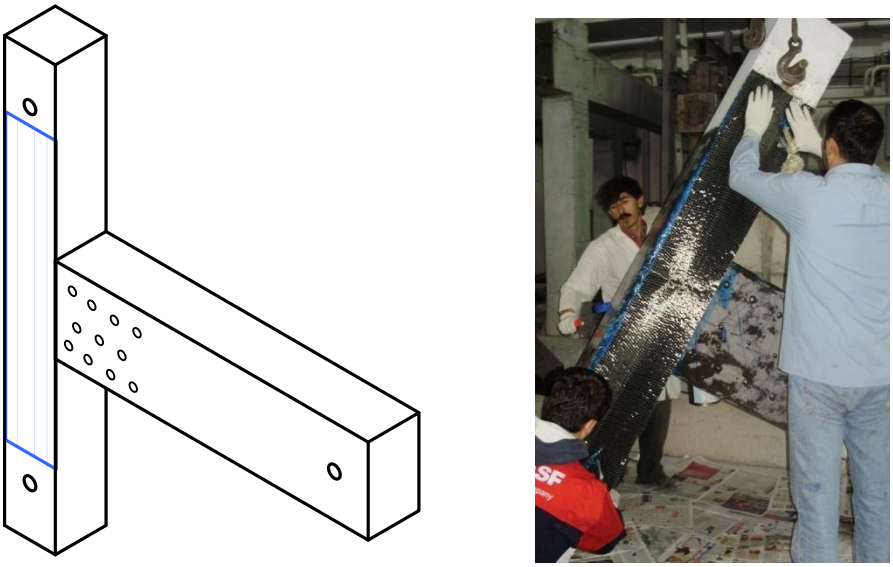

Figure 2.15. CFRP Application for Column Flexure

Step 3: As discussed in the wrapping steps of the FRP1 specimen, the idea for the application of the column wraps was to increase the confinement effect in the columns, which was associated with the deficiency of widely-spaced column ties. In order to increase the ductility, 300 mm part of the column from the joint was wrapped with 3 layers of CFRP sheets at the top column and 2 layers of CFRP sheets at the bottom column as shown in Figure 2.16.

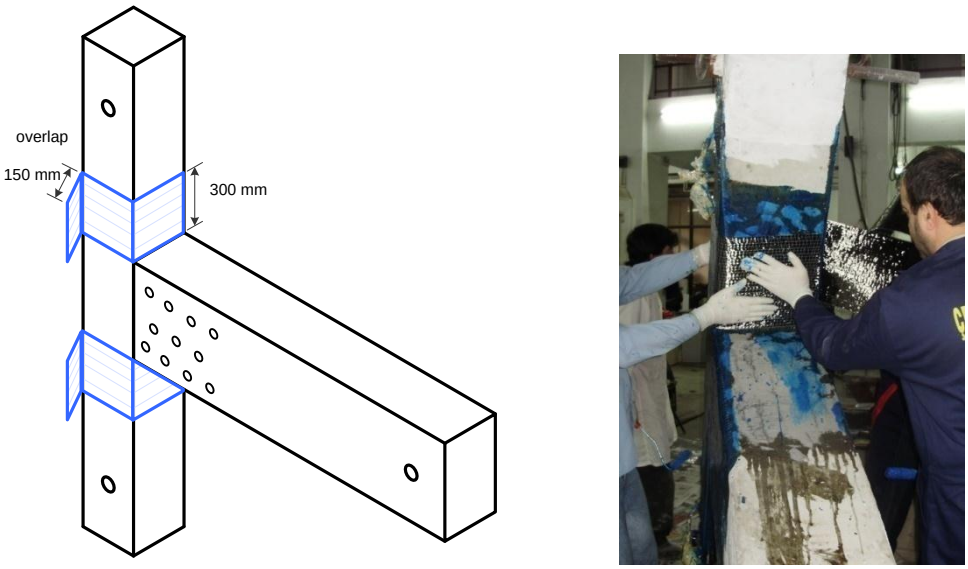

Figure 2.16. Column Wraps

Step 4: Three layers of U-shaped wrapping was applied to the joint that had the same dimensions and purpose as in the case of US3-FRP1 specimen. The application could be seen in Figure 2.17.

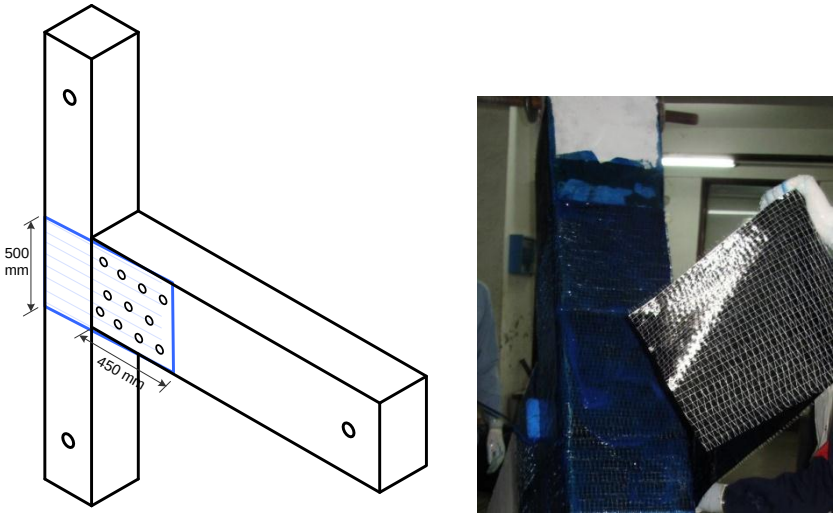

Figure 2.17. U Shape CFRP Application

Step 5: In this step, anchorages and the belt around the column were applied as shown in Figure 2.18.

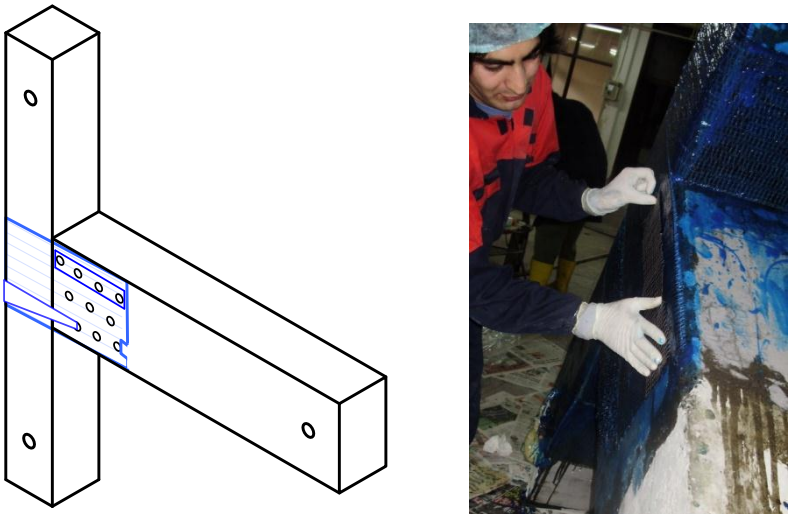

Figure 2.18. Belt and anchorage application

Step 6: Last step of the CFRP sheet installation was the application of the anchorage for the belt U-shaped wraps. The belt which was wrapped around the column and passing through the second hole, near to the column, was used for preventing the slip at the short embedment length of the beam reinforcement. The furthest bottom hole was used for preventing the debonding of U-shape by extending 100 mm part of the U-shape and passing through the hole to the other side of the beam. Anchorage holes in the middle part which have in CFRP sheets with (150mm x 500mm) dimensions, rest of hole in the bottom and those at the upper side which have in FRP sheets with (300mm x 500mm) dimensions were also used for preventing the occurrence of debonding.

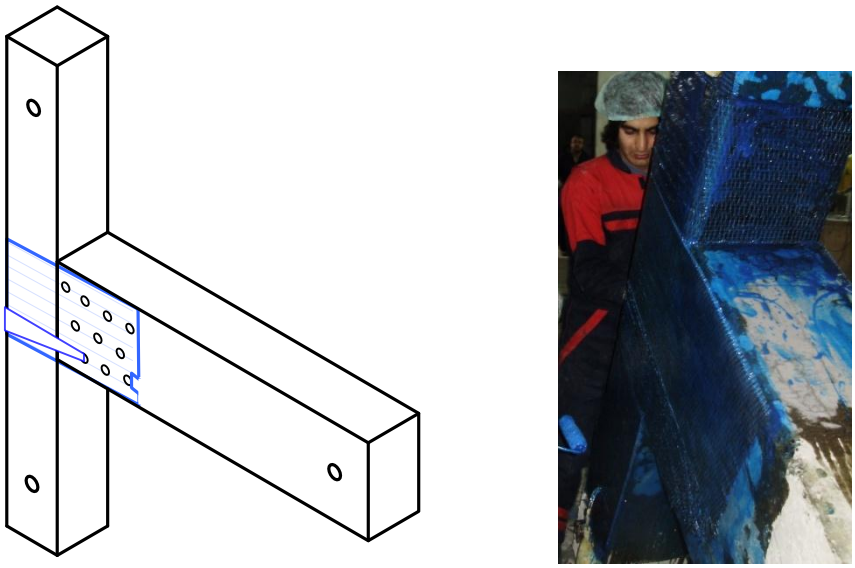

Figure 2.19. Belt and anchorage application

2.6. Test Setup

The loading setup is shown in Figure 2.20. The specimens were tested in beam horizontal position hinged at the free end of the beam. The column was in the vertical position and supported by universal pin at the bottom end. Constant axial load was applied by a load control with the vertical 1000 kN capacity actuator, while statically horizontal load was applied by displacement control with the horizontal actuator which has a capacity of 250 kN. Three cycles of the same amplitude in story drift were repeated and then displacement amplitude was increased. The amount of the axial force applied is 30% $f_c^{'} A_g$

where $f_c^{'}$ is the characteristic strength of concrete and A_g is gross cross-sectional area of column.

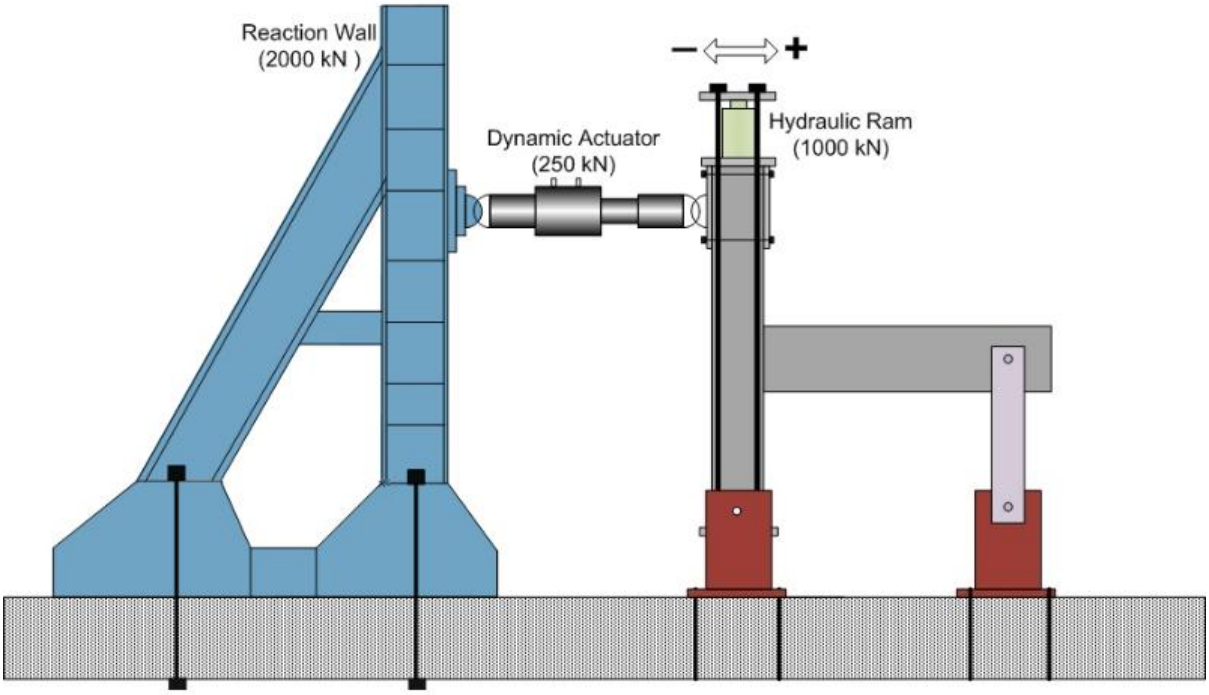

Figure 2.20. Test Setup

2.7. Instrumentation

In order to instrument the experimentation, two kinds of instrumentation applications were used. All the displacements at critical points were measured with Linear Variable Differential Transformers (LVDTs) and, strain of steel rebars and some critical zones on the CFRP sheets were measured by using strain gages. Total of 18 strain gages for US3-ACI specimen and 16 strain gages for each of US3-FRP1 and US3-FRP2, which were shown in Figure 2.21 and Figure 2.22, were mounted on the internal reinforcing bars to collect the strain values during the experiments. All of these strain gages were connected to the data acquisition system. In addition to the strain gages, displacement at the tip of the column and the deformation in the joint were monitored and measured by LVDTs and data transferred to the data acquisition system. LVDT locations were shown in Figure 2.23. And

also strain gage locations that put on US3-ACI and US3-FRP specimens were illustrated in Figure 2.21 and Figure 2.22.

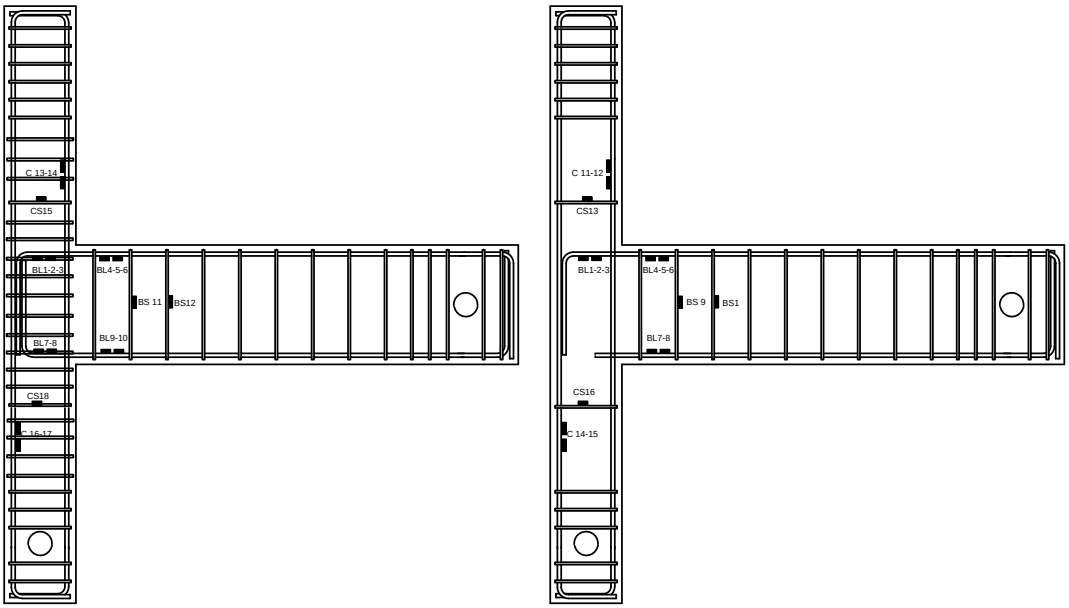

Figure 2.21. Strain gage Instrumentation on steel for US3-ACI and US3-FRP specimens

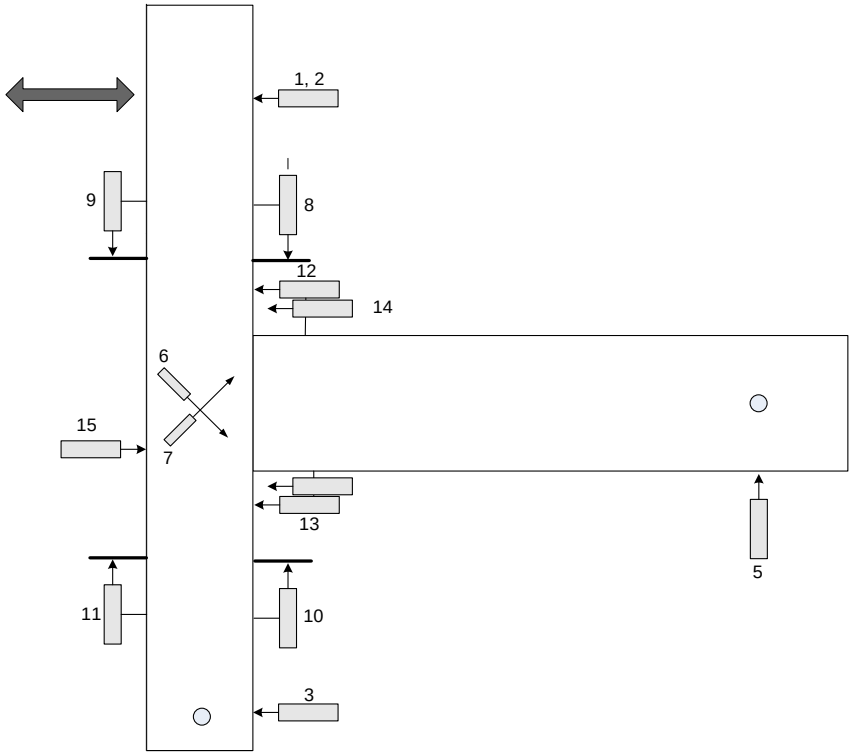

Figure 2.22. Dialgage Instrumentation

Strain gage location on FRP in Specimen US-3 FRP1 and US-3 FRP2

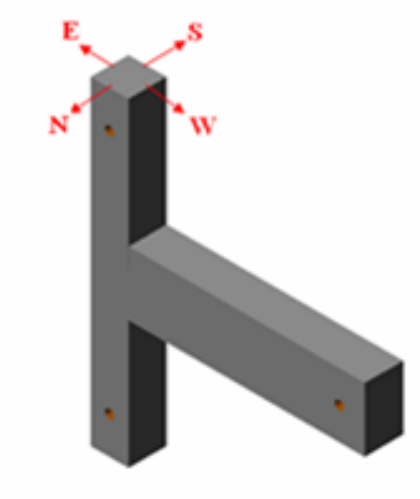

(a) 3D View

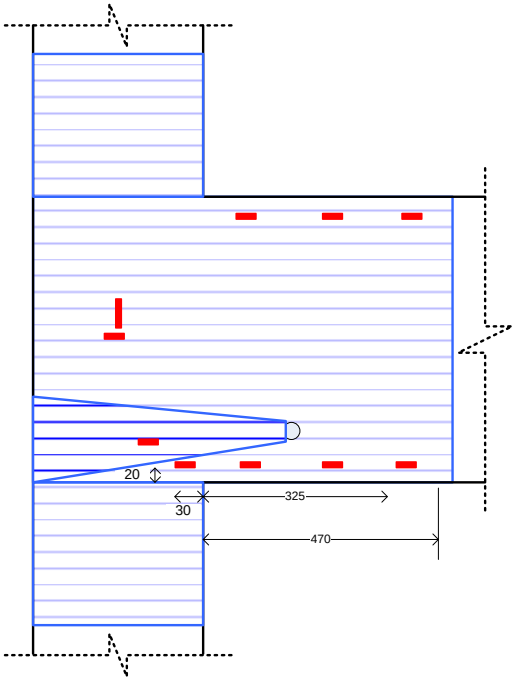

(b) North Face View

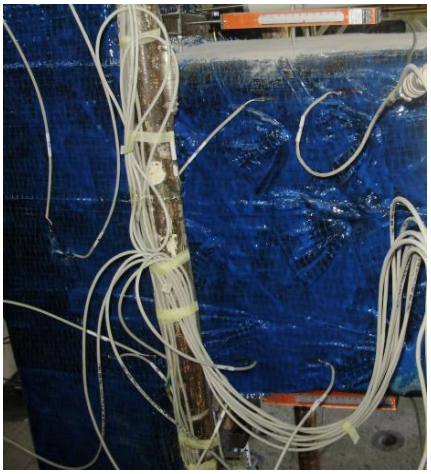

(c) Picture of North Face View

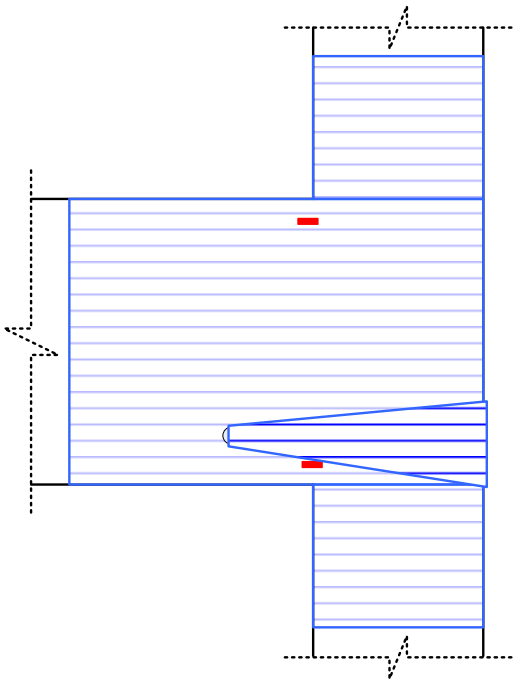

(d) South Face View

Figure 2.23. Strain gage instrumentation on FRP for US-3 FRP1 and US3-FRP2

2.8. Loading Pattern

The lateral load was applied based on the displacement control criteria. In any quasi-static cyclic loading, the specimens were subjected to predetermined numbers of displacement-controlled loading cycles as shown in Figure 2.25, and these load reversals were applied slowly in order to eliminate the effects of material strain rate (Sin 2004). Approximately 35-40 reversed cycles were applied throughout the test. All data were using TML 602 50 Hz. 50 channel data acquisition box. Crack propagation, CFRP fractures, debonding and other failures were recorded.

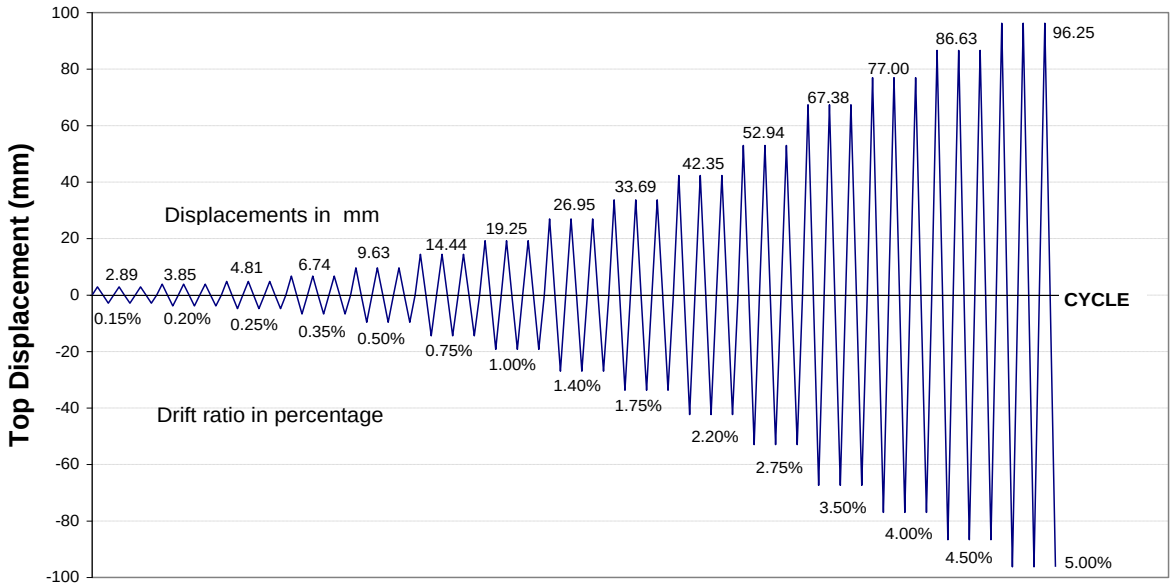

Figure 2.24. Loading Pattern based on ACI protocol

2.9. Test Procedure

Tests were performed according to ACI T1.01 recommendations. Minimum requirements of the test procedure could be summarized as follows:

- Test modules shall be subjected to a sequence of displacement-controlled cycles representative of the drifts expected under earthquake motions for that portion of the frame represented by the test module. Cycles shall be predetermined drift ratios.

- Three fully reversed cycles shall be applied at each drift ratio.
- The initial drift ratio shall be within the essentially linear elastic response range for the module. Subsequent drift ratios shall be values not less than one and one-quarter times, and not more than one and one-half times the previous drift ratio.
- Testing shall continue with gradually increasing drift ratios until drift ratio equals or exceeds 0.035.
- Data shall be recorded from the test such that a quantitative, as opposed to qualitative, interpretation can be made of the performance of the module. As continuous recording shall be made of the test module, drift ratio versus column shear force, and photographs shall be taken that show the condition of the test module at the completion of testing for each sequence of three cycles.

2.10.Load Corrections

Simplified free body diagram of the specimens is shown in Figure 2.26. Structural lateral load-lateral deformation (P-Δ) effects were neglected in the test setup. The beam-column joint subassemblies and testing method is in accordance with the specifications recommended by the *ACI committee of Acceptance Criteria for Moment Frames Based on Structural Testing*, ACI T1.1-01

In order to monitor the story drifts, joint rotations, crack openings, curvatures of the members, strain levels on the steel and CFRP materials several LVDTs, dial gauges and strain gauges were mounted on the test specimens. Cracks, CFRP fractures and debonding and failures were noted at the end of each 3-cycle loading sets. LVDTs used to measure the top displacement of specimens as shown in Figure2.27. Effect of support movement was incorporated in the measurement of the overall top displacement. Corrected top displacement, Δ, was calculated as indicated in Eq (2.2).

$$\Delta = \left(\frac{\Delta_1 + \Delta_2}{2} \right) - \Delta_3 - \left(\frac{1920}{1800} \right) \Delta_4 \qquad (2.2)$$

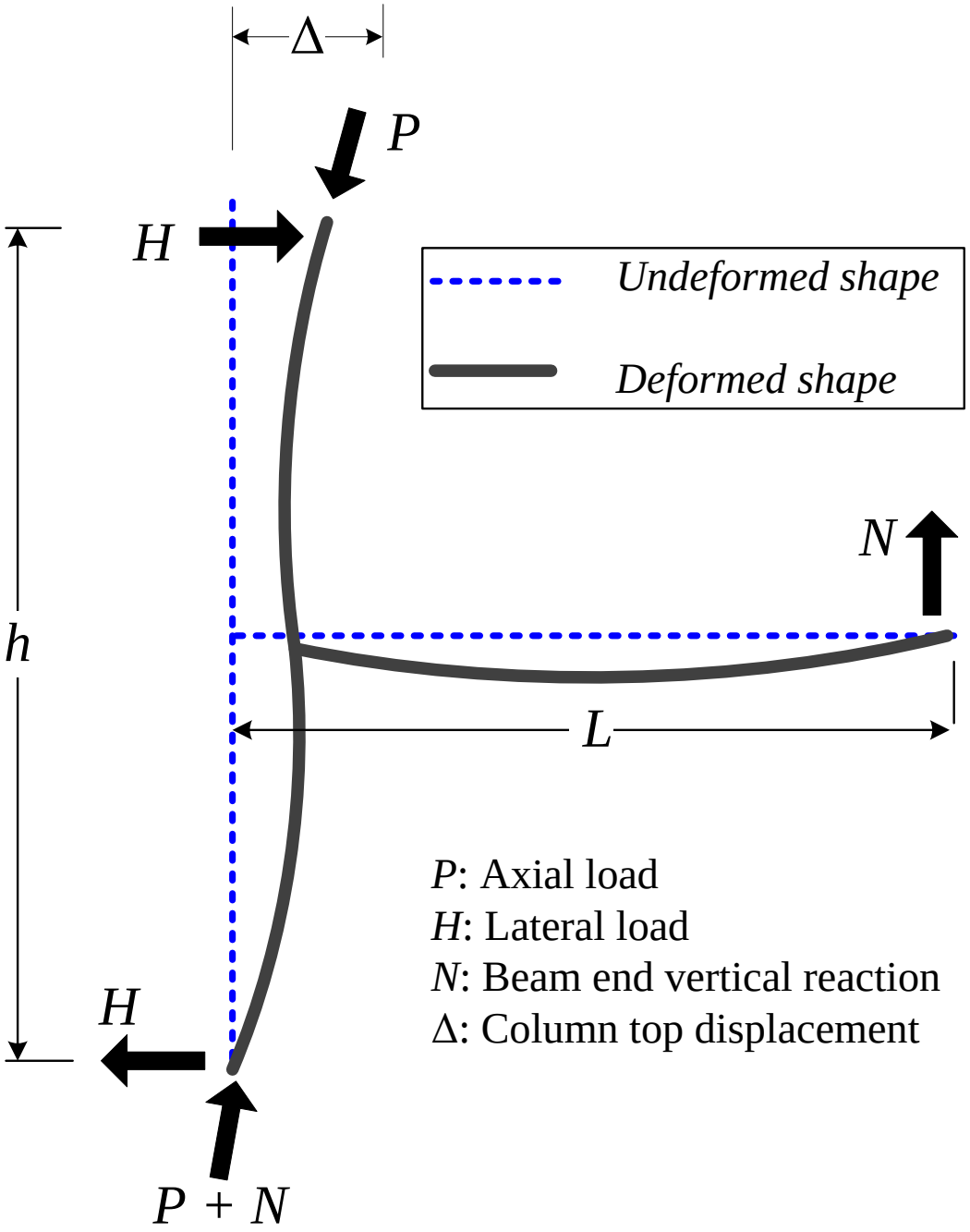

Figure 2.25. Simplified Free Body Diagram

Subscripts in Equation 2.2 indicate the number of the LVDT. For example, Δ_3 is the displacement measurement of LVDT 3 shown in Figure 2.27.

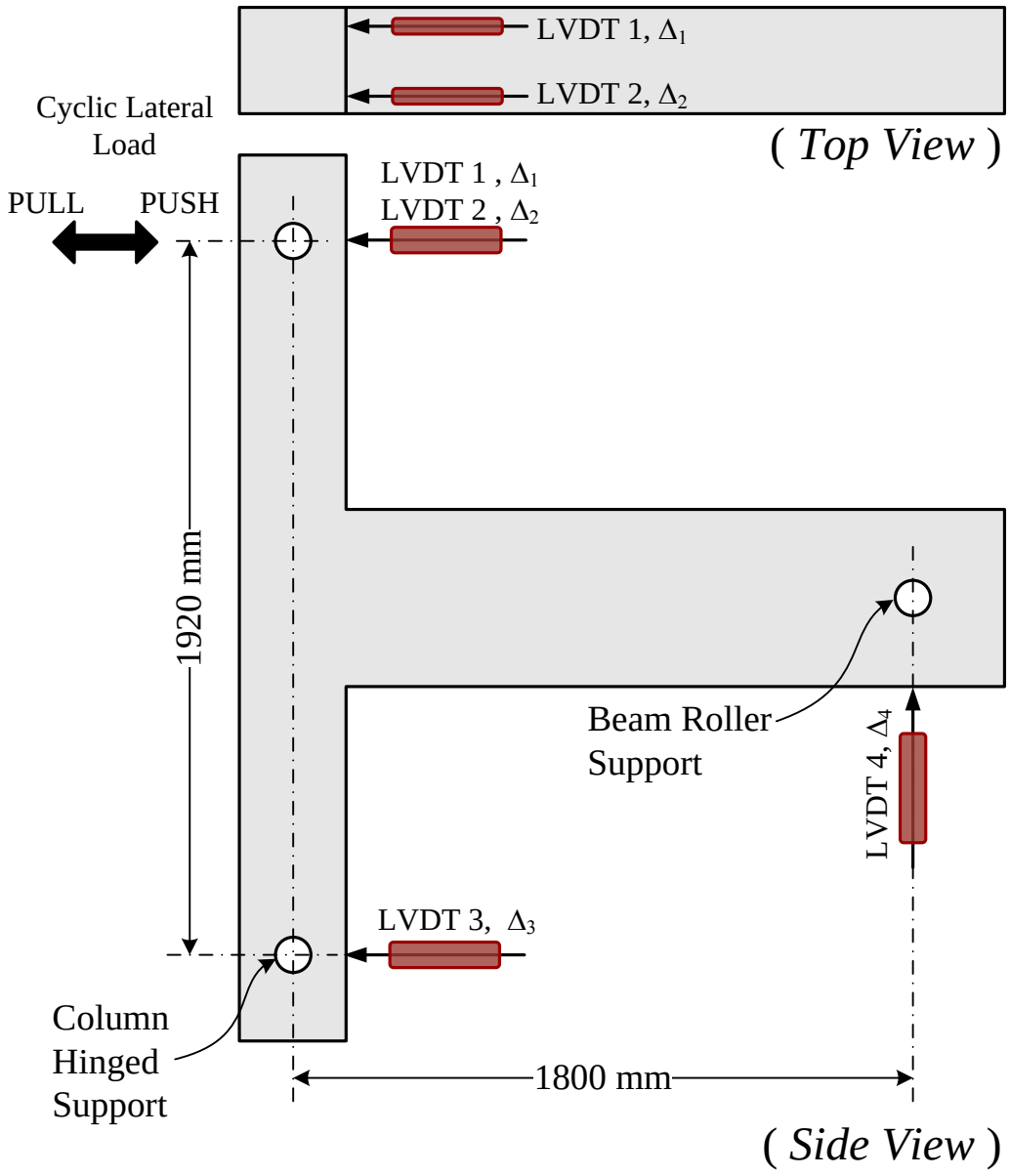

Figure 2.26. LVDT locations for measurement of top displacement

3. EXPERIMENTAL STUDY

3.1. General

In this chapter, test observations are discussed to give an insight to the overall behavior of the subassemblies and the experimental results for two RC beam-column joint specimens retrofitted with CFRP and one RC beam-column joint specimen detailed according to current ACI standards are presented. Also, comparisons of test results subjected to reversed-cyclic unidirectional loading are presented in this chapter. Overall behavior of each test specimen is discussed in terms of load-displacement hysteresis response, joint shear deformation, member deformations, crack formation, energy dissipations, stiffness degradations and failure modes. In addition, effectiveness of the wrapping configurations is evaluated through a comparison of ultimate drift and lateral load, stiffness degradations and amount of energy dissipations.

3.2. Test Observations

3.2.1. Specimen US3-ACI

This specimen's joint was detailed according to ACI 318-09 code. During testing it was observed that the first crack, which is flexural, occurred at the bottom of the beam, 15 mm away from the column when the lateral load was reached to 15 kN at a drift level of 0.15%. Up to drift level of 1.00% cracks occurred only in the beam. The first crack in the joint region was occurred at the drift level of 1.00% when the maximum load, 61 kN, was applied in push the direction. Then at the drift level 1.40%, first cracks were occurred also in pull directions in the joint region. At the drift level 1.75%, it has reached to the maximum lateral load capacity in both directions of loading. After the drift level 1.75%, the lateral load started to decrease gradually because of the crushing regions around the first crack that occurred in the joint. After this it was observed that crushing was obvious

because of debonding of reinforcement in the end parts of the beam in the joint. Figure 3.1 shows the crushing regions in the joint.

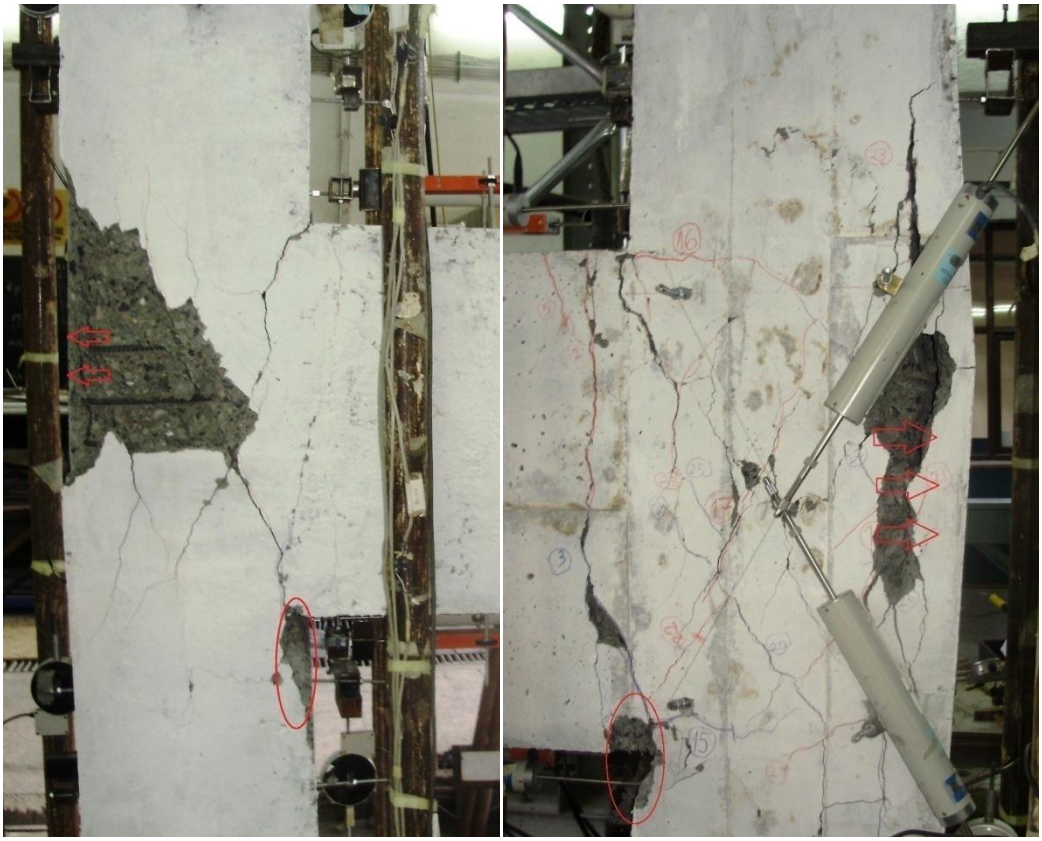

Figure 3.1. Crushing regions in the joint

The test was ended at the drift level of 4.00%, because of the fact that actuator displacement capacity was reached and the load carrying capacity decreased below the 50% of maximum load in the descending branch. Table 3.1 provides the load and crack pattern history for US3-ACI.

Table 3.1. Observations of US3-ACI

Drift (%)	Observations	Crack pattern
0.15	Max lateral load : (+) 15.38 kN (Push) : (-) 24.50 kN (Pull) CR1 : Flexural crack occurred at the bottom of the beam, 15 mm away from the column. Length of crack is 170 mm. CR2 : Flexural crack occurred at the top of the beam, 35 mm away from the column. Length of it is 250 mm.	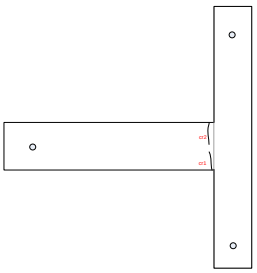
0.20	Max lateral load : (+) 18.70 kN (Push) : (-) 29.30 kN (Pull) CR1 : Flexural crack has extended 40 mm. CR2 : Flexural crack has extended 20 mm	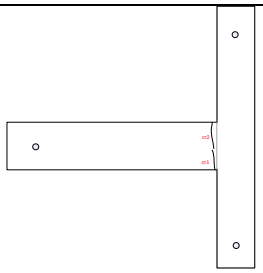
0.25	Max lateral load : (+) 20.05 kN (Push) : (-) 36.60 kN (Pull) CR1 & CR2 : joined CR3 : Flexural crack occurred at the top of the beam, 410 mm away from the column. Length of it is 260 mm.	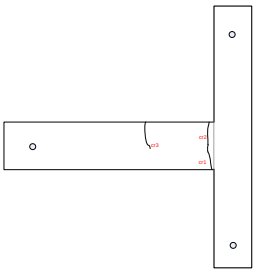
0.35	Max lateral load : (+) 26.40 kN (Push) : (-) 45.80 kN (Pull) CR3 : Flexural crack has bifurcated.	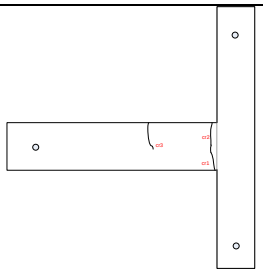

Table 3.1. Observations of US3-ACI (Continued)

Drift (%)	Observations	Crack pattern
0.50	Max lateral load : (+) 32.65 kN (Push) : (-) 59.10 kN (Pull) CR4 : Flexural crack occurred at the top of the beam, 80 mm away from the column. Length of crack is 80 mm. CR5 : Flexural crack occurred at the top of the beam, 650 mm away from the column. Crack length is 60 mm. CR6 : Flexural crack occurred at the top of the beam, 520 mm away from the column. Length of crack is 120 mm. CR7 : Flexural crack occurredat the top of the beam, 750 mm away from the column. Length of crack is 100 mm. CR8 : Flexural crack occurred at the top of the beam, 240 mm away from the column. Crack length is 100 mm. CR2 : extended and bifurcated. CR3 : extended 40 mm. .	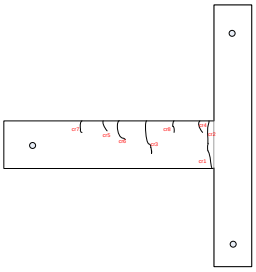
0.75	Max lateral load : (+) 46.90 kN (Push) : (–) 80.17 kN (Pull) CR9 : Flexural crack occurred at the bottom of the beam, 370 mm away from the column. Length of crack is 210 mm CR10 : Flexural crack occurred at the bottom of the beam, 660 mm away from the column. Length of crack is 210 mm CR11 : Flexural crack occurred at the top of the beam, 880 mm away from the column. Crack length is 150 mm CR5 : Extended to 210 mm. CR3 : Extended to 400 mm. CR5 : Extended to 330 mm.	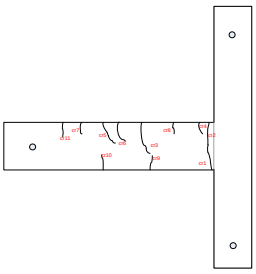

Table 3.1. Observations of US3-ACI (Continued)

Drift (%)	Observations	Crack pattern
1.00	Max lateral load : (+) 61.43 kN (Push) : (-) 86.00 kN (Pull) CR12 : Flexural crack occurred at the bottom of the beam, 880 mm away from the column. Length of crack is 100 mm CR13 : Flexural crack occurred at the bottom of the beam, 1010 mm away from the column. Length of crack is 100 mm CR14 : occurred in the joint length is 90 mm. CR15 : occurred in the joint length is 80 mm. CR16 : occurred in the joint length is 280 mm. CR17 : occurred in the joint length is 80 mm. CR10 : Extended and bifurcated. CR9 : Extended and bifurcated.	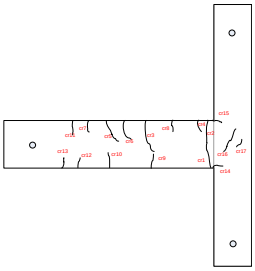
1.40	Max lateral load : (+) 73.40 kN (Push) : (-) 97.70 kN (Pull) CR14 : extended bifurcated CR1 & CR14: joined CR10 : extended 50 mm towards to top/bottom. CR9 : extended 60 mm towards to top/bottom. CR18 : occurred in the joint length is 80 mm. CR19 : occurred in the joint length is 80 mm. CR20 : occurred in the joint length is 80 mm. CR21 : occurred in the joint length is 80 mm. CR22 : occurred in the joint length is 80 mm. CR15 : bifurcated. CR4 : extended.	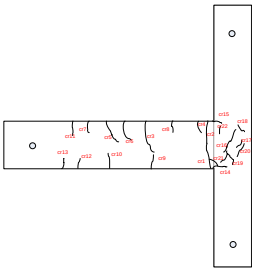

Table 3.1. Observations of US3-ACI (Continued)

Drift (%)	Observations	Crack pattern
1.75	Max lateral load : (+) 74.10 kN (Push) : (-) 103.90 kN (Pull) CR2: extended bifurcated CR15 & CR16: joined CR23: occurred in the joint length is 110 mm CR24 : occurred in the joint length is 90 mm CR25: occurred in the joint length is 100 mm. CR26 : occurred in the joint length is 120 mm. CR27 : occurred in the joint length is 150 mm. CR28 : occurred in the joint length is 110 mm. CR27 & CR18: joined CR29: flexural crack in the beam. CR30 : flexural crack in the beam. CR1 : crushed and widened.	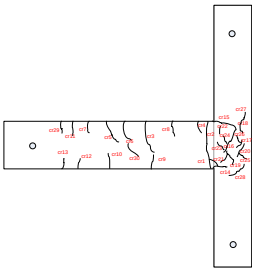 
2.20	Max lateral load : (+) 70.00 kN (Push) : (-) 96.30 kN (Pull) CR31: occurred in the joint length is 350 mm. CR32 : occurred in the joint length is 100 mm. CR33: occurred in the joint length is 300 mm.	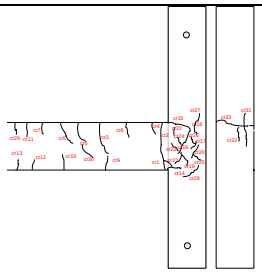
2.75	Max lateral load : (+) 59.70 kN (Push) : (-) 87.40 kN (Pull) CR31: crushing has started in an increasing rate.	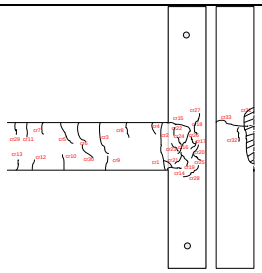

Table 3.1. Observations of US3-ACI (Continued)

Drift (%)	Observations	Crack pattern
3.50	Max lateral load : (+) 42.30 kN (Push) : (-) 75.50 kN (Pull) CR1 & CR2: has widened and crushing has started. CR27 & CR18:has widened and crushing has started.	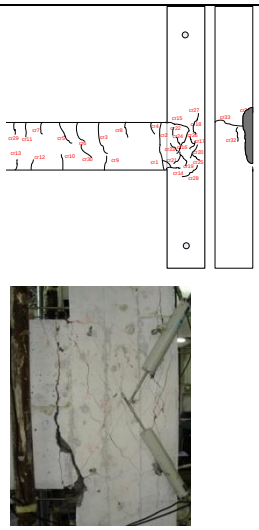
4.00	Max lateral load : (+) 29.10 kN (Push) : (-) 62.50 kN (Pull) CR27 & CR18:has crushed. Joint is crushed.	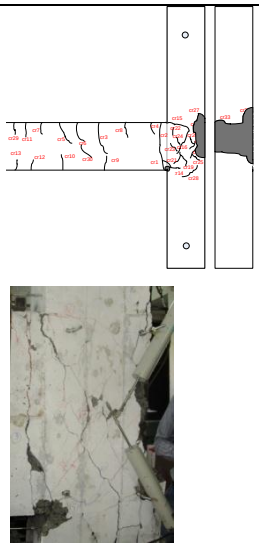

3.2.2. Specimen US3-FRP1

In this specimen, cracks were developed only in the beam when drift level reached at 2.75%. The first flexural crack occurred at the bottom of the beam close to the CFRP surface when the drift was 0.35% in push direction. The location was 570 mm away from the face of the column and the crack length was 170 mm. During the experiment the cracks occurred at the joint region cannot be traced due to the CFRP wrapping. Maximum applied lateral load was 78 kN at a drift level of 1.4% in the push direction and 145 kN at adrift level of 2.20% in the pull direction.

The debonding of U-shape CFRP was observed from both bottom and top sides of the beam when the drift level was 1.75%. However, before the maximum load was reached at push direction at the drift level 1.40%, noises were heard revealing that there was debonding. Especially, the region of the debonded area on the crack pattern was larger in the top side of the beam. It was apparent that the anchorage length was inadequate. Additional anchorages should have been used for especially for the top side of the beam where the debonding occurs.

The test was ended at the drift level of 4.00%, because of the fact that actuator displacement capacity was reached and the load carrying capacity decreased below the 50% of maximum load in the descending branch.

After the completion of the experiment, the CFRP wraps were removed from the concrete surface for visual inspection and it has been observed that the concrete in the joint was crushed to some extent and the crack pattern was different from the US3-ACI specimen. The detailed crack propagations for US3-FRP1 are given in Table 3.2.

Figure 3.2. Main cracks after removing the CFRP sheets

Table 3.2. Observations of US3-FRP1

Drift (%)	Observations	Crack pattern
0.15	Max lateral load : (+) 16.10 kN (Push) : (-) 35.00 kN (Pull)	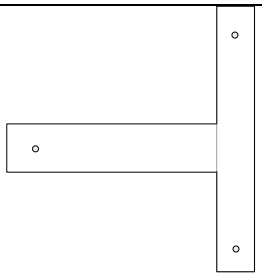
0.20	Max lateral load : (+) 21.70 kN (Push) : (-) 33.50 kN (Pull)	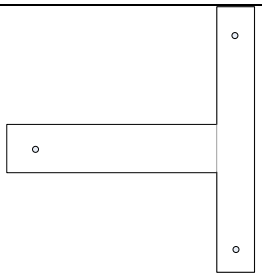
0.25	Max lateral load : (+) 26.80 kN (Push) : (-) 42.10 kN (Pull)	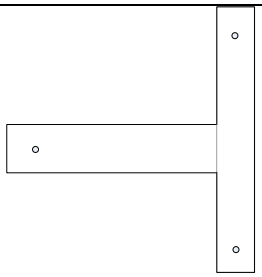
0.35	Max lateral load : (+) 32.00 kN (Push) : (-) 54.90 kN (Pull) CR1 : This is a flexural crack, occurred in push direction (at the bottom of the beam), and the location is 570 mm away from the face of the column. Crack length is 170 mm.	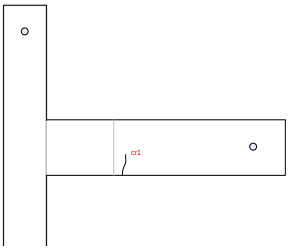
0.35	Max lateral load : (+) 32.00 kN (Push) : (-) 54.90 kN (Pull) CR1 : This is a flexural crack, occurred in push direction (at the bottom of the beam), and the location is 570 mm away from the face of the column. Crack length is 170 mm.	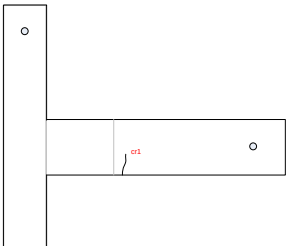

Table 3.2. Observations of US3-FRP1 (Continued)

Drift (%)	Observations	Crack pattern
0.50	Max lateral load : (+) 40.50 kN (Push) (Pull) : (-) 68.30 kN (Pull) CR2 : This is another flexural crack in pull direction 545 mm away from the face of the column. This crack was able to be observed only from the top. The crack can not be seen from the faces of the beam since FRP was bonded. Length of it is 270 mm. CR3 : In the same drift level but now in pull direction a symmetrical crack of Cr1 occurred. The distance from column is 550 mm and its length is 240 mm.	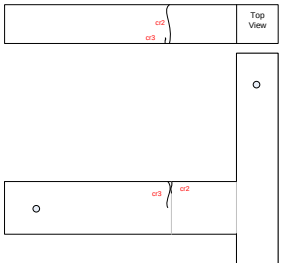
0.75	Max lateral load : (+) 55.20 kN (Push) : (–) 89.00 kN (Pull) CR4 : In pull direction a flexural crack occurred. The distance from the face of the column is 710 mm and its length is 250 mm CR5 : Another flexural crack 860 mm away from the face of the column occurred. The length of the crack is 110 mm and in the subsequent cycles it forked. CR6 : A flexural crack occurred. The distance from the face of the column is 970 mm and its length is 100 mm. CR7 : A flexural crack occurred at the top of the beam. The distance from the face of the column is 400 mm and length is 170mm CR8 : It started from the top of the beam at the distance of 630mm from the face of the column and its length is 250 mm. CR3 :It has extended	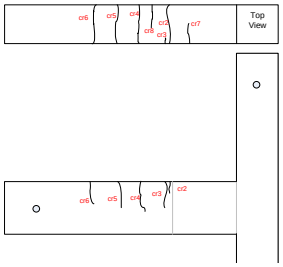

Table 3.2. Observations of US3-FRP1 (Continued)

Drift (%)	Observations	Crack pattern
1.00	Max lateral load : (+) 63.30 kN (Push) : (-) 106.00 kN (Pull) CR9 : It started from the top of the beam. The distance from the face of the column is 260 mm and its length is 200 mm. CR10 : A flexural crack occurred. The distance from the face of the column is 1130 mm and its length is 100 mm. CR11 : A flexural crack occurred at the bottom of the beam. The distance from the face of the column is 720 mm and length is 220mm CR12 : Another flexural crack occurred at the bottom of the beam. The distance from the face of the column is 970 mm and length is 100mm CR4 :It has extended FRP debonding has started	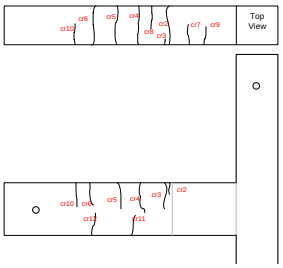
1.40	Max lateral load : (+) 77.90 kN (Push) : (-) 125.10 kN (Pull) CR14 : Just at the connection of the beam and the column, a crack opening was observed. This crack was exactly at the top connection line as shown in the sketch. CR13 : This is a crack symmetric to CR14 at the botteom of the beam.	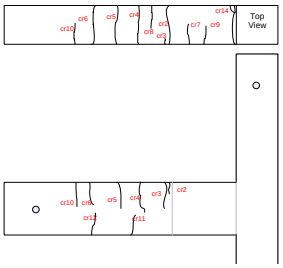

Table 3.2. Observations of US3-FRP1 (Continued)

Drift (%)	Observations	Crack pattern
1.75	Max lateral load : (+) 69.80kN (Push) : (-) 138.60 kN (Pull) Debonding increase was observed. It can be said that anchorages are handling with the stress. U shape almost dont have any bond on the surface of beam. Load has started to decrease in push direction. CR15 : A flexural crack occurred on the surface of the beam on FRP side. The distance from the face of the column is 460 mm and its length is 150 mm. CR16 : A flexural crack that has a 130 mm length and a 430 mm distance from the column, occurred at the bottom of the beam. CR17 : A flexural crack occurred. The distance from the face of the column is 40 mm and its length is 100 mm.	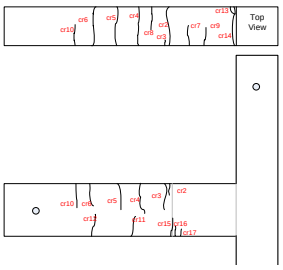 
2.20	Max lateral load : (+) 74.99 kN (Push) : (-) 144.70 kN (Pull) Debonding increase was observed and can be seen clearly. Load has increased again in Push direction. CR16 & CR17: has joined. CR17 : has widened. CR18 : A flexural crack occurred. The distance from the face of the column is 430 mm and its length is 110 mm	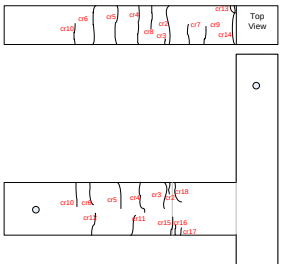
2.75	Max lateral load : (+) 66.80 kN (Push) : (-) 139.00 kN (Pull) CR19 : A flexural crack occurred. The distance from the face of the column is 930 mm and its length is 90 mm. CR20 : A flexural crack occurred. The distance from the face of the column is 1360 mm and its length is 70 mm. CR21 : A flexural crack occurred. The distance from the face of the column is 1390 mm and its length is 200 mm.	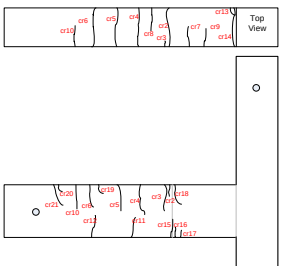

Table 3.2. Observations of US3-FRP1 (Continued)

Drift (%)	Observations	Crack pattern
3.50	Max lateral load : (+) 57.10 kN (Push) : (-) 114.70 kN (Pull) FRP strip, which surrounds the column as belt, and U shape FRP that extends to the beam totally ruptured It can be said that it is totally debonded and Anchorage failures were started.	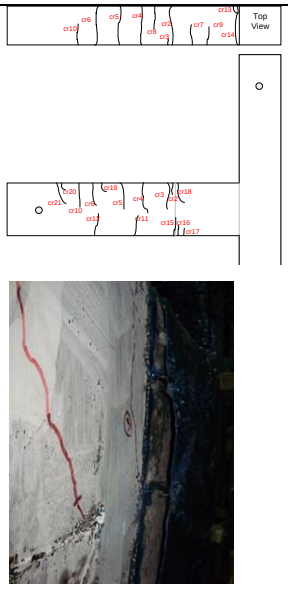
4.00	Max lateral load : (+) 34.00 kN (Push) : (-) 68.20 kN (Pull) All anchorages in beam and CFRP has debonded.	

3.2.3. Specimen US3-FRP2

Shortly after the test started, first crack occurred at the top portion of the beam and at the end of the U-shape CFRP when the lateral load was 73 kN and the drift was 0.50% in the pull direction. Up to drift level of 1.75% there were cracks only in the beam. At the drift level of 1.75% there were cracks in the both top and bottom corners of the beam near the column.

When the drift level was 2.20%, the lateral load reached the maximum capacity in both push and pull directions. In the push direction the maximum load was 103 kN and in the pull direction it was 153 kN. In addition, during this drift level, debonding was

observed in the bottom part of the beam. After this drift level the lateral load decreased rapidly in the push direction and a hinge occurred in the bottom part of the beam at the end of U shape as shown in Figure 3.3.

Figure 3.3. Hinge occurred in the beam and joint didn’t crushed

After removal of CFRP, Figure 3.3 reveals that failure has been in the beam which is desired failure mode. There is no crush in the joint but a hinge in the beam at the end of U-shape of CFRP.

Table 3.3. Observations of US3-FRP2

Drift (%)	Observations	Crack pattern
0.15	Max lateral load : (+) 17.60 kN (Push) : (-) 21.70 kN (Pull)	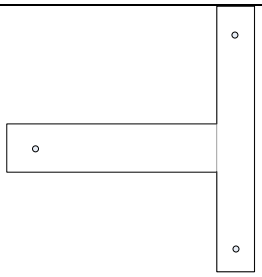
0.20	Max lateral load : (+) 21.10 kN (Push) : (-) 30.00 kN (Pull)	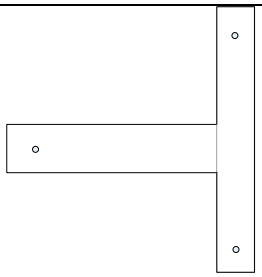
0.25	Max lateral load : (+) 23.70 kN (Push) : (-) 43.30 kN (Pull) CR1 : This is a flexural crack, occurred in pull direction (at the top of the beam), and the location is 540 mm away from the face of the column. Crack length is 40 mm.	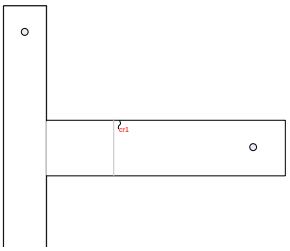
0.35	Max lateral load : (+) 32.70 kN (Push) : (-) 54.80 kN (Pull)	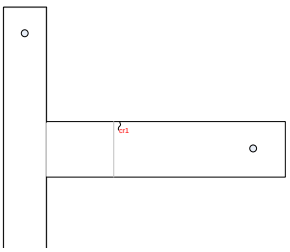
0.50	Max lateral load : (+) 41.20 kN (Push) : (-) 73.30 kN (Pull) CR2 : Flexural crack occurred at the bottom of the beam, 530 mm away from the column with a length of 140 mm. CR3 : Flexural crack occurred at the top of the beam, 850 mm away from the column with a length of 120 mm. CR1 : has extended and widened.	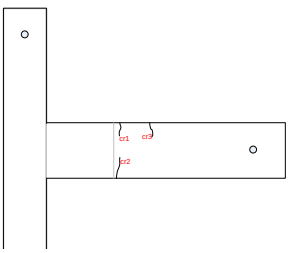

Table 3.3. Observations of US3-FRP2 (Continued)

Drift (%)	Observations	Crack pattern
0.75	Max lateral load : (+) 56.50 kN (Push) : (-) 95.20 kN (Pull) CR4 : Flexural crack occurred at the bottom of the beam, 620 mm away from the column with a length of 240 mm. CR5 : Flexural crack occurred at the top of the beam, 740 mm away from the column with a length of 340 mm. CR6 : Flexural crack occurred at the top of the beam, 870 mm away from the column with a length of 120 mm. CR7 : Flexural crack occurred at the top of the beam, 530 mm away from the column with a length of 140 mm. CR8 : Flexural crack occurred at the top of the beam, 1050 mm away from the column with a length of 110 mm. CR9 : Flexural crack occurred at the top of the beam, 120 mm away from the column with a length of 190 mm. CR10 : Flexural crack occurred at the top of the beam, 60 mm away from the column with a length of 130 mm.	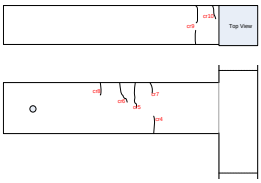
1.00	Max lateral load : (+) 71.90 kN (Push) : (-) 110.50 kN (Pull) CR11 : Flexural crack occurred at the top of the beam, 1200 mm away from the column with a length of 140 mm CR10 & CR9: has extended CR1 : has widened CR12 : Flexural crack occurred at the bottom of the beam, 900 mm away from the column with a length of 120 mm. CR13 : Flexural crack occurred at the bottom of the beam, 880 mm away from the column with a length of 80 mm. CR14 : Flexural crack occurred at the top of the beam, 5 mm away from the column with a length of 50 mm. CR15 : Flexural crack occurred at the top of the beam, 460 mm away from the column with a length of 250 mm. CR5 & CR6: has extended.	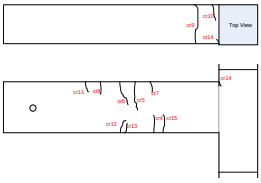

Table 3.3. Observations of US3-FRP2 (Continued)

Drift (%)	Observations	Crack pattern
1.40	Max lateral load : (+) 87.30 kN (Push) : (-) 127.20 kN (Pull) CR16 : Flexural crack occurred at the bottom of the beam, 1200 mm away from the column with a length of 900 mm. CR17 : Flexural crack occurred at the bottom of the beam, 310 mm away from the column with a length of 110 mm. CR18 : Flexural crack occurred at the top of the beam, 400 mm away from the column with a length of 130 mm. CR19 : Flexural crack occurred at the top of the beam, 1200 mm away from the column with a length of 150 mm. CR20 : Flexural crack occurred at the bottom of the beam, 5 mm away from the column with a length of 40 mm. CR4 & CR6: has extended. CR14 : has extended and bifurcated.	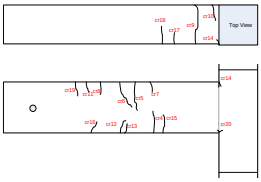
1.75	Max lateral load : (+) 98.70 kN (Push) : (-) 146.00 kN (Pull) CR4 & CR7 : has bifurcated CR15 : has extended CR1 : has widened to 1 mm.	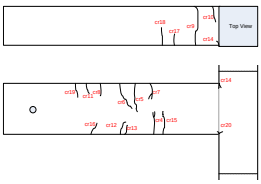
2.20	Max lateral load : (+) 103.10kN (Push) : (-) 153.50 kN (Pull) CR21 : Flexural crack occurred at the bottom of the beam, 850 mm away from the column with a length of 350 mm. CR22 : Flexural crack occurred at the top of the beam 1010 mm away from the column with a length of 460 mm. CR1 : has widened to 3 mm. Debonding has started between middle and bottom anchorages. CR1 & CR18 : has joined. CR1 & CR2 : has joined. CFRP debonded.	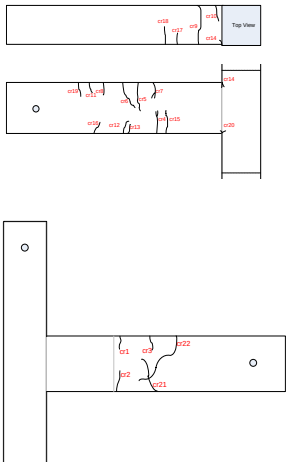

Table 3.3. Observations of US3-FRP2 (Continued)

2.75	Max lateral load : (+) 39.00 kN (Push) : (-) 140.80 kN (Pull) Load has decreased rapidly. At the point where FRP ends there has been a hinge at beam. The width of crack at hinge is 5 mm.	
3.50	Max lateral load : (+) 15.60 kN (Push) : (-) 135.30 kN (Pull) Slip and crushing occurred at hinge location.	
	Hinge is obvious. After peeling of the CFRP sheets.	

3.3. Analysis of Test Results

In this section, test results obtained from data acquisition system are plotted in terms of load-deformation and strain. All the experimental graphs such as Load-Drift envelopes, Load-Displacement envelope curves, Moment-Curvature relationships of beam and columns, Shear deformation-Load relationships of the joint panel were revealed. In order to have some idea about yielding process of beam longitudinal bars, straingauges versus displacement graphs for all specimens are also shown. Moreover, stiffness degradation and some energy graphs were compared in this section.

In “push” direction of loading, beam bottom rebars are in tension indicating “positive strains” and top rebars are in compression indicating “negative strains.” In “pull” direction of loading, the stresses and signs change accordingly. Figure 3.4 illustrates a schematic drawing of typical deformed shape of the beam-column joint test specimen.

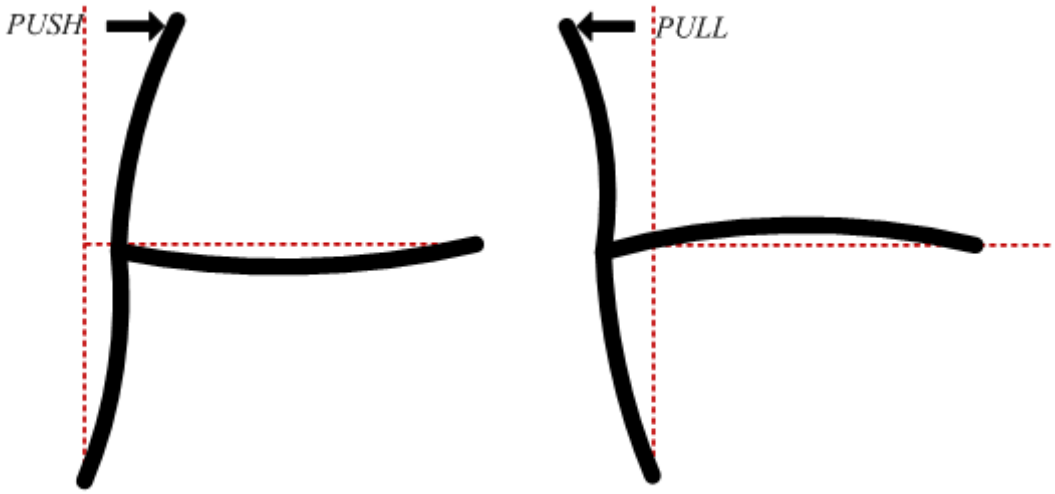

Figure 3.4. Push and Pull Directions of Loading

3.3.1. Load vs. Displacement and Drift Relationships

The Load vs. Displacement and Drift relationship of all three specimens were determined separately. It is apparent that the lateral load capacity of specimens increased after the CFRP retrofitting. For all specimens, Load vs. Displacement and Drift relationships are given in Figure 3.5 to Figure 3.7. Pull direction represents tension at top of the beam, whereas, in push direction tension is at the bottom of the beam.

Diagonal shear cracks were formed at the joint region of US3-ACI. Therefore, it could be said that the failure was governed by the crushing of joint core concrete before the yielding of beam reinforcements. Because of the fact that the amounts of longitudinal reinforcement was different in top (3ϕ20) and bottom (2ϕ20) of the beam, there was almost a 2/3 ratio between the lateral load capacities in push and pull direction of loadings. Figure 3.5 shows the load vs. displacement and drift relationship of US3-ACI specimen. And also, as it is observed from the Figure 3.5; the load capacity did not increase after the drift level

of 1.40% in the push direction. However, it increased until the drift level of 2.20% in the pull direction. The reason for this is the yielding of longitudinal reinforcement in the bottom portion of the beam as shown in Figure 3.8.

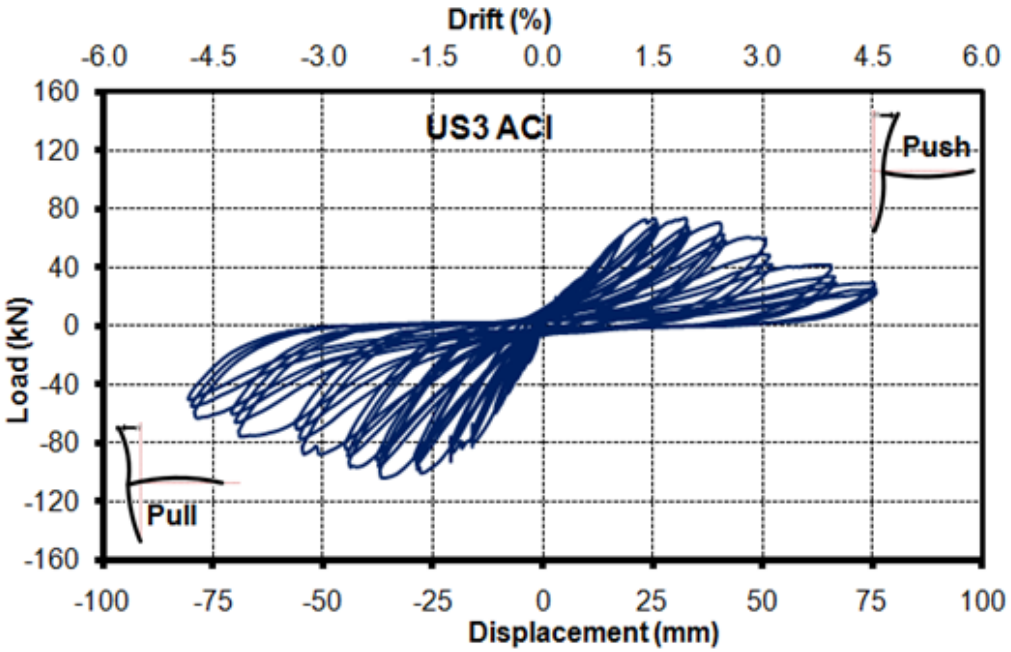

Figure 3.5. Lateral Load vs. Top Displacement

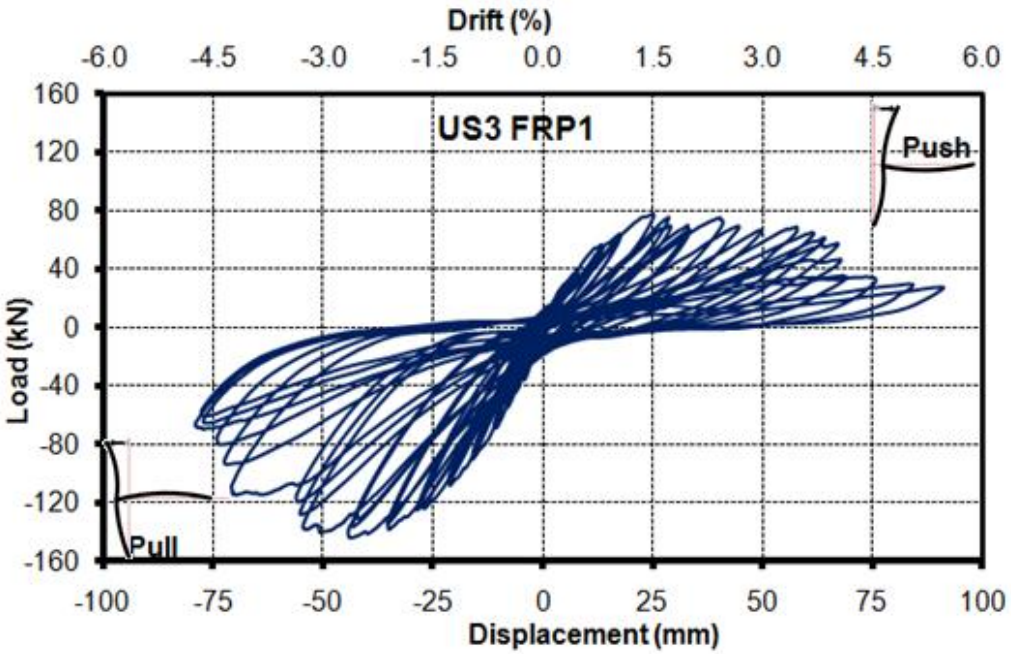

Figure 3.6. Lateral Load vs. Top Displacement

For US3-FRP1, it could be said that after the CFRP application as defined in section 2.5.3.1., the behavior of beam column specimen was improved significantly by applying the anchorage belts as seen in Figure 2.13. Therefore, the slipping of beam bottom rebar problem was solved. Due to the debonding of FRP material in the top part of the beam (Table 3.9- 1.75% drift), decreases in strength was observed in pull direction at a drift level of 2.20%. However, in push direction, the maximum load was observed at 1.40% because of debonding in bottom part of the beam.

Lateral load capacity of US3-FRP2 specimen was improved significantly when compared to specimen US3-FRP1 since the anchorage configuration was altered as described in section 2.5.3.2. From Figure 3.7, it could be observed that the load capacities in both push and pull directions of specimen US3-FRP2 increased by 30% and 10%, respectively as compared to specimen US3-FRP1. Also, no apparent crushing observed in the joint region and hinging occurred at end of FRP wrapping on beam.

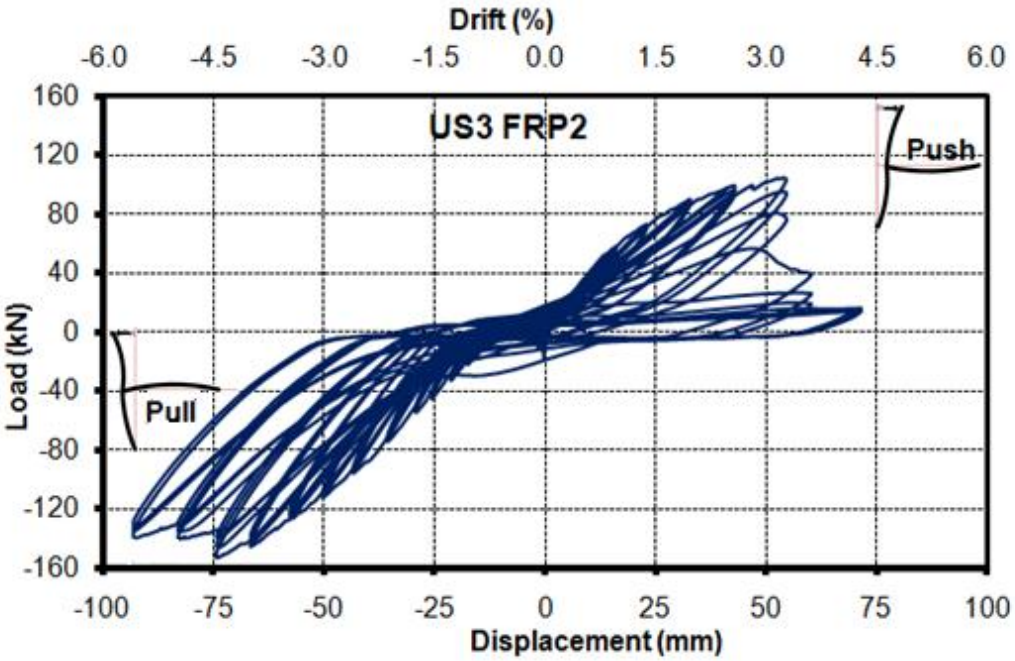

Figure 3.7. Lateral Load vs. Top Displacement

Straingauge data for both specimens revealed that no yielding occurred at beam longitudinal rebars. This is due to the fact that the joint region was confined and stiffened by FRP material.

3.3.2. Strain vs Displacement Relationships for Beam

Details of these rebars were given in the previous chapter. Strain level of longitudinal beams was very important in determination of possible plastic hinge zones. Figure 3.8 illustrates the location strain gauges on re-bars.

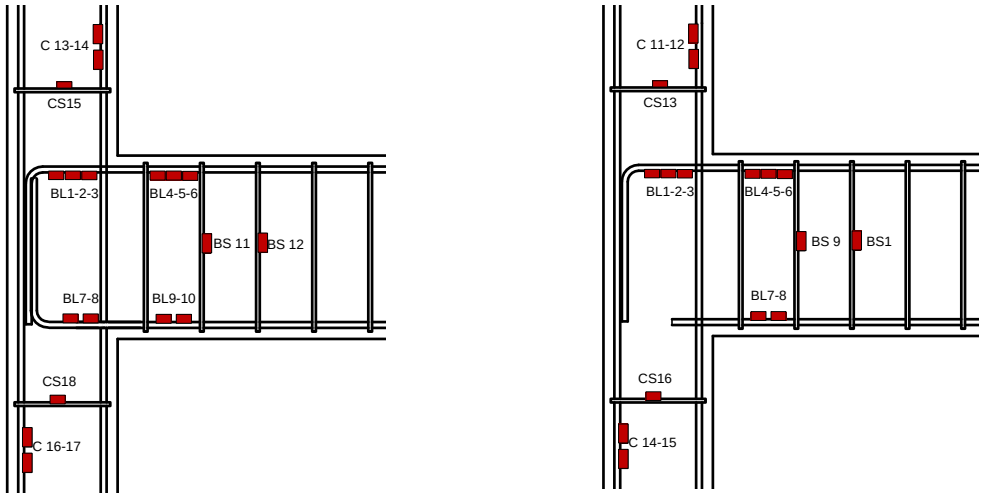

(a) Sg. instrumentation for US3-ACI (b) Sg instrumentation for US3-FRP1 and FRP2

Figure 3.8. Location of strain gauges on rebars

Top rebars were numbered from 1 to 6 and bottom rebars were numbered from 7 to 8. Straingauge readings from some bars were not reasonable and some straingauges did not function, therefore these readings cannot be expressed. Expressed straingauge data for beam longitudinal bars is revealed in Figures 3.9 – 3.11.

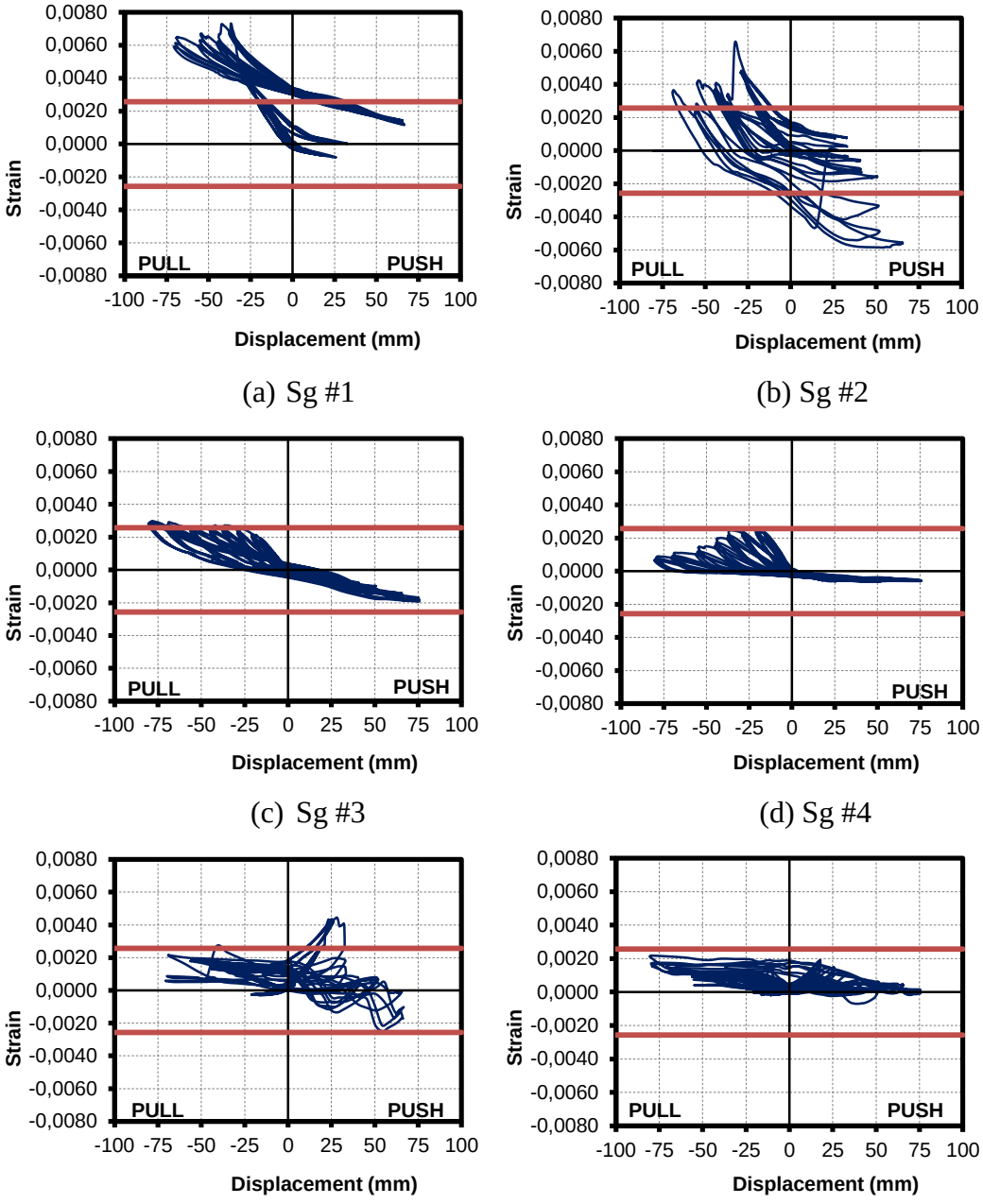

(a) Sg #1 (b) Sg #2

(c) Sg #3 (d) Sg #4

(e) Sg #7 (f) Sg #8

Figure 3.9. Strain vs. Displacement relationship for US3-ACI specimen beam longt. bars

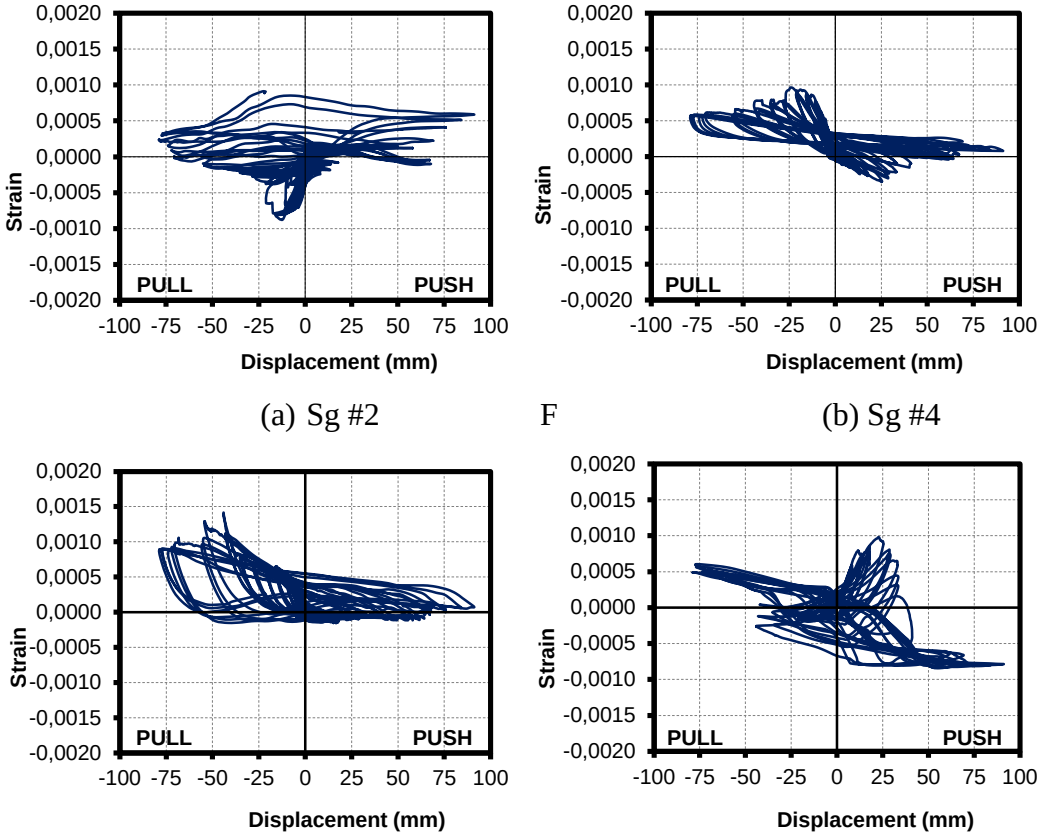

(a) Sg #2 F (b) Sg #4

(c) Sg #6 (d) Sg #8

Figure 3.10. Strain vs. Displacement relationship for US3-FRP1 specimen beam longt. bars

Figure 3.10-(d) illustrates the strain versus drift response of one of the bottom rebars of longitudinal beam for US3-FRP1. Figure 3.10-(a) to Figure 3.10-(c) shows the strain versus displacement relationship of top rebars of US3-FRP1 one specimen.

Strain values of FRP retrofitted specimens expressed similarity with its own lateral load versus displacement hysteresis. Strain level was lower than the expected yielding level of around 1000 μs as shown in Figure 3.9 and Figure 3.10. Whereas the specimen could overcome higher lateral load levels, strain levels were lesser due to contribution of FRP sheets in flexural capacity of beam. In the push direction of loading, re-bars were under compression.

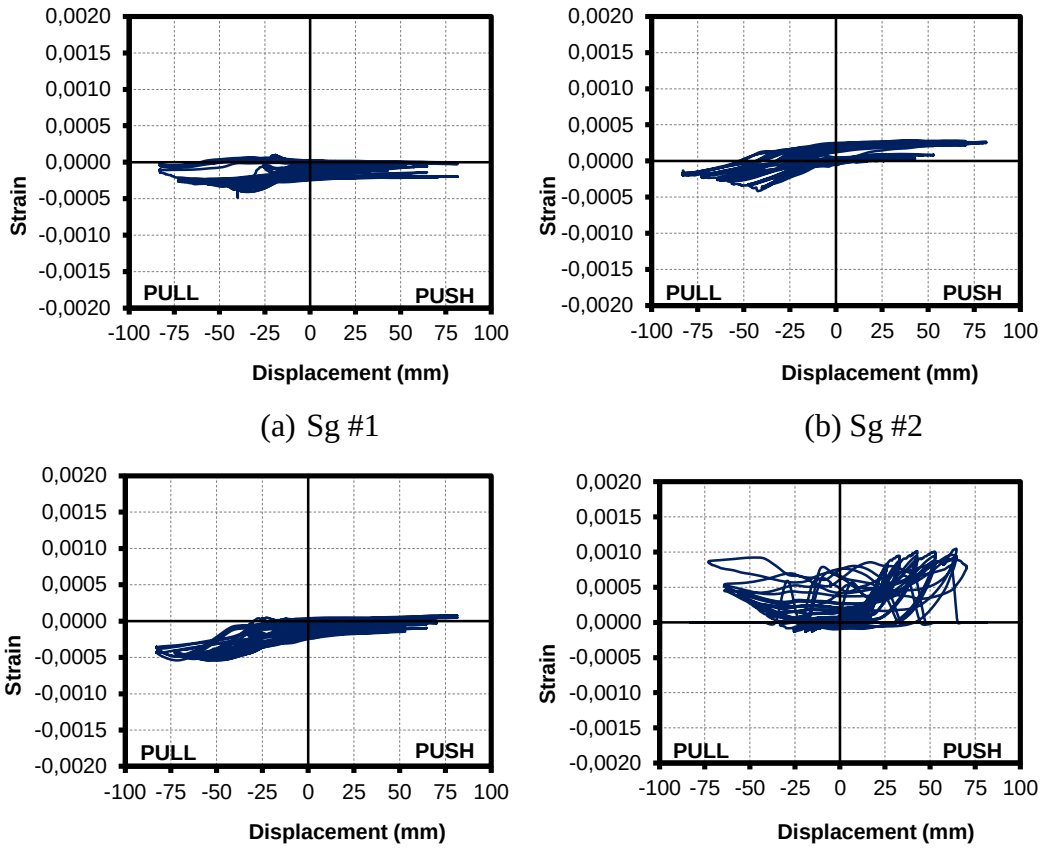

(a) Sg #1 (b) Sg #2

(c) Sg #3 (d) Sg #8

Figure 3.11. Strain vs. Displacement relationship for US3-FRP2 specimen beam longt. bars

3.3.3. Moment vs. Curvature Relationships

Average curvature readings were taken at four different locations on beam-column joint specimen using LVDTs. The placement of displacement sensors close to the maximum tensile and compressive strain regions of the columns and beams allows an average curvature measurement along the gauge length of the sensors. The curvature measurement, instrumentation and calculation are described in Figures 3.12 and shown in Figure 3.13.

Curvature readings could be obtained at the possible plastic hinge region of the columns and the beams. The moment-curvature relationships of column bottom portion (CB), top portion (CT) and beam (B) for all specimens were presented in Figures 3.14 to 3.16 for all specimens.

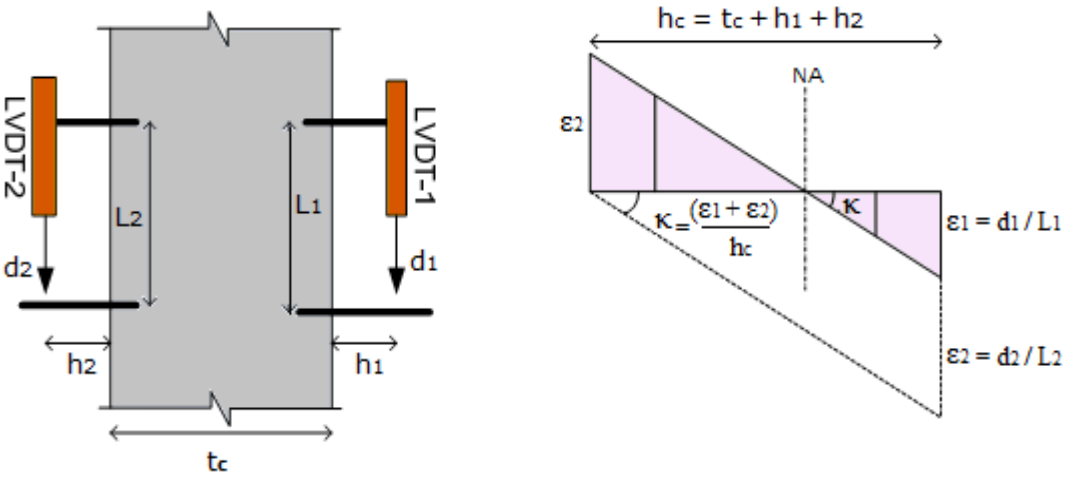

Figure 3.12. Curvature Calculations

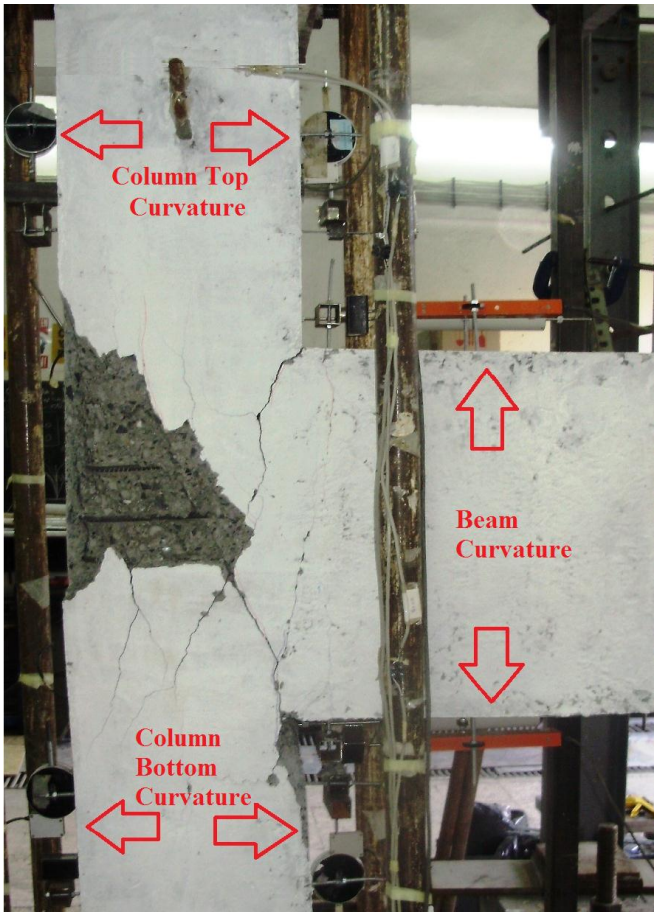

Figure 3.13. Curvature Readings

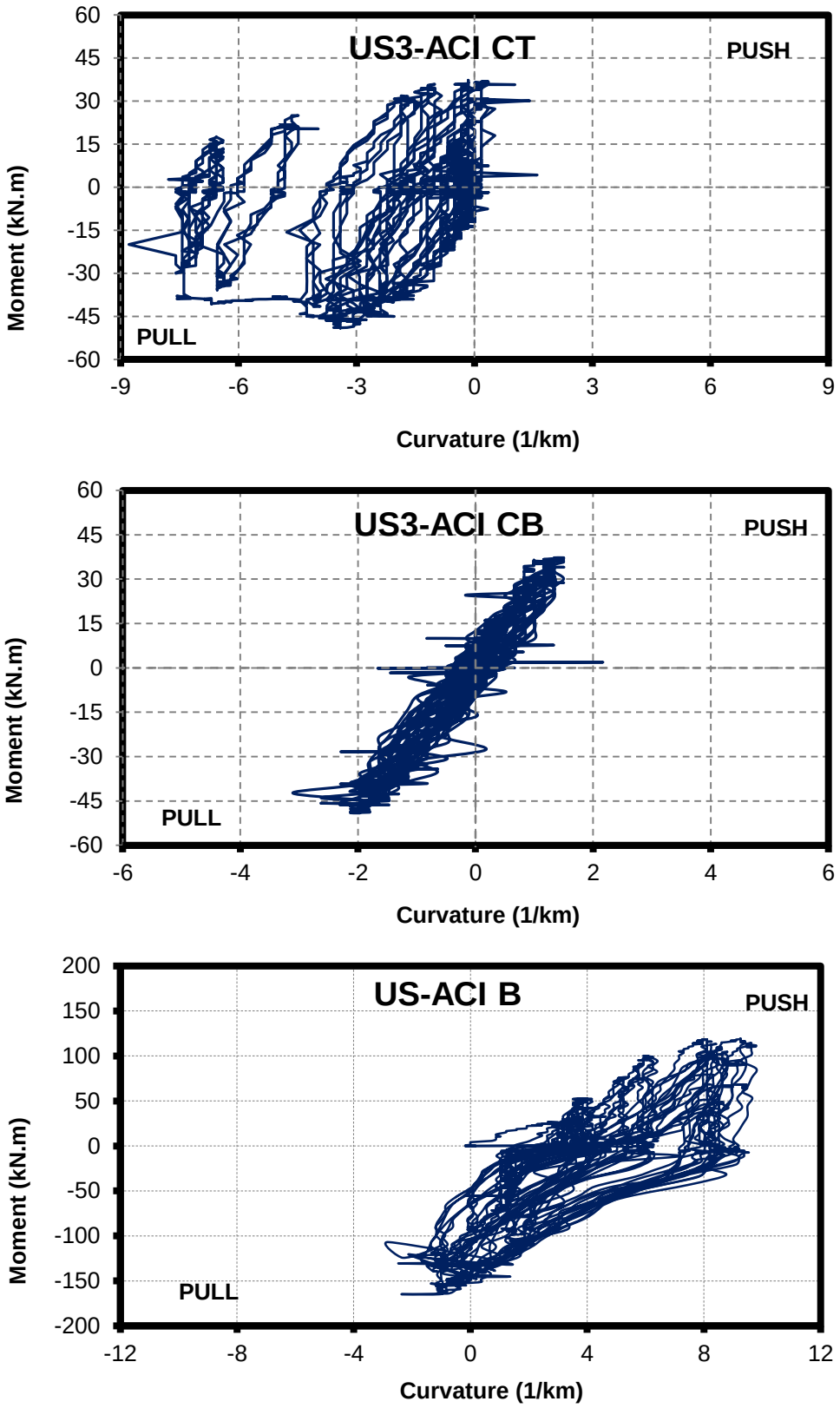

Figure 3.14. Moment vs. Curvature relationship diagrams for US3-ACI

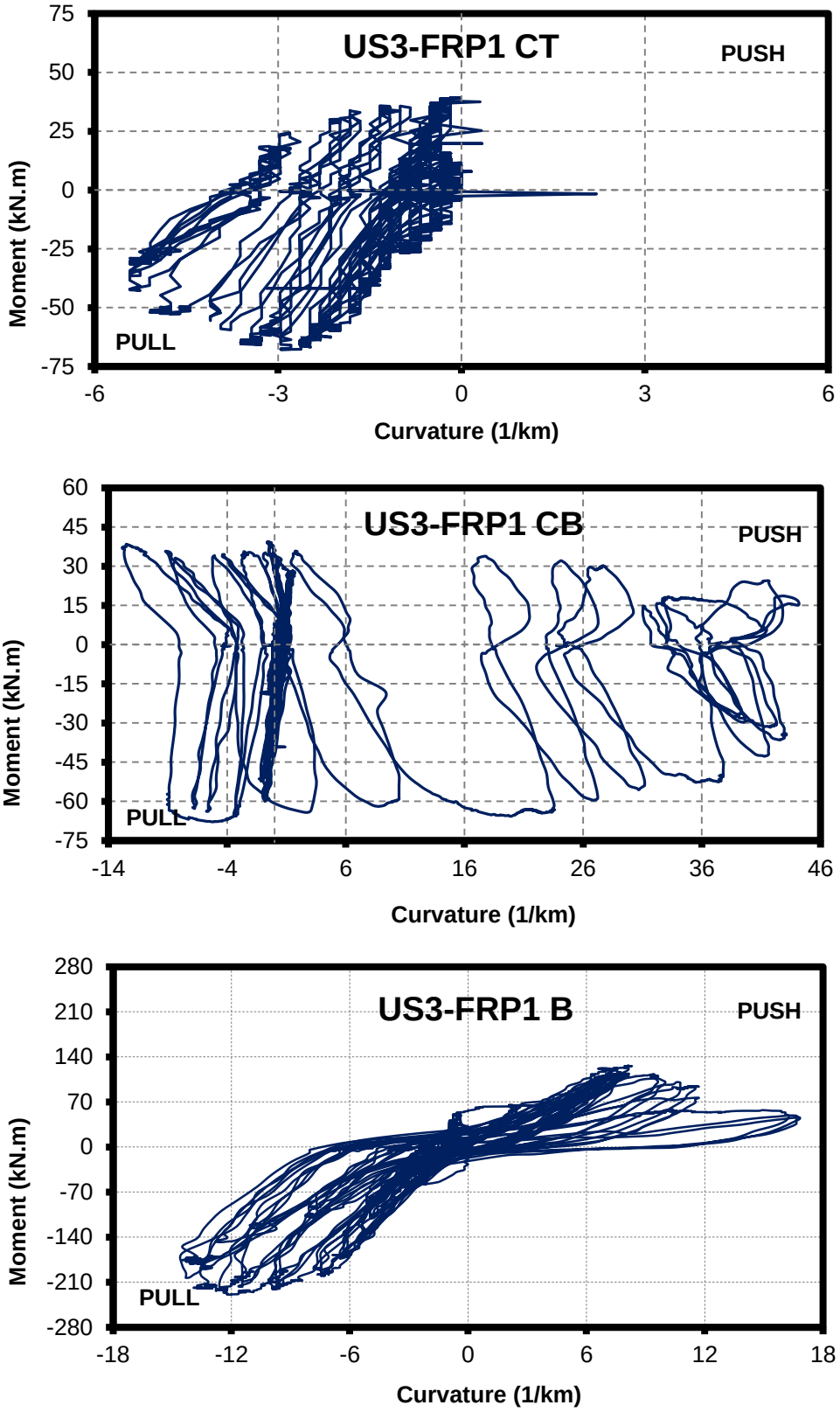

Figure 3.15. Moment vs. Curvature relationship diagrams for US3-FRP1

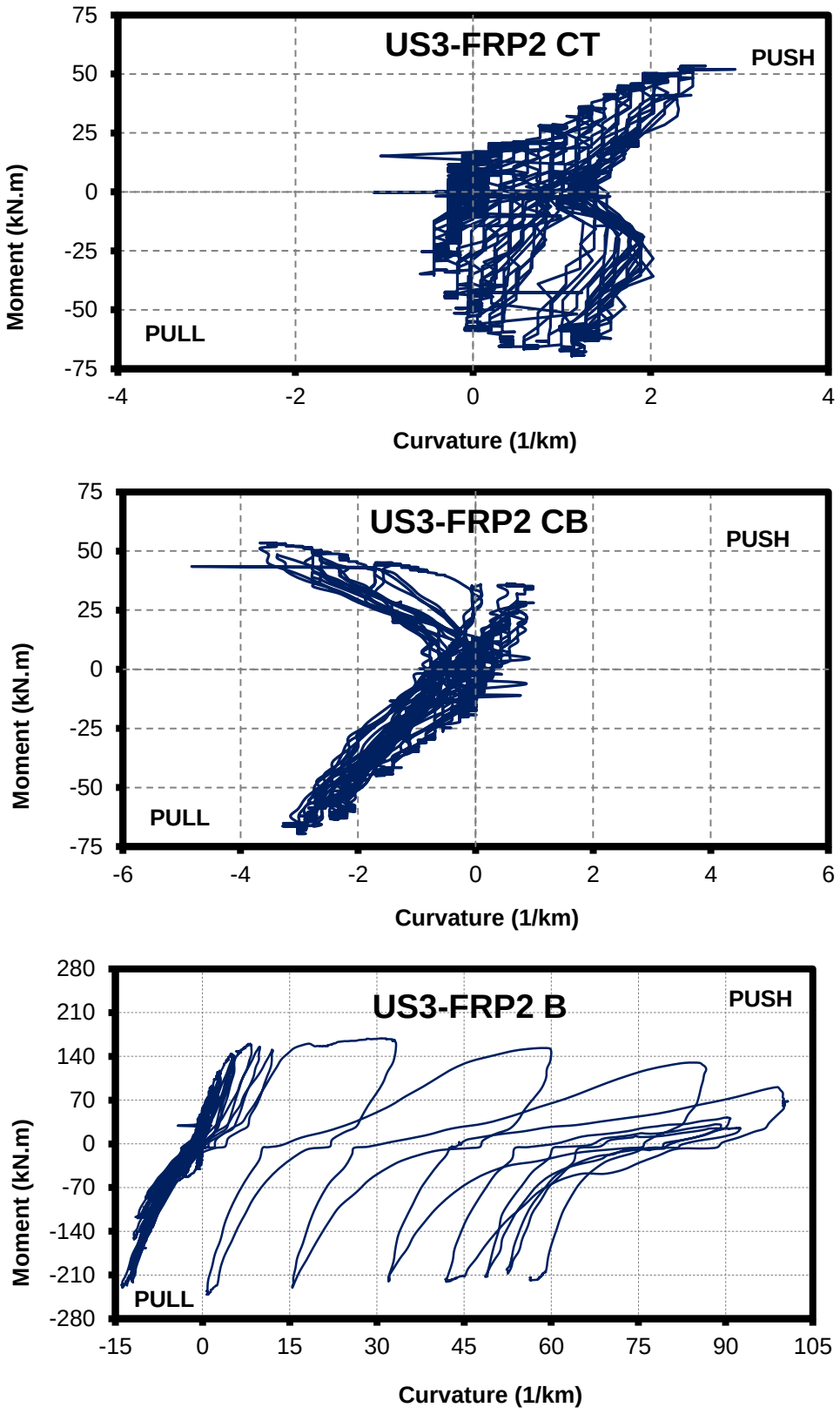

Figure 3.16. Moment vs. Curvature relationship diagrams for US3-FRP2

As it is seen from Figures 3.14 to 3.16, the curvature values of beams were greater than that of column curvature values. This is because of length of beam is greater than length of columns. Moreover, because there were not any significant deformations in columns, the moment curvature values re not that much larger. However, because of the hinge occurred in the beam, for the US3-FRP2, beam curvatures are greater than column curvature values of other specimens.

3.3.4. Joint Shear Deformations

Joint regions are vulnerable to the shear effects due to insufficient transverse reinforcement. Shear deformations were measured at the joint panel with the two diagonal LVDTs as seen in Figures 3.17 and 3.18.

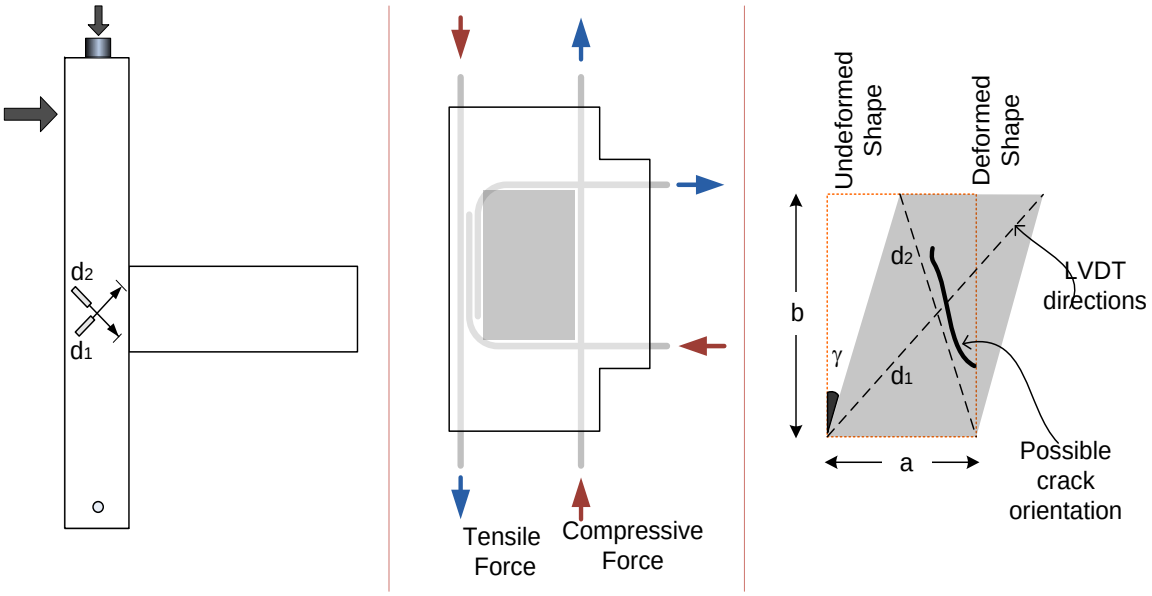

Figure 3.17. Shear Calculations

Assuming that the height and the width of the shear panel do not change due to small shear deformations, by using the given equation below Eqn (3.1), lateral load versus shear deformation relationships of the joint panels were obtained and presented for all specimens in Figures 3.19 to 3.21.

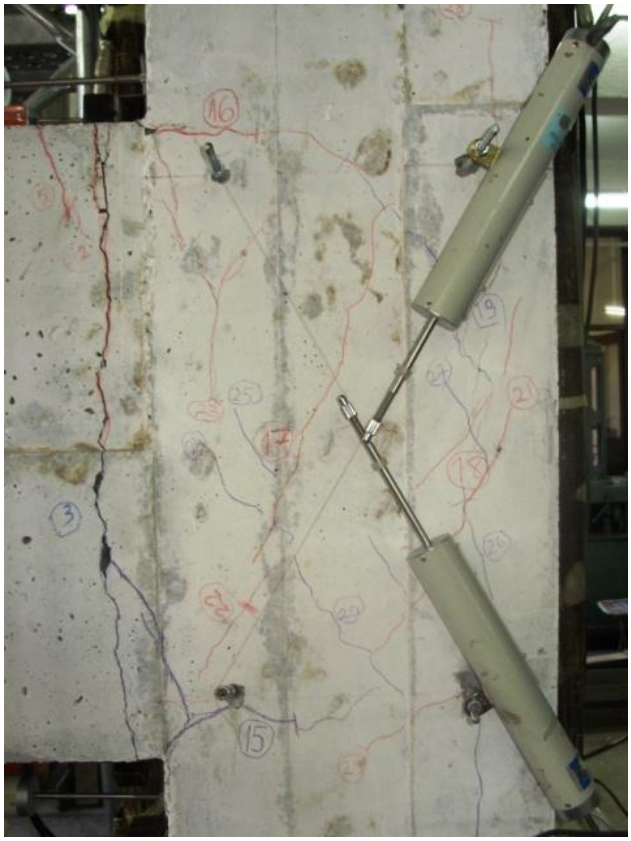

Figure 3.18. Shear Measurements

By using the data obtained from these LVDTs, the shear deformation of the joint could be calculated according to Eqn (3.1).

$$\gamma = tan^{-1}\left(\frac{\sqrt{d_1^{\,2} - b^2} - \sqrt{d_2^{\,2} - b^2}}{2b}\right) \tag{3.1}$$

Where, γ is the shear deformation in radians; a and b are the undeformed joint dimensions; and d_1 and d_2 are gauge lengths of diagonally placed LVDTs.

Figure 3.19 shows the lateral load vs. shear deformation relationship for US3-ACI specimen. As it was observed, shear deformation in the joint has increased up to 0.04 radians at successive higher drift levels. When this specimen's behavior compared with CFRP-retrofitted specimens, there is a significant change in the behavior in terms of joint

shear deformations. The ACI specimen, although it was designed according to current practice, its behavior was somewhat inferior than that of CFRP-retrofitted specimens.

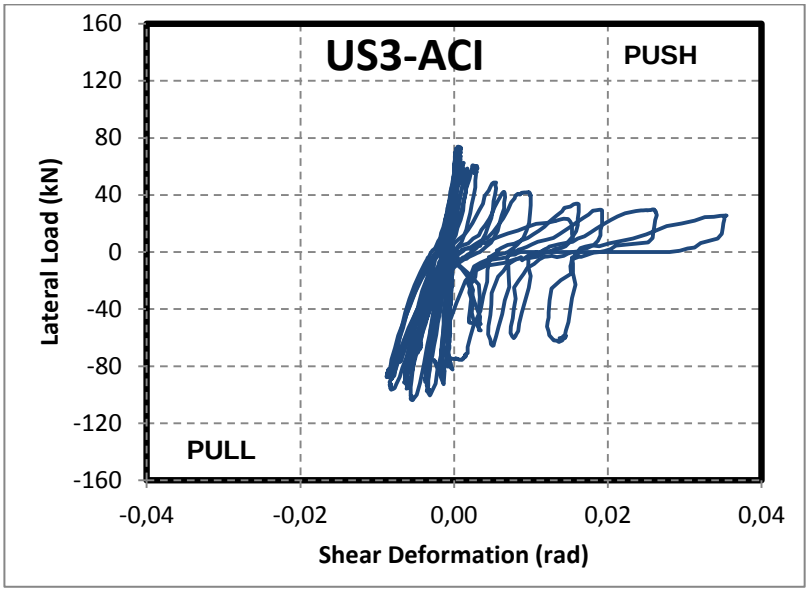

Figure 3.19. Lateral Load vs. Shear Deformation relationship for US3-ACI

As Figure 3.20 shows, compared to US3-ACI, US3-FRP1 specimen where it displayed almost less than half of the shear deformations of US3-ACI specimen.

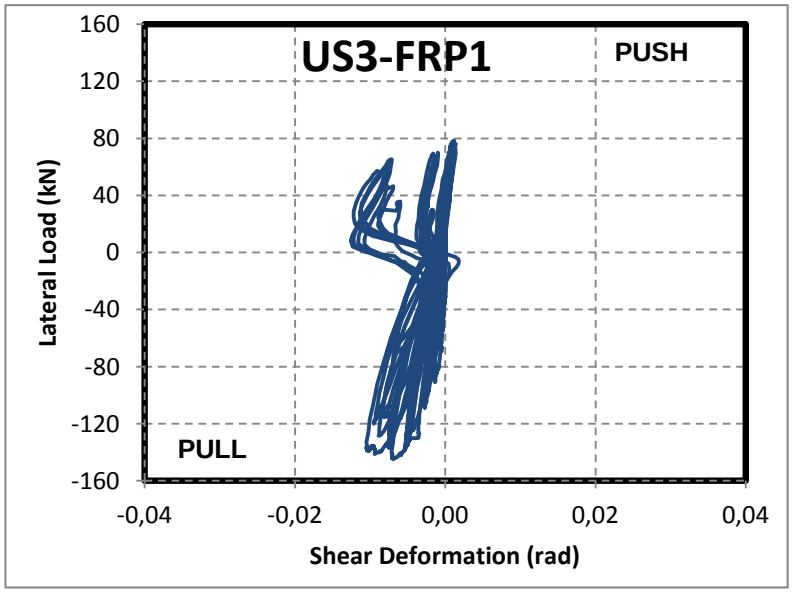

Figure 3.20. Lateral Load vs. Shear Deformation relationship for US3-FRP1

The US3-FRP2, when compared with its companion US3-FRP1 and also to US3-ACI, displayed the least amount of shear deformations, as shown in Figure 3.21. The reason for this was the improved anchorage configuration and thus the failure mechanism was directed towards formation of hinges in the beam and no concrete crushing in joint panel region.

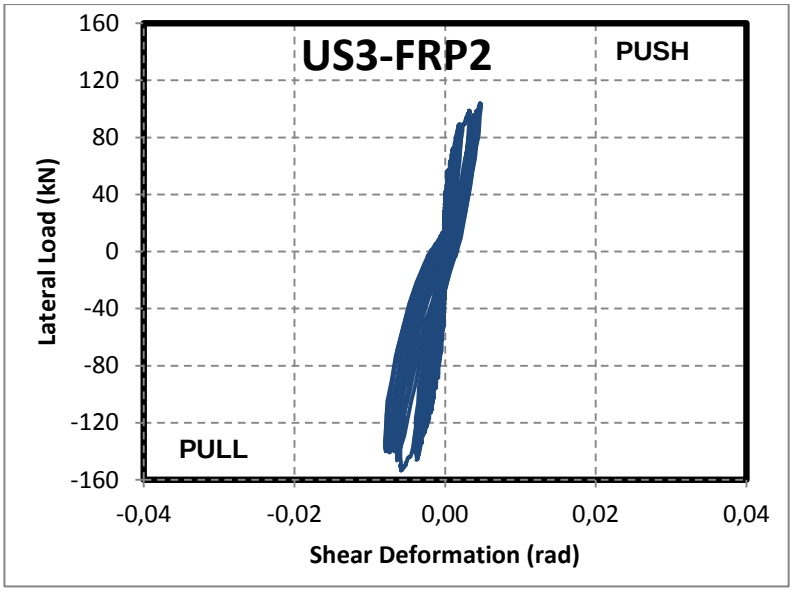

Figure 3.21. Lateral Load vs. Shear Deformation relationship for US3-FRP2

3.3.5. Stiffness Degradation

Stiffness degradation is another important parameter that indicates the behavior of structural elements, especially during cyclic loading, in terms of the amount of degradation by excessive deformations and separations. Flexural and shear cracking, bond slip effects, joint shear deterioration, cover crushing and spalling are the main factors influencing the stiffness degradation.

For all specimens, as shown in Figure 3.22, stiffness was computed for each cycle in push and pull directions of loading separately from the slope of each cycle for corresponding drift level.

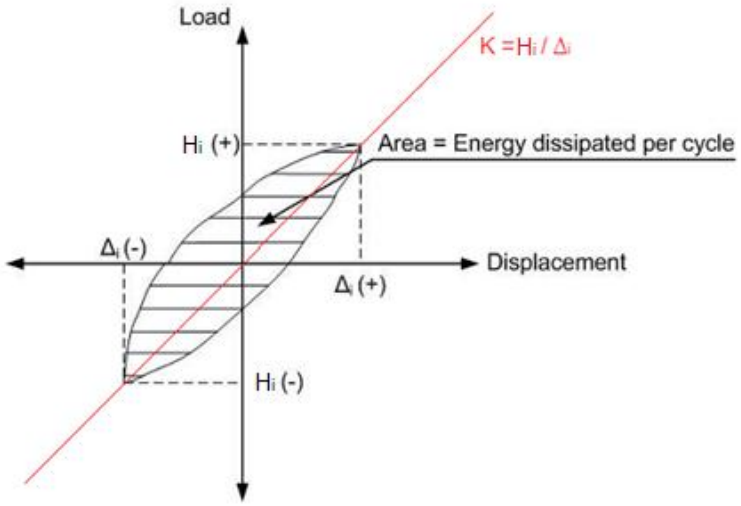

Figure 3.22. Stiffness and Dissipated Energy Calculations

The effect of joint shear and bond slip failures on stiffness degradation was investigated for each specimen. Figures 3.23 through 3.25 show the stiffness vs. drift response relationships of all specimens in push and pull directions of loadings.

Figure 3.23 shows stiffness vs. drift relationship for US3-ACI specimen. Since there is adequate confinement in joint supplied by stirrups, there was no brittle failure observed, however, the stiffness degraded at 2.50% of drift level.

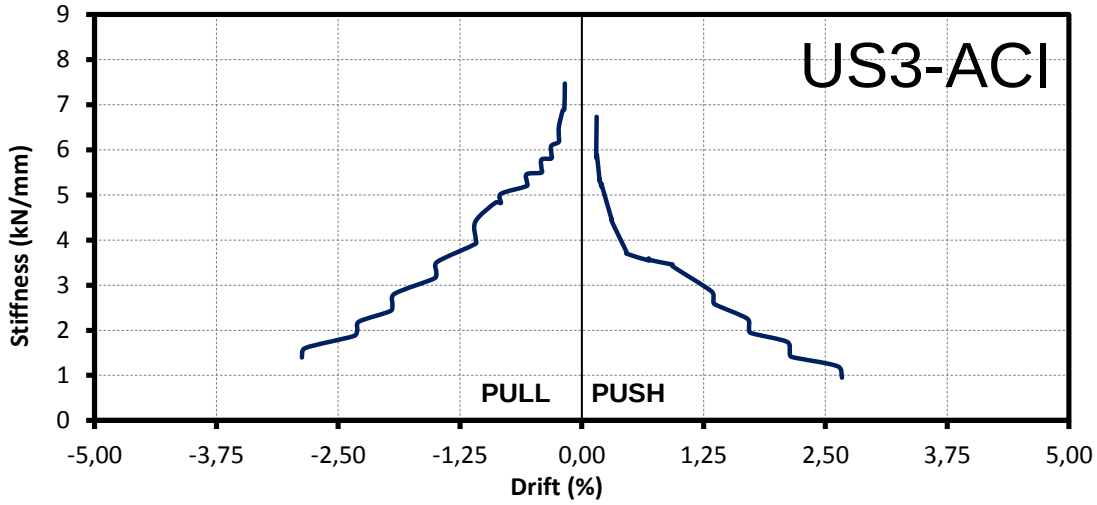

Figure 3.23. US3-ACI stiffness vs. Drift relationship

Figure 3.24 shows the stiffness vs. drift relationship of US3-FRP1 specimen. The degradation lasted up to 3.75% and there was no sharp decrease in the stiffness observed.

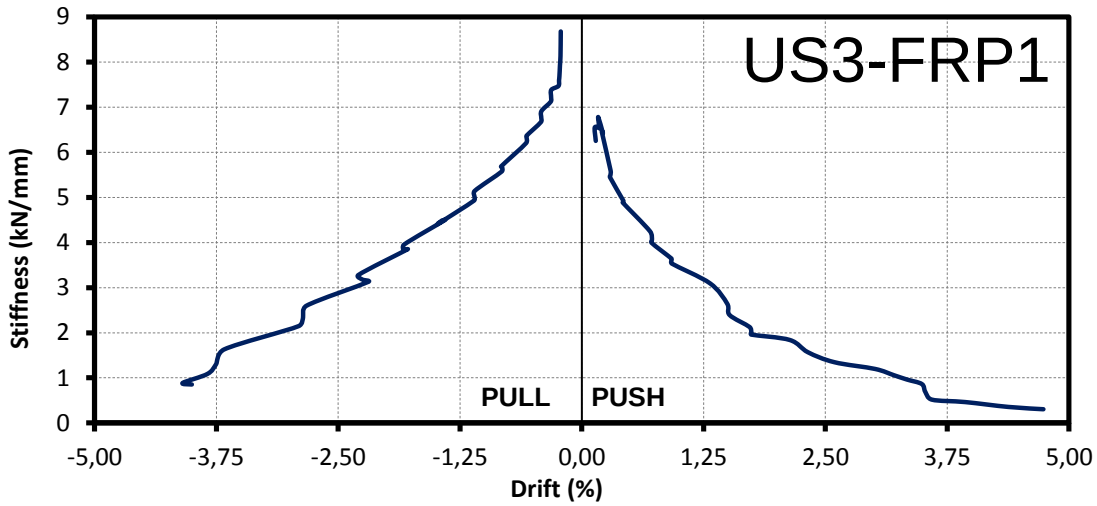

Figure 3.24. US3-FRP1 stiffness vs. Drift relationship

Almost similar behavior was obtained in the case of US3-FRP2 as compared to US3-FRP1, where stiffness degradation lasted up to 3.75%. As it is seen in Figure 3.25, in the pull and push direction behaviors are not symmetric since some data during the experiment was shifted and could not be corrected at a later stage. Thus, push direction data is valid in this case.

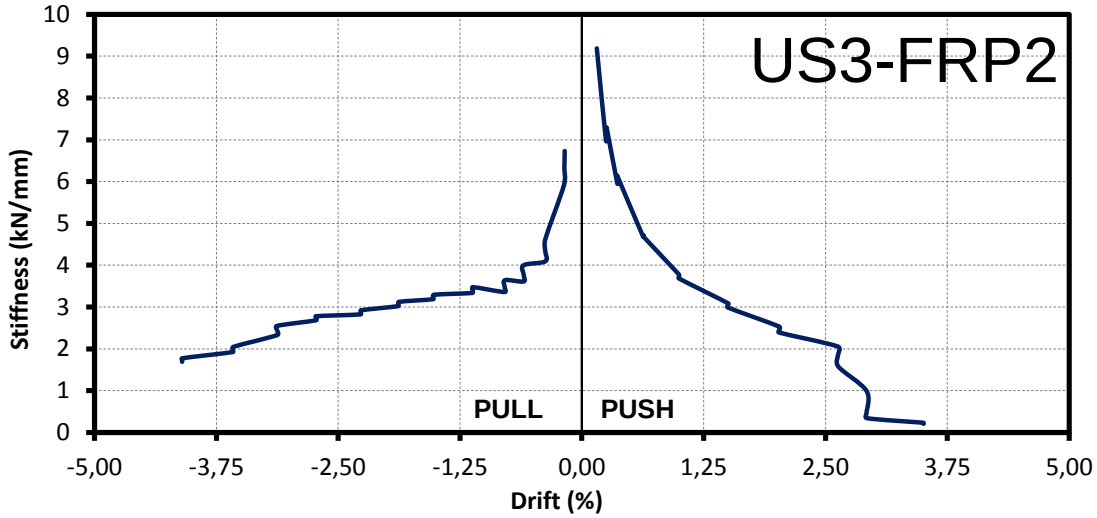

Figure 3.25. US3-FRP2 Stiffness vs. Drift relationship

To conclude the behaviors of all three specimens, especially after the application of retrofitting materials, the joint behavior became more ductile since the rate of degradation of the stiffness values of each cycle decreased.

3.3.6. Energy Dissipation

The capability of a structure to dissipate energy has a strong influence on the response of seismic action. Therefore, ductile behavior of beam-column joints in RC structures is significant since it is correlated with desired energy dissipation potential of structure. Beam-column joint region is a crucial part of the structural system since its behavior dictates the overall response. Therefore, the joint region should not fail under any circumstance and due to strong column-weak beam design philosophy all energy dissipation should take place in the hinging region of the beam.

The dissipated energy was obtained by calculating the enclosed area of individual hysteresis loops from load vs. displacement relationships at particular drift levels as shown in Figure 3.22. The cumulative energy dissipated was calculated by summing up the areas of the consecutive loops throughout the test.

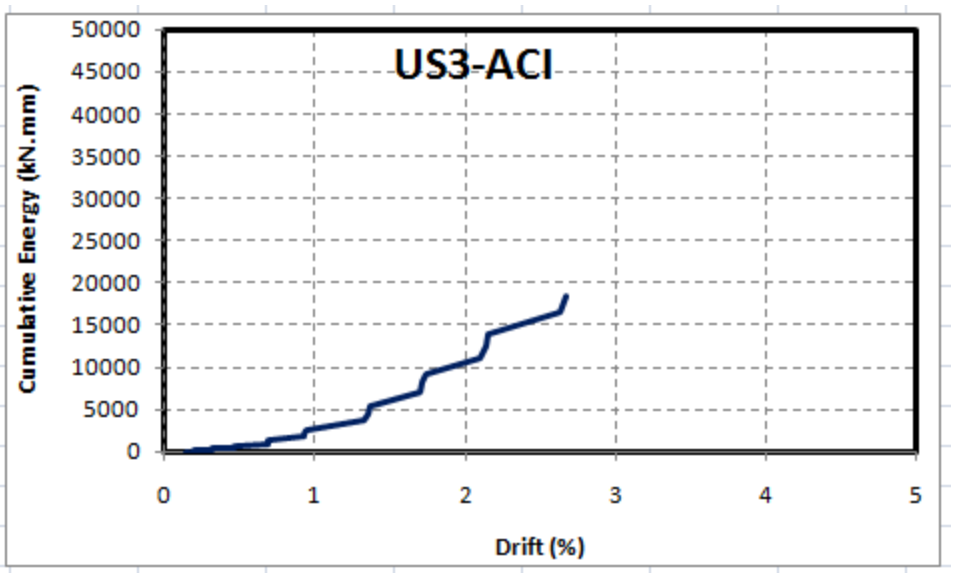

Figure 3.26. Cumulative Energy Dissipation vs. Drift relationship for US3-ACI

Figures 3.26 to 3.28 show Cumulative Dissipated Energy relationships of specimens. Due to high shear deformations occurred in the ACI-US3 specimen, the full strength potential could not be reached and dissipated less energy than that of retrofitted specimens. While comparing US3-FRP1 and US3-FRP2, both displayed almost the same energy dissipation capacities. However, the later reached the same level of energy dissipation at lower drift levels. This also shows the effectiveness of the improved anchorage configuration.

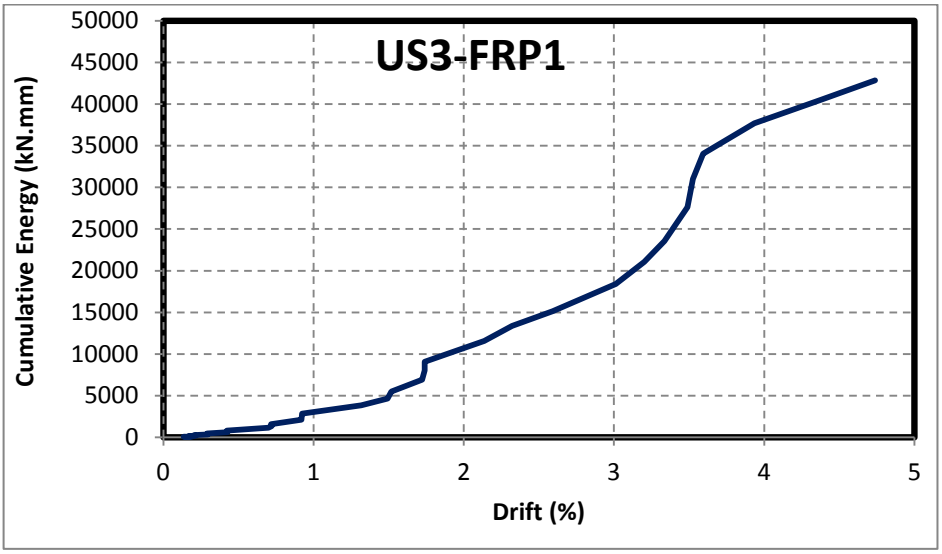

Figure 3.27. Cumulative Energy Dissipation vs. Drift relationship for US3-FRP1

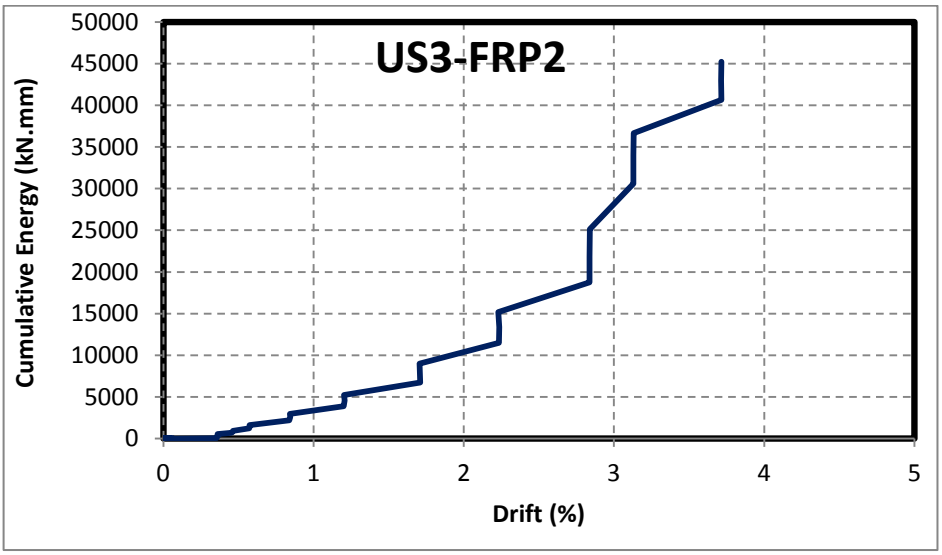

Figure 3.28. Cumulative Energy Dissipation vs. Drift relationship for US3-FRP2

3.4. Comparative Analyses with Previous Studies

3.4.1. Comparison of Test Results

3.4.1.1.Latereal Load versus Displacement. It is obvious that retrofitting technique incrased lateral load capacity of specimens that are strengthened with the applied technique compared to US3-ACI specimen in Figure 3.28. As for retrofitted specimens, although US3-FRP2 specimen has better load carrying capacity in both directions, it is possible to express that the specimen behaved similar to the previous CFRP retrofitted specimen in pull direction of loading. In push direction of loading an increase of 30 percent was observed compared to US3-FRP1. This difference observed in push direction of loading is caused by debonding of CFRP occurred from the beam surface.

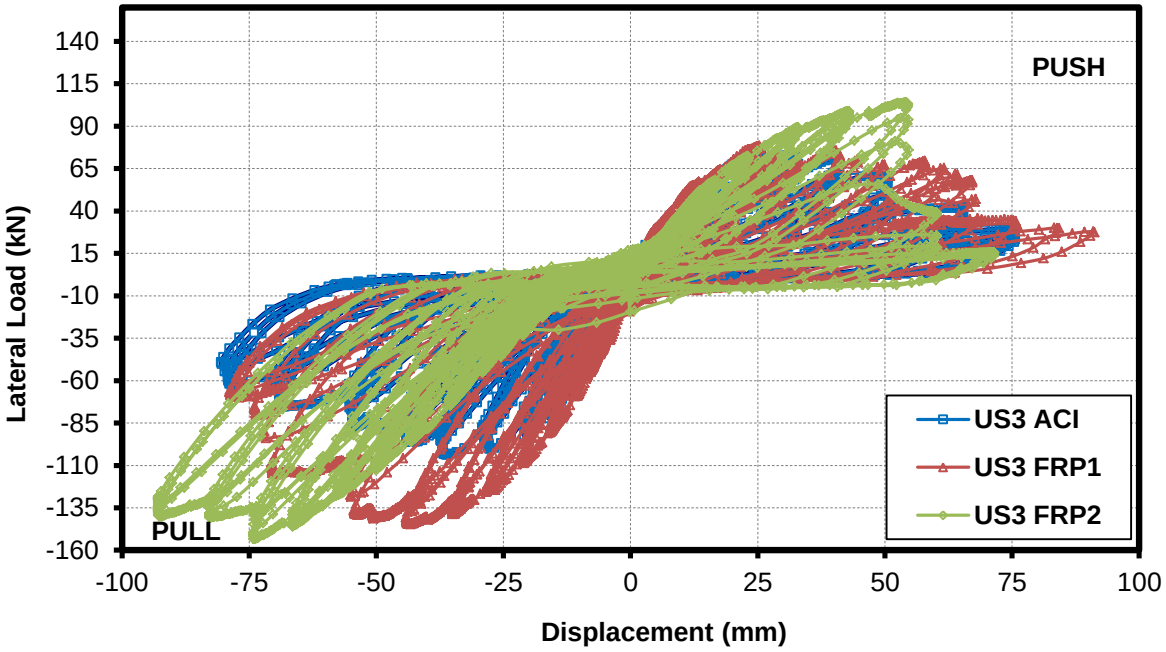

Figure 3.29. Lateral Load vs. Displacement Relationship comparison for specimens

3.4.1.2.Load versus Shear Deformation. One of the main aims of retrofitting technique applied was to be capable of limiting joint shear deformations in order to have a more ductile behavior. While the joint shear deformations were around 0.04 radians, they were decreased by US3-FRP1 and these deformations are the least with US3-FRP2. So, it is

evident that retrofitting technique caused a very important improvement in joint shear deformations as shown in Figure 3.29.

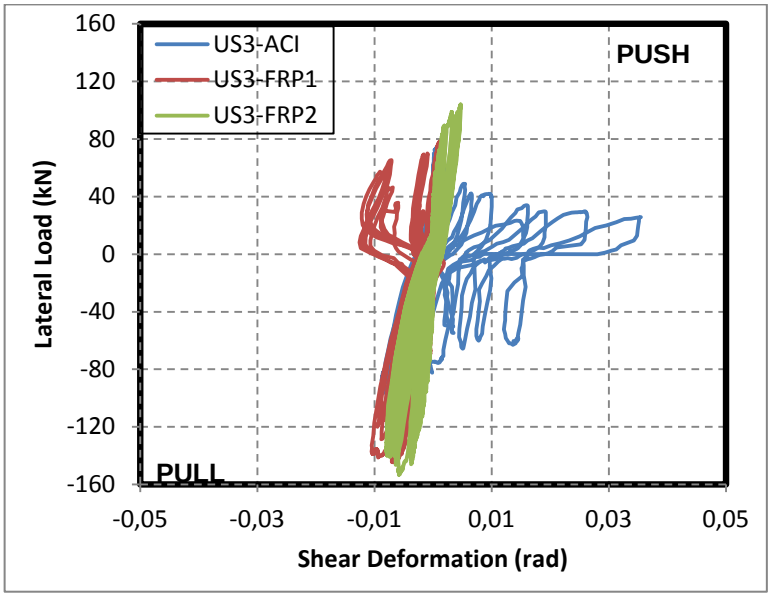

Figure 3.30. Lateral Load vs. Shear Deformation relationship comparison for specimens

3.4.1.3.Stiffness versus Drift. As it is seen in Figure 3.30, stiffness degradation rate was nearly same for all specimens in push direction of loading. However, Stiffness vs. drift response of retrofitted specimens was quite better than that of ACI specimen in pull direction of loading. Not only initial stiffness of retrofitted specimens but also stiffness values in consecutive cycles throughout the test were higher.

3.4.1.4.Cumulative Dissipated Energy versus Drift. It was obvious from the Figure 3.31 that the US3-ACI specimen showed poor energy dissipation capacity compared to the retrofitted specimens. In US3 specimens those are retrofitted, by using the effective wrapping methodology, high energy dissipation capacities were achieved as shown in Figure **Error! Reference source not found.**3.31. Also, the hysteretic cycles became fat in retrofitted specimens. Therefore, the area under the hysteretic loops which shows the dissipated energy increased in those specimens. This resulted in higher cumulative energy capacity.

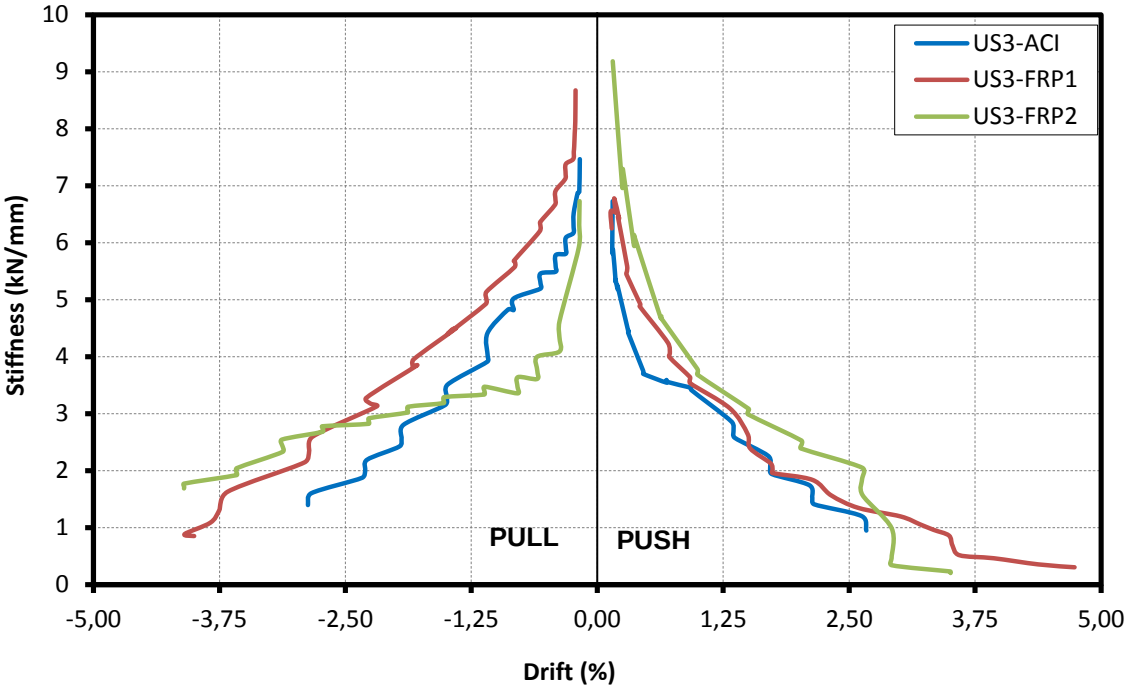

Figure 3.31. Stiffness vs. Drift relationship comparison for specimens

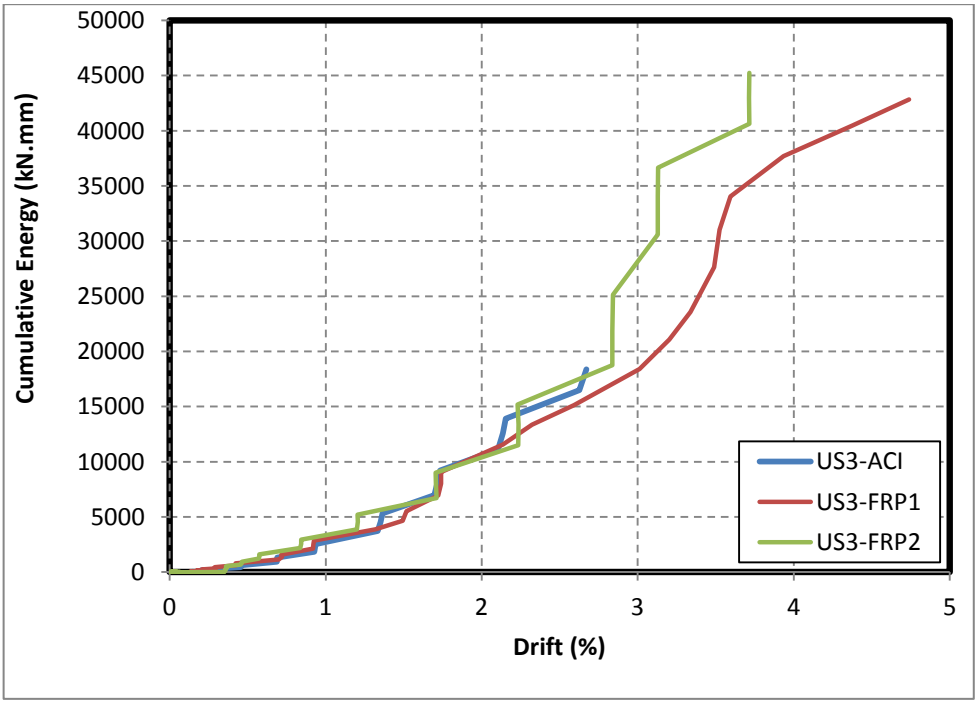

Figure 3.32. Cumulative Energy vs. Drift relationship comparison for specimens

3.4.2. Comparison of Test Results with Previous Experiments

In this section, test results shall be compared with the previous tests, namely US3-CONTROL and US3-FRP, conducted by Altay (2010).

3.4.2.1.Lateral Load versus Displacement Relationship. Figure 3.32 shows lateral load capacity comparison with previous tests. It is well seen, in specimen US3-FRP2 that had improved anchorage techniques, maximum lateral load increased approximately 2.5 times in push direction of loading and 2 times in pull direction of loading compared to US3-CONTROL. While comparing with US3-ACI specimen, maximum lateral load capacity increased about 30 percent in pull direction and 50 percent in push direction of loading. It is possible to express that retrofitting definitely lead to an increase in lateral load capacity of specimens while 3 retrofitted specimens are compared with control specimens.

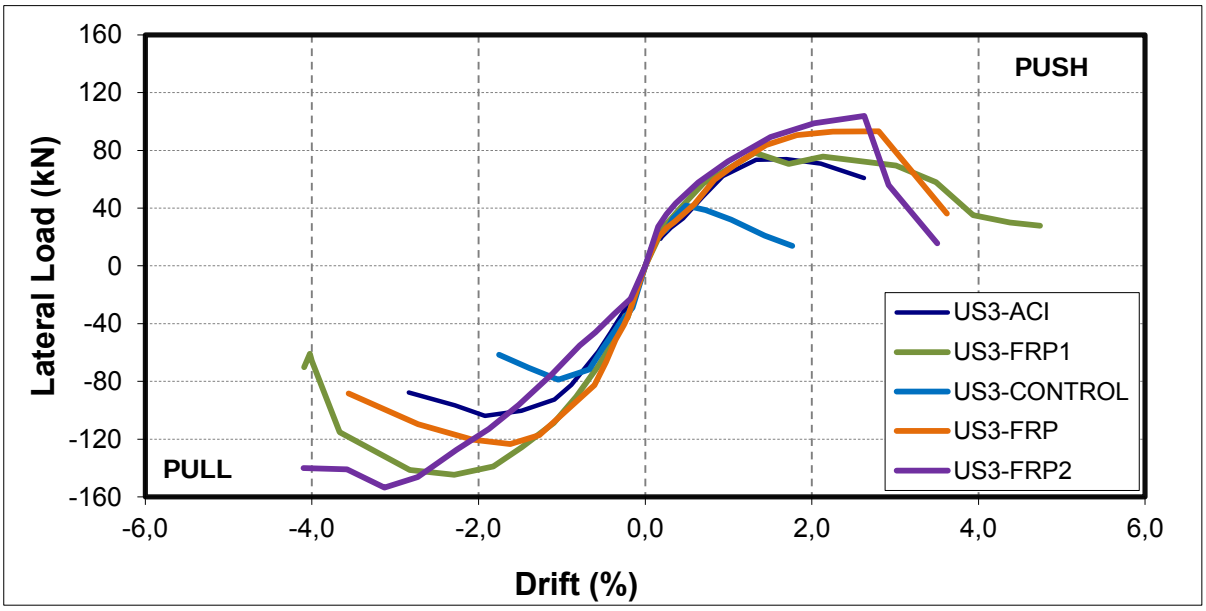

Figure 3.33. Lateral Load vs. Drift Backbone curve comparison with previous tests

3.4.2.2.Lateral Load versus Shear Deformation Relationship

Figure 3.33 shows the lateral load versus shear deformation relationships of all five specimens and it was very obvious that, US3-ACI and US3-CONTROL specimens have

brittle failure due to large shear deformations. However, CFRP retrofitted specimens showed a ductile behavior.

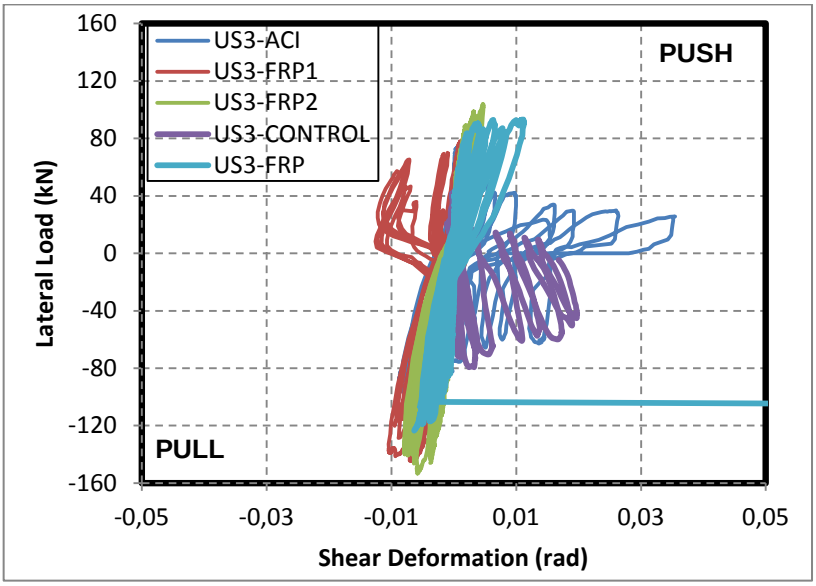

Figure 3.34. Lateral Load vs. Shear Deformation relationship for all tests

3.4.2.3.Stiffness versus Drift Relationship. Figure 3.34 reveals the fact that behavior of retrofitted specimens were more ductile in both push and pull directions of loading since joint shear and bond-slip failures were limited and/or delayed. Therefore, it can be said that CFRP sheets acted as additional reinforcement. Also US3-CONTROL has the least ductile behavior because of sharp decreases in both pull and push directions of loading.

3.4.2.4.Cumulative Dissipated Energy versus Drift Relationship. Figure 3.35 shows the energy dissipated per cycle for all specimens. Since energy dissipation consists of energy dissipated by the steel reinforcement, energy dissipated by friction along existing cracks in concrete, and energy dissipated during the formation of new cracks; it was observed that dissipation was low in the first drift levels. In US3-ACI and US3-CONTROL specimens, energy dissipated per cycle became nearly constant as the drift increased while it improved gradually in retrofitted specimens. For all specimens, energy dissipation was smaller at the repeat cycles of each drift level when they were compared with their corresponding first cycles as a result of the stiffness and strength degradation during the repeated cycles.

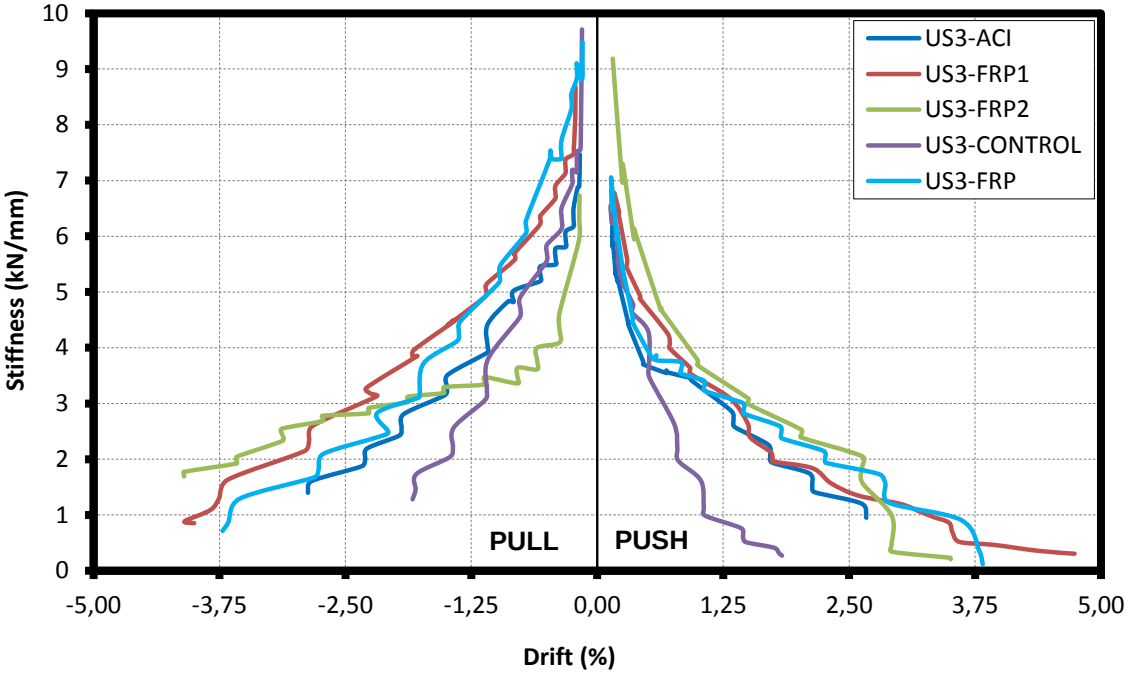

Figure 3.35. Stiffness vs. Drift relationship comparison with previous tests

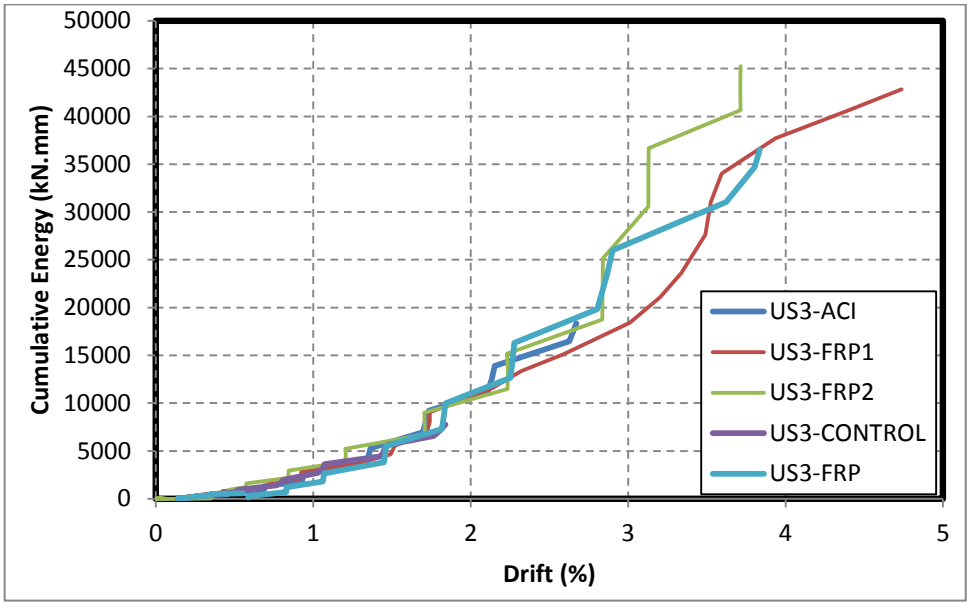

Figure 3.36. Cumulative Energy vs. Drift relationship comparison with previous tests

3.5. Numerical Analysis

In this section, numerical analysis of specimens was done and then it was compared with test results. The numerical model that was developed by Osman Kaya et al (2010) in MS Excel, is going to be used in order to analyze the specimens' behavior.

3.5.1. Model to Predict The Behavior

The analytical model was based on strut and tie model and it mainly checks tensile and compressive stresses on possible failure locations under incremental lateral loads. The lateral load capacity was obtained from the load when the first failure initiated.

3.5.1.1.Model Description. All forces around and within a joint are identified as shown in the Figure 3.38. As it is also discussed in the section 1.3.2, the horizontal joint shear force (V_{jh}) is estimated as a result of subtraction of horizontal column shear force (V_{c1}) from tensile force in the beam's longitudinal reinforcement (T_b) at the top section. Model derivation consists of five simple steps.

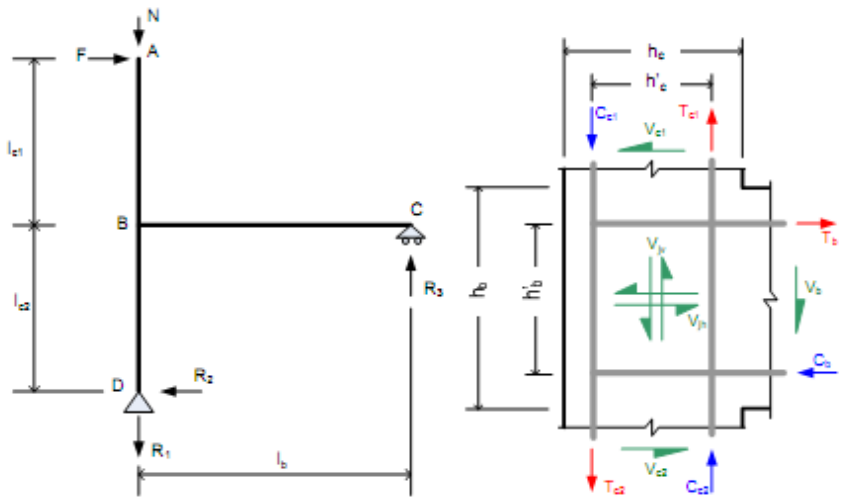

Figure 3.37. Identified forces for the joint model

At first step, all reactions and internal forces are calculated using equilibrium equations and by using the reactions calculated, the moments at the joint region were determined as given in Eq (3.6) and Eq (3.7).

$$M_{c1} + M_{c2} = M_b \tag{3.6}$$

$$F \times l_{c1} + F \times l_{c2} = R_3 \times l_b \tag{3.7}$$

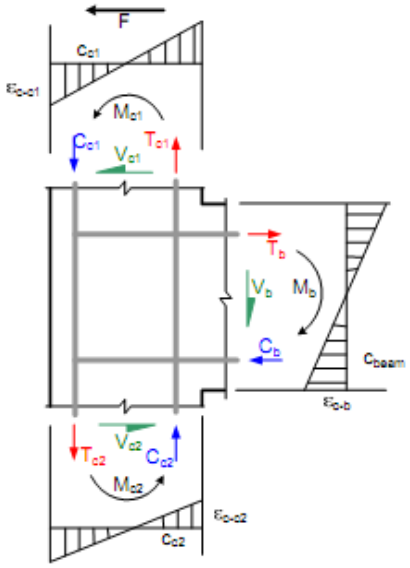

Figure 3.38. Sectional Analysis

In the second step, section is analyzed and the moment (M) and curvature (κ) values are determined. Also, for any lateral loads (F) of column, the corresponding moments, and accordingly extreme fiber compressive and tensile strain of the section (ε_c, ε_t), compression depths of columns and beam (c_{c1}, c_{c2}, c_b), and tensile forces of beam reinforcements (T_b) can be determined from back calculation of Sectional Analysis, as shown in Figure 3.37.

In the third step, forces coming from the beam and columns, were transferred into the joint region. The compression depths of the column and beam sections, calculated from the section analysis and the compression strut area of the joint is shown in Figure 3.38. The compressive strut area has no constant depth; it varies along the diagonal of the joint region. Therefore the effective depth should be determined for calculation of the effects of

concrete on shear. The effective depth of compressive strut can be determined from the depth of equivalent rectangular area along the diagonal axis of the joint region.

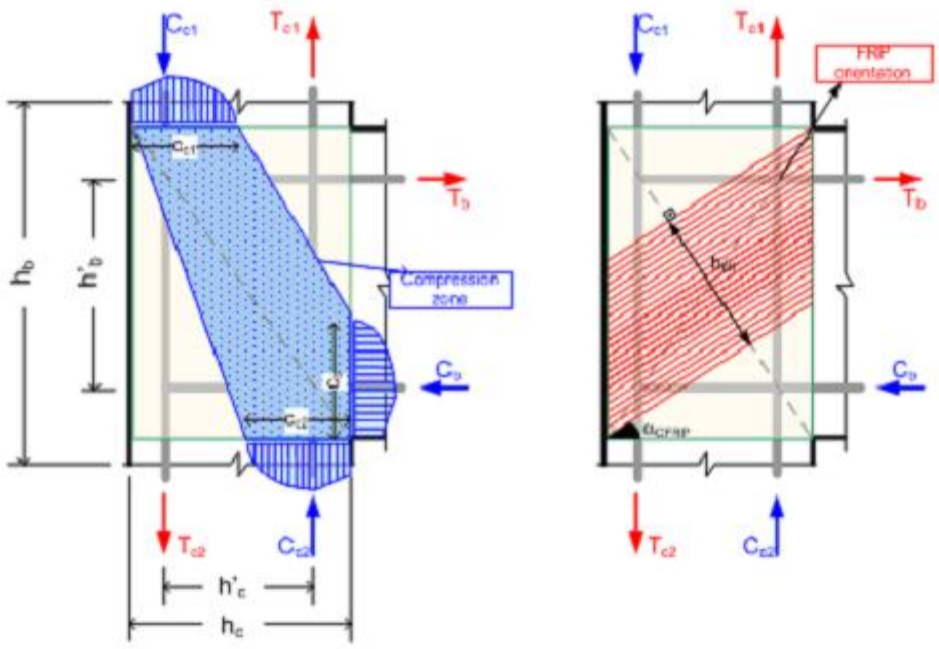

Figure 3.39. Forces acting on joint region and compression and tension struts

The effective area of diagonal strut A_{str} and the effective area of the CFRP sheets A_{CFRP} are calculated as defined in Eq (3.8) and Eq (3.9).

$$A_{str} = a_s \times b_s \tag{3.8}$$

$$A_{CFRP} = b_{eff} \times n \times t \tag{3.9}$$

In the above equations, a_s is the effective depth of the diagonal strut, b_s is the width of the diagonal strut, b_{eff} is the effective width of CFRP, n is the number of the CFRP layers, and t is the theoretical thickness of the one layer of CFRP sheets.

At Fourth step, the mechanism of the joint region is simplified as a statically indeterminate truss system with compression and tension members as seen in Figure 3.39. By applying a unit shear force to the top member, using any structural analysis software, forces exerted on each member of truss were solved and shown in Figure 3.39.

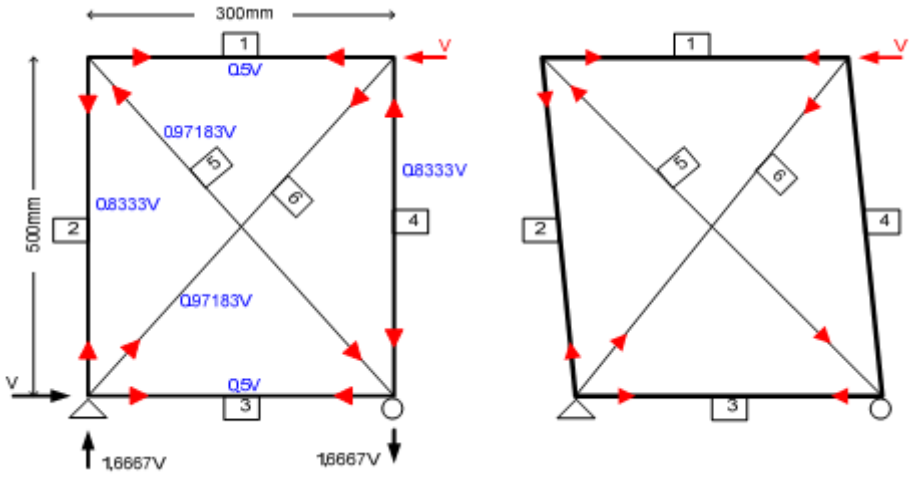

Figure 3.40. Proposed truss system

Final step consists of the calculation process of stresses considering possible five failure mechanisms that are observed from experiments and by considering background knowledge. Stresses for these failure mechanisms, crushing or concrete at joint, the yielding of beam longitudinal reinforcement for control specimens, and rupture of CFRP sheets due to tension failure ($f_{CFRP\text{-}\gamma 2}$), rupture of CFRP sheets due to shear failure ($f_{CFRP\text{-}\gamma 2}$) and yielding of the beam reinforcement at the end of CFRP wrapping region (f_s), calculated. For each considered failure mechanism, lateral load capacity determined by using stresses. The maximum lateral load capacity of the strengthened specimens is determined by the smallest lateral load capacity calculated by using the $f_{CFRP\text{-}\gamma 1}$, $f_{CFRP\text{-}\gamma 2}$ and f_s.

As a summary of model for analysis, at first, dimensions of the column beam and the joint region were introduced and then the amount of steel and CFRP materials, and the characteristic properties of the concrete, steel and CFRP materials were introduced. Afterwards, a unit lateral load was applied. By using the equilibrium equations, all the reaction forces and moments at the joint regions were calculated. In the sectional analysis procedure, for each lateral load increment, moment and the corresponding curvature values are obtained. And accordingly, strain and stress distributions of beam and column sections and the forces of the reinforcements can be determined. The geometry of the compression

strut in the joint was determined by the compression depths of the beam and the column sections. Thus, the forces exerted within the joint regions were obtained.

3.5.1.2.Material Models.

Concrete: The average concrete strength of the specimen was determined as f'_c = 30 MPa from the compression test described in Section 2.4. Modulus of Elasticity of concrete (E_c) which is taken from ACI 318R-08, is calculated according to Eq (3.2) and the strain value at the maximum strength was calculated from Eq (3.3)

$$E_c = 4700\sqrt{f'} = 4700 \times \sqrt{30} = 25743\ MPa \tag{3.2}$$

$$\varepsilon_0 = 2\frac{f'_c}{E_c} = 2 \times \frac{30}{30125} = 0.00199 \tag{3.3}$$

Functions of the pre-peak and post-peak Hognestad curve are defined by Eq (3.4) and Eq (3.5).

$$\sigma_{pre} = f'_c\left[\left(2 \times \frac{\varepsilon}{\varepsilon_0}\right) - \left(\frac{\varepsilon}{\varepsilon_0}\right)^2\right] \tag{3.4}$$

$$\sigma_{post} = f'_c - f'_c \times (\varepsilon - \varepsilon_0) \times \left(\frac{0.15 \times f'_c}{\varepsilon_u - 2 \times \frac{f'_c}{E_c}}\right) \tag{3.5}$$

The tensile strength of concrete, f_t, was taken as the 8% of the compressive strength of concrete. Figure 3.41 shows stress vs. strain relationship of compression test for concrete cylinders.

Steel: Tri-linear steel model was used. Yield strength of the reinforcements was determined as fy = 514 MPa by tensile tests as described in Section 2.4. The Modulus of Elasticity of the steel was taken as Es = 200000 MPa. Figure 3.40 shows stress vs. strain relationship of tension test for longitudinal steel bars.

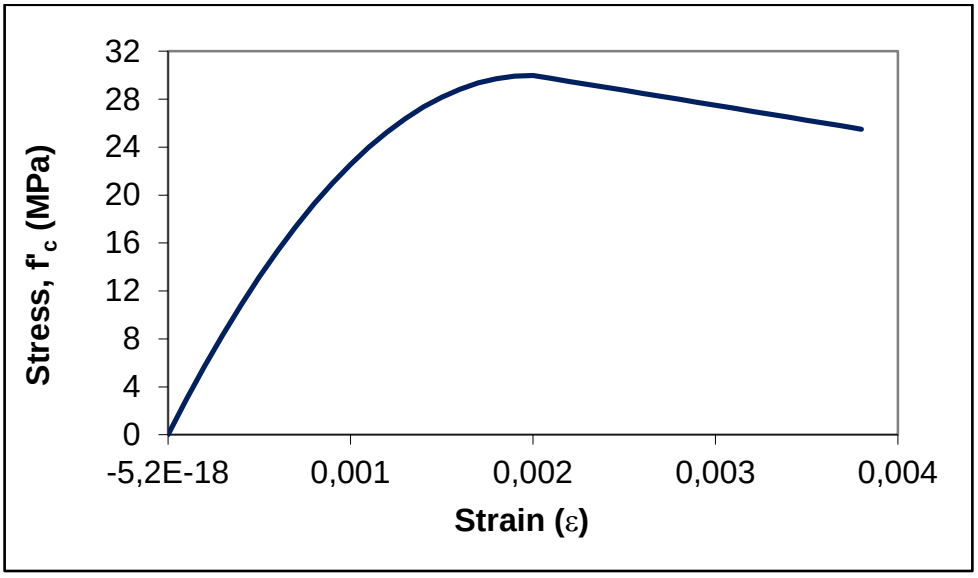

Figure 3.41. Concrete Model (Hognestad)

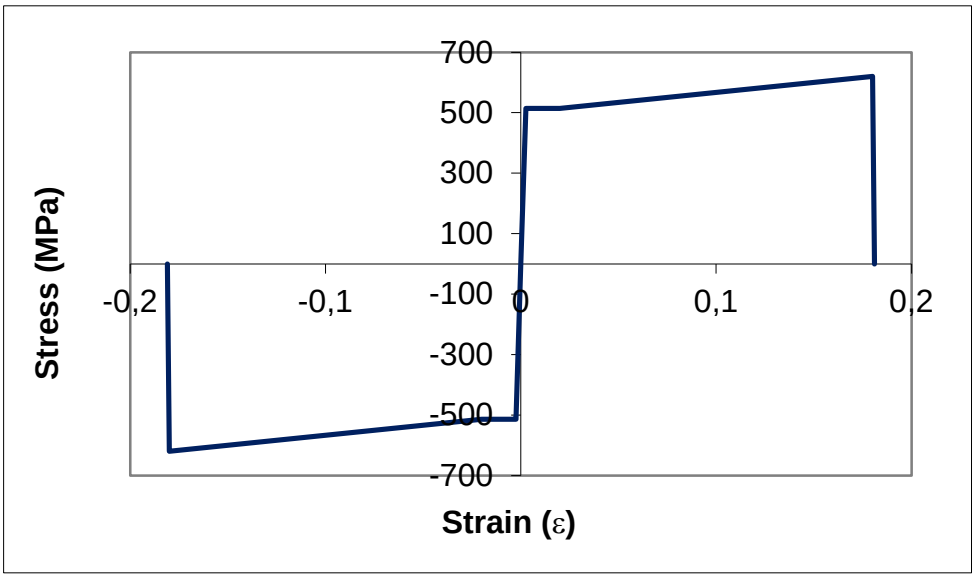

Figure 3.42. Steel Model

CFRP: The material properties of the CFRP fibers and adhesives were given in Section 2.4. When CFRP fibers and epoxy were combined, the ultimate strength and the Modulus of Elasticity of the matrix decrease significantly. From the CFRP strain values measured during the experiments and the observations, the ultimate strength of the matrix was taken as 70% of ultimate strength of fibers. Also, the modulus of Elasticity was taken as 200 GPa which was 20% less than the value given in manufacturers data.

3.5.1.3.Parameters. Input parameters entered to model are mainly listed as below.

Geometry of beam and column: b, hb, hc, etc.

Steel reinforcement ratios: ρ_s, ρ_s', $\rho_{t,}$ etc.

CFRP reinforcement: *n, t, g, L*, etc.

Material properties: f'_c, f_y, $f_{U\text{-}CFRP}$, E_c,E_s, E_{CFRP}, etc.

3.5.2. Comparison of Shear Model Results with Experimental Results

The proposed model was used to predict the lateral load capacity of the test specimens. Table 3.15 illustrates the comparisons of experimental and analytical lateral load capacities.

Table 3.4. Comparison of Model Results with Experimental Results

Specimen ID	f'c	Fy	N/Agf'c	Ftest (kN)		Fcalc (kN)		Ftest/Fcalc		Failure Mode
	Mpa	Mpa		push	pull	Push	pull	push	pull	
US3-ACI	30	514	0.26	73.8	103.9	76.4	100.9	0.97	1.03	Joint Shear
US3-FRP1	30	514	0.26	78.4	144.7	79.4	160.8	0.99	0.90	Beam Yielding / Debonding of CFRP
US3-FRP2	30	514	0.26	103.9	153.5	109.1	160.8	0.95	0.95	Beam Yielding
US3-CONTROL	26	450	0.26	41.9	79.3	68.2	67.2	0.61	1.18	Joint Shear
US3-FRP	26	450	0.26	93.3	123.4	68.2	140.6	1.37	0.88	Joint Shear

For each specimen, model offered five lateral load capacities. These capacities were, as discussed before, determined due to failure mechanism that the specimen had. Proposed capacities were “beam yield FRP” which assumes that hinge occurs at the end of FRP region, “beam yield failure” which assumes that yield occurs close to column surface, two “concrete compression failures” that are assumed for joints with tie and without tie, and “FRP rupture failure”

For each test and specimen, the observed failure mechanism and lateral load capacity are determined by model and then comparisons are done. As Table 3.15 reveals, US3-FRP1 and US3-FRP2 specimens are very compatible with the proposed maximum load capacities of model.

Specimens US-CONTROL and US-FRP were not estimated well. This may arouse because of some factors. Especially for US-FRP specimen, since there were not enough anchorages, debonding effect had been observed in pull direction and thus its lateral load capacity decreased.

4. CONCLUSIONS AND RECOMMENDATIONS

4.1. Conclusions

Observations from recent earthquakes revealed that beam-column joints are indeed the weakest link in the overall structural framing system. Thus, such subassemblies that are not properly designed as per current provisions need to be retrofitted in order to strengthen the joint regions and shift the progressive failure mechanisms to beams and columns. Therefore, improperly designed joint regions are subjected to mainly shear-type of failures.

When the joint region is retrofitted using FRP materials, debonding of that material from concrete surface during cyclic actions should not take place. In this study, the effects of different anchorage techniques applied to the retrofitted beam-column joints to prevent debonding were examined.

The experimental study included two CFRP specimens of US3-FRP1 and US3-FRP2 that were retrofitted with different anchorage configurations in order to prevent debonding of CFPR material from the concrete surface. Both configurations substantially enhanced the structural performance of the beam-column joints in terms of lateral load, drift, dissipated energy, and stiffness capacities when compared to as-built beam-column joints, and as well as, to properly, in accordance with ACI guidelines, designed, US3-ACI specimen. It was concluded that the shear deformations were controlled and also the observed joint behavior became more ductile. Overall, lateral load capacities of CFRP retrofitting specimens were increased significantly. Rates of decrease in their stiffness degradation patterns were also improved. As a conclusion of these enhancements, energy dissipation capacity of the joint reached approximately twice of those of control specimens.

In the proposed retrofitted specimen of US3-FRP2 that had improved anchorage configuration, maximum lateral load increased approximately 2.5 times in push direction

of loading and 2.0 times in pull direction of loading compared to US3-CONTROL specimen. While comparing with US3-ACI specimen, maximum lateral load capacity increased about 30% in pull direction and 50% in push direction of loading. Beam hinging and hence a ductile behavior was maintained in pull direction of loading in both US3-FRP1 and US3-FRP2. This effect in general shows the effectiveness of the CFRP wrapping configurations in terms of ultimate loads.

CFRP wrapping configuration prevented the joint shear failure and caused a desired failure mode which is plastic hinging at the beam. In US3-FRP1, joint shear failures were delayed to an acceptable drift level, however joint shear failures were eliminated in US3-FRP2 specimen. In the CFRP-wrapped specimens, in the pull direction of loading, the debonding of the top portion of U-shaped CFRP sheet was the governing failure mode for the US3-FRP1 but due to the improved anchorage technique, debonding prevented. Hence, US3 specimens can be retrofitted effectively with the proposed wrapping configuration and anchorage technique.

Thus, the research shows that application of CFRP retrofitting method on a seismically deficient joint of a real structure can be easily achieved by using methodologies of anchorage and wrapping which were applied on the research.

Generally, experimental results were compatible with proposed model results in the condition that debonding prevented. This can be clearly seen at US3-FRP2 specimen. Lateral load capacities of model and experimental results were almost same. Thus, it can be said that proposed model works if there is no debonding problem.

4.2. Recommendations

Further experimental research could substantiate the present study and also provide further refinement of the anchorage configuration for CFRP retrofitting in the strengthening of beam-column joints.

REFERENCES

ACI Committee 318, Building Code Requirements for Structural Concrete (ACI 318-08) and Commentary, American Concrete Institute, USA, 2008.

ACI-ASCE Committee 352, Recommendations for Design of Beam-Column Joints in Monolithic Reinforced Concrete Structures (ACI 352R-02), American Concrete Institute, USA, 2002.

ACI T1.1-01, Acceptance Criteria for Moment Frames Based on Structural Testing, American Concrete Institute, 2001.

Alcocer, S. and J. O. Jirsa, 1993, "Strength of Reinforced Concrete Frame Connections Rehabilitated by Jacketing", *ACI Structural Journal*, Vol. 90, No. 3, pp. 249–261.

Almusallam, T. H. and Y.A. Al-Salloum, 2007, "Seismic Response of Interior RC Beam-Column Joints Upgraded with FRP Sheets.II: Analysis and Parametric Study", *Journal of Composites for Construction*, Vol.11, No. 6, pp. 590–600.

Altay, S., A. Parvin, C. Yalcin, and O. Kaya, 2007, "Evaluation of Existing Bond-Slip Models for R/C Joints", *The 9th Canadian Conference on Earthquake Engineering (9CCEE) Ottawa*.

Akguzel, U. and S. Pampanin, 2010, "Effect of Axial Load Variation on the Retrofit of Exterior Reinforced Concrete Beam-Column Joints", *NZSEE Conference*, No. 42, March.

Altay, S., 2009, *Experimental Investigation and 3D Cyclic Finite Element Simulation of R/C Exterior Beam-Column Joints Retrofitted with CFRP Composites*, Ph.D

Dissertation, Boğaziçi University, Istanbul.

Antonopoulos, C. P. and T. C. Triantafillou, 2003, "Experimental Investigation of FRP-Strengthened RC Beam-Column Joints", *Journal of Composites for Construction ASCE*, Vol. 7, No. 1, pp. 39–49.

Bakir, P. G. and H. M. Boduroglu, 2002, "A New Design Equation for Predicting the Joint Shear Strength of Monotonically Loaded Exterior Beam-Column Joints", *Engineering Structures*, Vol. 24, No. 8, pp. 1105–1117.

Beres, A., R. N. White and P. Gergely, 1992, *Seismic Performance of Interior and Exterior Beam-to-Column Joints Related to Lightly Reinforced Concrete Frame Buildings: Detailed Experimental Results*, Report No. 92-7, Cornel University, Ithaca, NY., November.

Beres, A., S. EI-Borgi, R.N. White, P. Gergely, 1992, "*Experimental results of repaired and retrofitted beam-column joint tests in lightly reinforced concrete frame building*", NCEER Technical report, No.25, State University New York, Buffalo, October.

Beres, A. B., 1994, *Experimental and Analytical Study of the Performance of Reinforced Concrete Frames with Non-Ductile Details*, Ph.D. Dissertation, Cornel University, Ithaca, NY.

Bonacci, J. and S. Pantazopoulou, 1993, "Parametric Investigation of Joint Mechanics", *ACI Structural Journal*, Vol. 90, No. 1, pp. 61–71.

Ghobarah, A., T. S. Aziz, A. Biddah, 1997, "Rehabilitation reinforced concrete frame connections using corrugated steel jacketing", *ACI Structural Journal*, Vol. 4, No. 3, pp. 283–294.

Gergely, J., C. P. Pantelides and L. D. Reaveley, 2000, "Shear strengthening of RCT-Joints Using CFRP Composites", *Journal of Composites for Construction* ASCE, Vol. 4, No. 2, pp. 56–64.

Granata, P.J. and Parvin, A., 2001, "An Experimental Study on Kevlar Strengthening of Beam-Column Connections", *Composite Structures*, Vol. 53, No. 2, pp. 163–171.

Gökgöz, E., 2008, *Experimental Research On Seismic Retrofitting Of RC Exterior Beam-Column-Slab Joints Upgraded With Carbon Fiber Reinforced Polymer (CFRP) Sheets*, M.S. Thesis, Boğaziçi University, Istanbul.

Hanson, N. W. and H. W. Connor, 1967, "Seismic Resistance of Reinforced Concrete Beam-Column Joints", Journal *of the Structural Division ASCE*, Vol. 93, pp. 533–560.

Hwang, S. J and H. J Lee, 1999, "Analytical Model for Predicting Shear Strength of Exterior Reinforced Concrete Beam-Column Joint for Seismic Resistance", *ACI Structural Journal*, Vol. 96, No. 5, pp. 846–857.

Kim, J., J. M. LaFave and J. Song, 2007, "A new statistical approach for joint shear strength determination of RC beam-column connections subjected to lateral earthquake loading", *Structural Engineering and Mechanics*, Vol. 27, No. 4, pp. 439–456.

Kim, J. and J. M. LaFave**,** 2009, *Joint Shear Behavior of Joint Shear Behavior of Reinforced Concrete Beam-Column Connections subjected to Seismic Lateral Loading*, NSEL Report Series Report No.20, University of Illinois at Urbana-Champaign November.

Kazuhiro, K., O. Shunsuke and A. Hiroyuki, 1991, "Development of Design Criteria for RC Interior Beam-Column Joints – Design of Beam-Column Joints for Seismic

Resistance (SP-123)", *American Concrete Institute*, Detroit, Vol. 123, pp. 97–123.

Kaya, O., 2009, Seismic Retrofitting of RC Beam – Column Joints Using Composite Materials, Ph.D Dissertation, Boğaziçi University, Istanbul.

Kim, J. and J. M. LaFave, 2007, "Key influence parameters for the joint shear behaviour of reinforced concrete (RC) beam–column connections", *Engineering Structures*, Vol. 29, pp. 2523–2539.

Mukherjee, A., M. Joshi, 2005, "FRPC reinforced concrete beam-column joints under cyclic excitation", *Composite Structures*, Vol. 70, pp. 185–199.

Mukherjee, A. and M. Joshi, 2005, "FRPC Reinforced Concrete Beam-Column Joints Under Cyclic Excitation", *Composite Structures*, Vol. 70, No. 2, pp. 185–199.

Popov, E. P., V. V. Bertero and S. Viwathanatepa, 1975, "Analytical and Experimental Hysteretic Loops for R/C Subassemlages", *Fifth European Conference on Earthquake Engineering*, Istanbul, No. 89, September.

Pantelides , C. P., Y. Okahashi and L. D. Reaveley, 2008, "Seismic Rehabilitation of Reinforced Concrete Frame Interior Beam-Column Joints with FRP Composites", *Journal of Composites for Construction*, Vol.12, No. 4, pp. 435–445.

Prota, A., A. Nanni, G. Manfredi, and E. Cosenza, 2004, "Selective Upgrade of Underdesigned Reinforced Concrete Beam-Column Joints Using Carbon Fiber-Reinforced Polymers", *ACI Structural Journal*, Vol.101, No. 5, pp. 699–707.

Pampanin, S., D. Bolognini, and A. Pavese, 2007, "Performance-Based Seismic Retrofit

Strategy for Existing Reinforced Concrete Frame Systems Using Fiber-Reinforced Polymer Composites", *Journal of Composites for Construction*, Vol.11, No. 2, pp. 211–226.

Scarpas, A. and T. Paulay, 1981, *The Inelastic Behavior of Earthquake Resistant Reinforced Concrete Exterior Beam-Column Joints*, University of Canterbury, Christchurch, New Zealand, Report No. 81-2, February.

Scot, R. H., 1996, "Intrinsic Mechanism in Reinforced Concrete Beam Column Connection Behavior", *ACI Structural Journal*, Vol. 93, No. 3, pp. 336–346.

Shiohara, H., 2001, "New Model for Shear Failure of RC Interior Beam Column Connections", *Journal of Structural Engineering ASCE*, Vol. 127, No. 2, pp. 152–160.

Tsonos, A. G., 1999, "Lateral load response of strengthened reinforced concrete beam to column joint", *ACI Structural Journal*, Vol. 96 No. 1, pp. 46–56.

Topçu, İ., 2008, *Experimental Research On Seismic Retrofitting Of R/C Corner Beam-Column-Slab Joints Upgraded With Carbon Fiber Reinforced Polymer (CFRP) Sheets*, M.S Thesis, Boğaziçi University, Istanbul.

Uma, S.R. and A. M. Prasad, 2004, *Seismic Behavior of Beam Column Joints in Reinforced Concrete Moment Resisting Frames*, Earthquake Code, No. 31, IIT Madras, India.

Womack, K. C., M. W. Halling And R. M. Moyle, 2000, "Full Scale Testing Of Concrete Beam-Column Joints Using Advanced Carbon-Fiber Composites", *12WCEE Conference*, Utah State University, No. 1478, Utah.

Wang, Y. C. and K. Hsu, 2009, "Shear Strength of RC Jacketed Interior Beam- Column

Joints without Horizontal Shear Reinforcement", *ACI Structural Journal*, Vol. 106, No. 2, pp. 222–232.